Nanostructured polymeric aqueous dispersions containing quantum dots

PhD candidate: Alicia De San Luis González
Supervisors: Prof. Jose Ramon Leiza
Prof. María Paulis

Table of contents

Chapter 1. Introduction

1.1. Quantum dots

1.1.1. General aspects

Colloidal quantum dots are dispersions of semiconductor nanocrystal of sizes between 2 nm and 10 nm, which were discovered by Alexey Ekimov in 1981[1] and described by L. E. Brus and coworkers during the early 80s. Brus et al. modelled the excited electronic states of small semiconductor crystallites comparing them with bulk materials and observing some interesting differences. From these studies, the influence of the quantum dots (QDs) size on their energy and subsequently on their properties was deduced, being this the base of their development[2–5]. As semiconductors, the electronic band structure of quantum dots is based on a conduction band and a valence band separated energetically by the band gap (Figure 1.1).

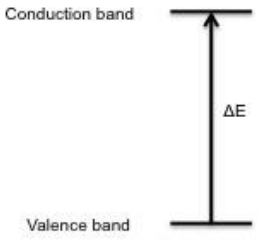

Figure 1.1 Electronic band structure of quantum dots.

Normally, the energy levels of the valence and the conduction band in a semiconductor particle are continuous. However, when the size of the semiconductor is smaller than the Bohr exciton radius these energy levels become discrete resulting in a size-dependent band gap[6]. This is called quantum confinement effect. The presence of discrete energy levels in their

electronic structure makes QDs to be sometimes referred as artificial atoms, as they show a structure similar to the one that would correspond to atoms[7,8].

The dependency of the band gap with the particle size is defined by Equation 1.1, which shows an inversely proportional relationship between the bang gap energy (ΔE) and the size (R); the bigger is the radius of the nanocrystals the smaller is the band gap.

$$\Delta E = \frac{\hbar^2 \pi^2}{2R^2}\left(\frac{1}{m_e^*} + \frac{1}{m_h^*}\right) - \frac{1.8\, e^2}{\varepsilon R}$$

Equation 1.1 Change in the bandgap width as a function of the size of the QD.

e = electron elementary charge

ε = bulk dielectric constant

m_e^* and m^*_h = effective mass of the electrons and the holes, respectively

R = nanoparticle radius

The size-dependence of the band gap influences the electronic and optical properties of the quantum dots, especially on their fluorescence emission. For fluorescence to happen, first a jump of an electron from the valence band to the conduction band has to occur. This creates an electron hole in the valence band upon absorption of a photon. Then, the electron and the hole are attracted by electrostatic Coulombic forces and recombined, generating an exciton emitting light in fluorescence form. As mentioned above, and as a consequence of the quantum confinement effect, the smaller is the particle size the bigger is the band gap between the valence band and the conduction band, meaning that more energy is emitted when the electron

and the hole are recombined. Therefore, smaller particles emit light at shorter wavelengths, blue range of the visible spectra, whereas bigger particles emit light at longer wavelengths, in the red range of the visible spectra (Figure 1.2).

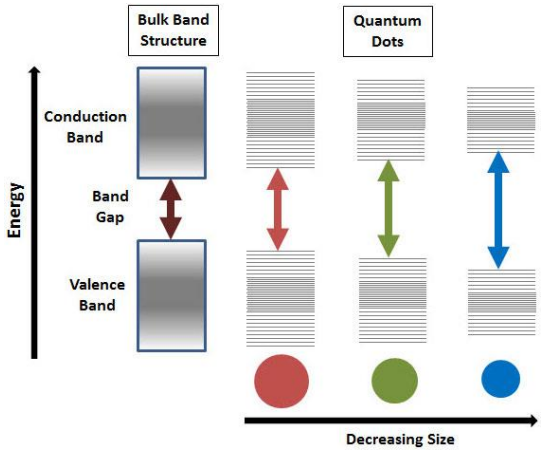

Figure 1.2 Quantum confinement effect (http://www.sigmaaldrich.com/technical-documents/articles/materials-science/nanomaterials/quantum-dots.html#ref).

1.1.2. Structure

Quantum dots are made of combinations of different periodic elements, especially from groups II and VI (CdSe, CdS…), but also from groups III and V (InAs, GaAs…) or groups IV and VI (PbSe). The final crystal structure, in all the cases, depends mostly on the synthesis conditions, being the most common structures zinc blend, wurtzite and sodium chloride[9–11]. Colloidal quantum dots, especially the ones from groups II-VI, has been extensively investigated[10], being the most extended synthetic route the one proposed by Murray and

coworkers[12]. They synthesized good quality trioctylphosphine oxide (TOPO) coated CdE (E = S, Se, Te) nanocrystals by hot injection of the precursor solutions (Figure 1.3). In this method, the surface modifier (TOPO) is placed in the reaction vessel in solid form under magnetic agitation, and the temperature of the flask is increased to 300ºC melting the TOPO. Then, two solutions are prepared, one containing the cadmium reagents and the other one containing the "E" reagents. The two solutions are then loaded in a single syringe. After cooling down the flask, the solutions mixture is injected in a shot increasing suddenly the temperature to 180ºC. Afterwards, the temperature is increased gradually to 230ºC-260ºC. Depending on the reaction time CdE particles of different sizes are obtained.

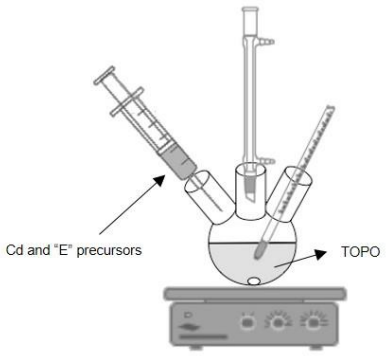

Figure 1.3 Hot injection set-up.

This technique gives a good control of the nucleation, which provides narrow particle size distributions of QDs with high luminescence. However, the nanocrystals produced present defects on their surface leading to electron leaks during time, and therefore, to a loss on their optical properties. In order to circumvent this, QDs are usually passivated with another semiconductor material with a similar crystal lattice to avoid incompatibilities and loss of

luminescence[13–16]. Even if hot injection technique is extensively used for the synthesis of QDs, more recently, good quality quantum dots have also been synthesized using supercritical fluid technology. This technique allows reducing the reaction time and to overcome miscibility problems as well as the synthesis of larger amounts of good quality product[11,17].

Depending on the band gap of the bulk material that composes the core and the shell, three types of core-shell systems can be distinguished, Type I, Reverse Type I and Type II[16] (Figure 1.4). In Type I (CdSe/ZnS)[13] the band gap of the shell is bigger than the one of the core, being both electrons and holes confined in the core. In this case the shell acts as a protection of the core, so the loss of the optical properties of the nanocrystal is mainly reduced. In Inverse Type I (ZnSe/CdSe)[18] the opposite situation is presented, the band gap of the core is bigger than the band gap of the shell. In this case the position of the electrons and the holes depends on the thickness of the shell being partly or entirely confined in the shell. Finally, in Type II core-shell QDs (CdTe/CdSe)[19] either the valence band or the conduction band of the shell is situated in the band gap of the core. Consequently, the electron and the hole are separated and situated in different parts of the final structure[19].

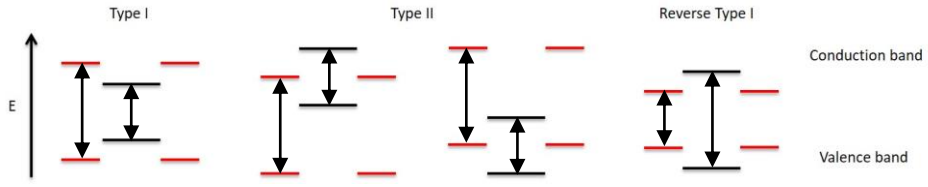

Figure 1.4 Scheme of the bandgap alignment between the core (blue) and the shell (red) material in a core-shell system. From left to right: Type I, Type II (two cases) and Inverse Type I. (Reproduced from reference[16])

In the three cases the thickness of the shell has a great impact on the final properties of the nanocrystal[15,16]. For example, the thickness in the ZnS shell in CdSe/ZnS Type I particles causes a slight red shift both in the absorbance and the emission peak. This red shift is probably due to partial leakage of excitons into the ZnS shell. In the two other types, as the electrons and holes are delocalized in the core and in the shell, the increase in the thickness of the shell drives to a notable red shift. Taking all these factors into account, a good equilibrium between an effective protection of the core in order to avoid photobleaching and maintenance of the tunability in the emission wavelength depending on the final size, has to be reached. This way highly luminescent nanocrystals can be obtained.

In fluorescence, the luminescence efficiency is defined by the quantum yield, which is the ratio between the number of photons emitted and absorbed. This value increases significantly when synthesizing core-shell quantum dots nanocrystals avoiding photodegradation.

Most of the quantum dots presented so far are cadmium based, so potentially toxic when used for biological applications. Therefore, new heavy metal free quantum dots have been synthesized trying to obtain the same optical properties as for Cd-based nanocrystals[20], in order to use them for both optoelectronic and biological applications. In some cases, synthesis have been done by hot injection of the precursors[21–26]. On the other hand, other authors have developed new techniques aiming at obtaining properties similar to the ones of conventional QDs. For example, Li and Reiss developed the “heating-up method” obtaining high quantum yields[27]. As in the case of conventional Cd-based quantum dots, supercritical

fluid technology can also be used for the synthesis of those novel nanocrystals, such as GaN that present excellent optoelectronic properties and are biocompatible[28].

1.1.3. Surface chemistry

Independently from the inorganic shell, usually quantum dots are further coated with an organic compound (eg., trioctylphosphine oxide (TOPO) or octadecylamine) that acts as a stabilizer ligand in their synthesis[29,30]. Furthermore, the organic coating gives the QDs dispersibility in different solvents (water or organic solvents). Ligands normally influence the optical properties of the nanocrystals because they interact with its surface, and therefore, ligands have to be carefully chosen and incorporated. Typically, the organic ligand is incorporated when synthesizing the nanocrystal, as some of the precursors are dissolved in the presence of the ligand.

Additionally, most of the stabilizers used to coat quantum dots surface are hydrophobic, which makes difficult their dispersion in aqueous media and hence reduce their potential use in biological applications. Therefore, polymeric modifiers that are compatible with water and contain multiple functionalities have been implemented to achieve stable dispersion of QD in aqueous media[30]. Although many approaches have been developed to get polymer-coated quantum dots, most of them require a ligand exchange reaction that affects the fluorescence of the QDs by reducing their quantum yield[31]. Some examples are: the use of multidentate polymeric ligands[32,33]; attachment of the polymer chain to the QDs´ surface both via direct attachment of a functionalized polymeric chain to the surface[34], or via polymerization from the

surface of the nanocrystal[35]; or coating with dendrimeric materials[36,37]. An alternative to these ligand exchanges is the use of amphiphilic polymers in which the hydrophobic part interacts with the former organic modification of the quantum dot surface and the hydrophobic part is exposed to the outer side, obtaining good quality water dispersible quantum dots [38–40].

1.1.4. Properties

As discussed in the previous sections, thanks to their very small size (2-10 nm), quantum dots present a size dependent band gap that makes them exhibit some exceptional optical and electronic properties.

The most remarkable property of quantum dots is linked to their size-tunability, which is intimately related with their band gap size dependency. This means that maintaining the chemical composition of the nanocrystal, the emission wavelength is changed by varying their size. For example, in the case of CdSe/ZnS quantum dots, emission wavelength shifts from the blue to the red range by changing the size of the nanocrystal from 2 nm to 10 nm (Figure 1.5).

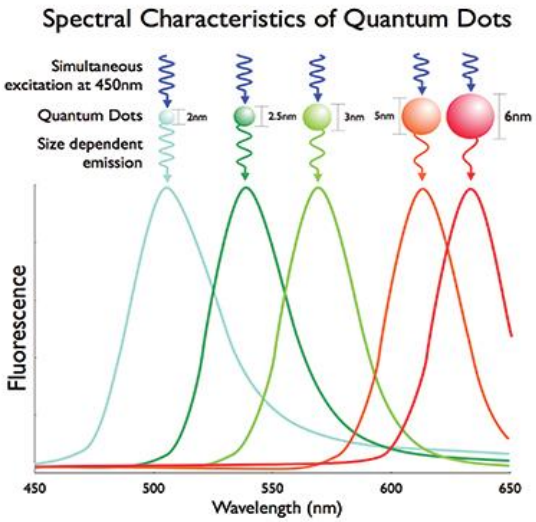

Figure 1.5 Fluorescence emission wavelength of CdSe/ZnS quantum dots dependending on their size.(Image taken from reference [41]).

Apart from their size-tunability, quantum dots present other remarkable optical properties. They present a narrow emission peak exhibiting small full width at half maximum, so their emission is very specific. Additionally, they absorb light in a wide range of wavelengths. Combining these two characteristics, different types of quantum dots or quantum dots of different sizes can be used at the same time illuminating the sample under the same excitation wavelength and obtaining fluorescence spectra in which overlapping of the peaks is avoided. Therefore, quantum dots can be used in biological labelling or bioimaging assays such as multiplexing.

Compared with organic dyes, quantum dots present many advantages, apart from the already highlighted size-tunability, specific emission peaks and broad absorbance. For

example, they are around 20 times brighter under UV light[42]. In terms of photostability, quantum dots are much more stable than organic chromophores. This is mainly due to the inorganic composition of QDs. In the case of chromophores, they are photochemically altered by the cleavage of covalent bonds, modifying their chemical structure and suffering from a decay in fluorescence emission intensity. This effect is called photobleaching. Regarding fluorescence lifetime, regardless the slower start of emission of QDs; their excited state decay curves are smoother presenting longer lifetimes than organic dyes. Quantum dots also present molar extinction coefficients 10 to 50 times larger than organic dyes, which is a notable advantage in limited photon absorbance conditions[39,43].

In spite of the inherent advantages provided by quantum dots (exceptional electronic and optical properties), one should also consider their potential drawbacks for certain applications. Thus, the most important drawbacks is their small size (that is needed to get size-tunability fluorescence), which makes them difficult to manipulate. Furthermore, their sensitivity upon degradation of their surface that leads to a loss of their properties, and their toxicity due to the heavy metals composition, are also important drawbacks. Therefore, there is a strong interest to protect quantum dots using polymers to facilitate their use in optoelectronic and biological applications, overcoming the drawbacks listed above. This way, QDs with easier manipulation and good dispersibility in several mediums will be available. Regarding their surface sensitivity, quantum dots would be protected against damage, so against loss of their properties. Furthermore, the working environment would be protected and the impact of their toxicity notably reduced.

1.2. Incorporation of quantum dots into colloidal polymer particles

A large number of researchers have attempted the production of colloidal polymer particles with encapsulated inorganic nanoparticles and more particularly with quantum dots. A careful review of these works clearly indicates that, not only there is not a general approach for the encapsulation of QDs, but also in most of the cases specific modification of the surface of the QDs and purification steps are required, which makes the methods difficult to scale-up. The most relevant methods developed for the encapsulation of quantum dots into polymer particles are the following:

- Incorporation into premade polymers
- Suspension Polymerization
- Emulsion Polymerization
- Miniemulsion Polymerization

A brief summary of these methods will be presented in the next sections.

1.2.1. Incorporation of QDs into premade polymers

With the aim of controlling the position and the number of quantum dots into the polymer particles, as well as to avoid possible degradation of the surface of the nanocrystals (by the interaction of the radicals when polymerizing in presence of QDs), several groups studied the

incorporation of QDs into already preformed polymer particles. Different ways of incorporation have been reported.

The simplest method is the swelling of the quantum dots into polymer microgels[44]. This has been reported both for quantum dots coated with organic ligands[44,45] and for water-dispersible nanocrystals[46]. However, in some of the cases the position of the quantum dots in the microgels was not the desired one, being found in the outer part of the particle. Regarding the microgel size, this has to be well controlled as it can change depending on the environment, pH, temperature, ionic strength, solvent and electric field. The tuning of these parameters was seen as an advantage for the incorporation of quantum dots in different reported works. For example Kuang et al.[47] entrapped CdTe QDs into microgel spheres by changing the pH. At low pH microgel particles were swollen trapping the QDs. Then, increasing the pH, the microgel shrinked and confined the nanocrystals inside. When the pH was increased to values higher than 11 QDs were released (Figure 1.6).

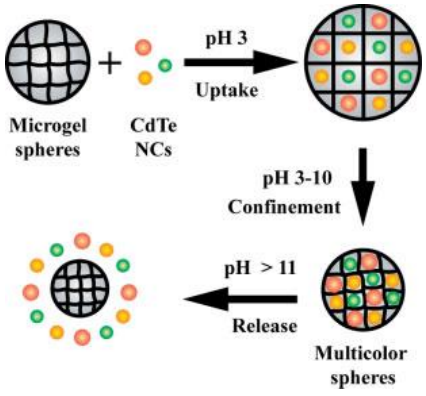

Figure 1.6 Schematic illustration of the loading of CdTe NCs in PNIPVP spheres and their controlled release by pH. (Image taken from reference [47]).

In-situ synthesis of quantum dots in polymer microspheres (e.g. microgels) has also been studied, carrying it on the surface of the polymer particles or directly inside[48,49] them. Many factors have to be controlled in order to get high quality nanocrystals into the microgels, such as the pH during the nanocrystal synthesis, the microgel composition, and the morphology of the microgel.

1.2.2. Encapsulation via suspension polymerization

Regarding encapsulation of quantum dots during a polymerization reaction, suspension polymerization has been one of the ways investigated for obtaining stable polymer particles-quantum dots hybrids. O´Brien et al.[50] first synthesized hexadecylamine CdSe QDs followed by a ligand exchange (with polymerizable ligands based on the TOPO structure) obtaining surface polymerizable QDs. Those quantum dots were encapsulated into polymer particles synthesized by suspension polymerization. The nanocrystals were dispersed in a styrene-divinyl benzene (DVB) monomer mixture. Polyvinyl alcohol was used as stabilizer and AIBN as initiator in the suspension polymerization. They obtained polymer beads of 38 μm size with a homogeneous distribution of QDs in them after polymerization (Figure 1.7 left image). This homogeneity in the distribution of the QDs, was shown by measuring the fluorescence in different parts of a bead (RDI 1, RDI 2…) and obtaining the same emission intensity, as shown in the fluorescence spectra of Figure 1.7 (right image).

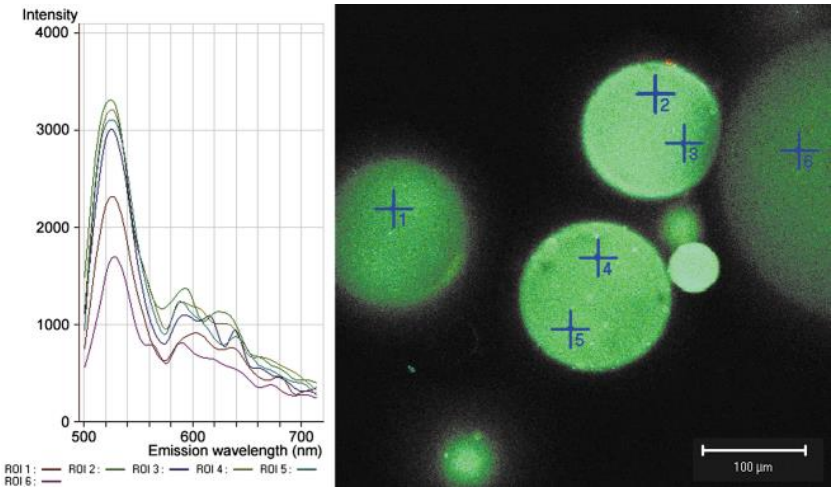

Figure 1.7 Fluorescence emission fingerprint of quantum dot containing polymer beads. Images taken from reference [50]

Bradley et al.[44] used two different ways to encapsulate TOPO coated CdSe QDs. On one hand, the quantum dots dispersed in chloroform were swollen into polystyrene microgel particles. On the other hand, the QDs were dispersed in a mixture of styrene and divinyl benzene (DVB), carrying out suspension polymerization using polyvinyl alcohol as stabilizer and benzoyl peroxide (BPO) as initiator. The localization of the QDs was studied by confocal microscopy. In the former case, the penetration of the nanocrystals depended on the swelling of the microgel particles; the higher the swelling, the higher the penetration of the QDs. In the latter case quenching of the fluorescence was observed when encapsulating CdSe QDs, so CdSe/ZnS QDs were used. In this case, the polymer particles in which the nanocrystals were located in the polymer particle-aqueous phase interface were obtained. In this report, no data about the fluorescence of the microgel particles was shown, just the localization of the QDs by confocal microscopy.

Sheng et al.[51] first produced TOPO coated CdSe/ZnCdS/ZnS quantum dots followed by a cap-exchange in which the TOPO molecules were substituted by an oligomeric phosphine ligand. The obtained QDs were then dispersed in ethanol for a pre-polymerization process with MMA, after which a shell of cross-linked PMMA protected the QDs. These PMMA modified QDs were incorporated in PS microparticles produced in suspension polymerization, using AIBN, poly(vinylpyrrolidone) (PVP) and ethanol as initiator, stabilizer and continuous medium respectively. The process led to quantum dot-embedded polystyrene microspheres (QD/PSMS) with 1.2 μm diameter. Fluorescent monodispersed microspheres stable under harsh conditions were obtained. Nevertheless, aggregation of quantum dots could not be prevented when increasing their concentration.

Even though QDs were incorporated into polymer particles by suspension polymerization process, a good control of either the position of the quantum dots or of the final fluorescence properties was achieved.

1.2.3. Encapsulation via emulsion polymerization

Emulsion polymerization has also been used for the encapsulation of quantum dots into colloidal polymer particles. Yang and Zhan[52] synthesized TOPO coated CdSe quantum dots and dispersed them in toluene. The dispersion was then added dropwise to the surfactant solution in water at room temperature. Then, the monomer mixture (styrene, divinyl benzene and methacrylic acid) and the initiator (AIBN) were added dropwise to the prepared emulsion in an ice bath. Finally, they increased the temperature to 70ºC carrying out the polymerization for

20 hours. They claimed a good control of the encapsulation of the quantum dots into the polymer particles avoiding aggregation of the nanocrystals, showing fluorescence microscopy images. Unfortunately, TEM micrographs and fluorescence spectra of the hybrid polymer particles were not provided to assess the encapsulation.

Cysteine acrylamine coated CdS and CdSe/CdS quantum dots were encapsulated by emulsion polymerization using two different methods[53]. In a first example, surfactant-free emulsion polymerization of styrene and sodium 4-styrenesulfonate using KPS as initiator was carried out, dispersing the QDs in the monomer. Polymer particles ranging from 177 nm to 226 nm were described, noting that after the polymerization some of the QD nanoparticles were not trapped into the polymer particles and were removed by ultrafiltration. Although nanocrystals could not be observed in the TEM micrograph shown and fluorescence emission spectra were not presented, they claimed stability of the fluorescence for more than two years. In a second example, CdSe/CdS QDs were first modified with vinylbenzyl (trimethyl)-ammonium chloride obtaining polymerizable groups on their surface. Those nanocrystals were then dispersed in a mixture of styrene and water containing sodium dodecyl sulfate as emulsifier carrying out the emulsion polymerization using AIBN as initiator. No TEM images in which the QDs could be observed were presented. Nevertheless, a fluorescence spectra comparing the CdSe/CdS signal before and after the emulsion polymerization was shown. A blue shift in the fluorescence emission wavelength was observed during the polymerization, as well as a wider final emission peak (Figure 1.8), meaning that the nature of the quantum dots did not remain unaltered during the polymerization process.

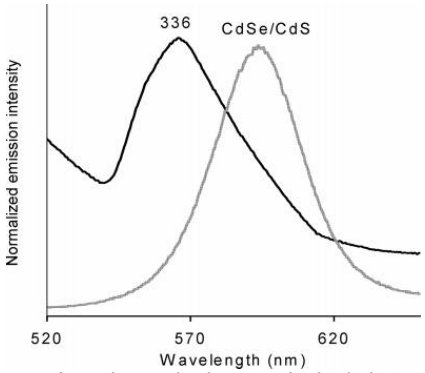

Figure 1.8 Fluorescence emission spectrum of cysteine acrylamine coated CdSe/CdS QDs before and after the emulsion polymerization process carried out using SDS and AIBN as emulsifier and initiator (336) (Image taken from reference [53]).

Finally, Lee et al.[54] synthesized TOPO coated CdSe and CdSe/ZnS quantum dots. In this work, encapsulation via emulsion polymerization using different monomers is explained. First the encapsulation of the CdSe QDs into polydivinyl benzene (pDVB) particles is shown. The QDs were dispersed in chloroform and then mixed with an aqueous solution of sodium bis(2-ethylhexyl) sulfosuccionate (AOT). After removing the excess of AOT from the surface of the QDs by dialysis and centrifugation, the aqueous solution of QDs was mixed with divinyl benzene (DVB) initiating the polymerization reaction with potassium persulfate (KPS). They claimed the synthesis of 20 nm size hybrid polymer particles with a successful encapsulation of the QDs (Figure 1.9a). The obtained hybrid polymer particles were characterized by UV-Vis absorbance observing a decrease of the absorbance during the encapsulation process, from the dispersion of the QDs in chloroform (Figure 1.9b). Moreover, a decrease of the fluorescence emission intensity from the dispersion of the QDs in chloroform to the final hybrid polymer particles was reported, as well as a red shift of the emission peak (Figure 1.9b inset). They proved the versatility of the method by using different monomers (styrene (S), vinyl pyridine (VPy) and methyl methacrylate (MMA)) for the encapsulation of CdSe QDs with and

without using DVB as cross-linker. The effect of the cross-linking in the polydispersity and structure was studied, presenting an improvement for the case of PS and PVPy hybrid polymer particles, but not for PMMA, where QDs were severely aggregated. Better results were obtained when CdSe/ZnS core-shell QDs were used in the same approach. Thus, fluorescence quenching during the process of encapsulation into pDVB particles was avoided (Figure 1.9). However, results for the other monomers were not shown, neither the evolution of the fluorescence during time.

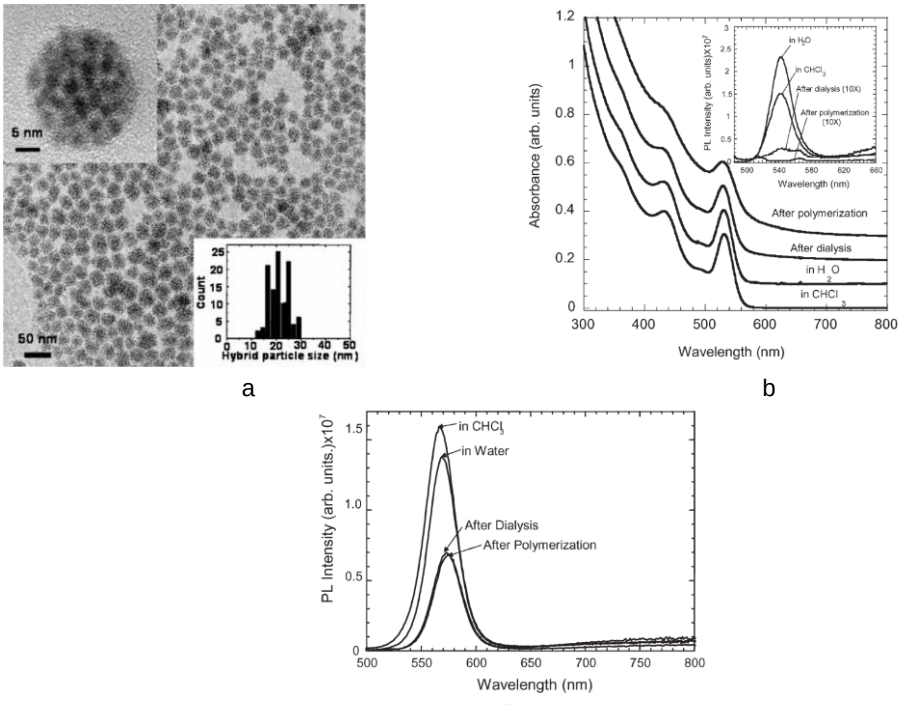

Figure 1.9 a) TEM micrographs of hybrid polymer particles pDVB/QDs. The upper inset is a high magnification image showing an individual pDVB/QDs hybrid polymer particle. The lower inset shows the particle size distribution. b) UV-VIS absorption spectra of CdSe nanocrystals at each step of the synthesis. Absorption spectra are offset for clarity. The curves in the inset are the corresponding photoluminescence spectra normalized to the optical density at the excitation wavelength. c) Photoluminescence spectra normalized to the optical density at the excitation wavelength of CdSe/ZnS nanocrystals at each step of the synthesis (Images taken from reference [54]).

From the examples above, it can be said that complete encapsulation of QDs into polymer particles by means of emulsion polymerization is difficult, unless polymerization is started from the surface of the QDs, after their surface modification to incorporate polymerizable groups.

1.2.4. Encapsulation via miniemulsion polymerization

Likely the simplest and more general method to encapsulate QDs in hydrophobic submicron polymer particles is by means of miniemulsion polymerization[55,56]; namely by generating an aqueous dispersion of nanodroplets of a polymerizing monomer where the surface coated QDs are compatible. The polymerization of the nanodroplet dispersion yields a dispersion of polymer nanoparticles that contain the quantum dots. The successful encapsulation of the inorganic nanoparticles into the polymer particles by miniemulsion polymerization depends on the monomer system, the initiator type, the surfactant concentration and the surface modification of the inorganic nanoparticles. All these factors determine the thermodynamic equilibrium morphology of the hybrid polymer-inorganic nanoparticle particles, which is the one that minimizes the surface energy of the system[57].

Fleischaker and Zentel[58] produced core/shell PS/PMMA nanoparticles with CdS/ZnS coated CdSe QDs integrated in the core. The core was produced by miniemulsion polymerization using hexadecane (HD) as co-stabilizer and sodium dodecyl sulphate (SDS) as emulsifier. The shell was produced by starved feeding of MMA to the hybrid core seeds. Unfortunately, the authors did not provide information about the location and distribution of the

QDs in the core particles neither regarding the fluorescence properties of the core particles. Nonetheless, the core/shell particles seem to be good candidates to produce colloidal crystals (Figure 1.10).

Figure 1.10 Colloidal photonic crystals from PS/PMMA core-shell spheres with embedded CdSe QDs (Image taken from reference [58]).

Esteves et al. claimed encapsulation of TOPO-coated CdS or CdSe QDs in polystyrene and polybutyl acrylate polymer particles produced by free radical[59] or AGET-ATRP (Activator Generated by Electron Transfer-Atom Transfer Radical Polymerization)[60,61] miniemulsion polymerization, yielding homogeneous nanocomposites where the optical properties of the QDs were maintained. However, the latexes were bimodal and QDs were only observed in the large population, and hence additional separation steps were necessary to get only the fluorescent colloidal particles.

Joumaa et al. extensively analysed the incorporation of CdSe/ZnS core-shell QDs into polymer colloids by miniemulsion polymerization investigating the effect of the type of coating (either trioctylphosphine oxide (TOPO) or vinyl-functionalized), the concentration of the QDs, and the surfactant concentration on the kinetics of the polymerization as well as the photoluminescence properties of the hybrid polymer particles[62]. They found that the kinetics of the polymerization was almost not altered by the presence of either type of QDs, the

fluorescence of the particles increased with the concentration of nanocrystals, and the fluorescence properties were superior for the TOPO-coated latexes. Interestingly, the authors provided very accurate TEM images of the location of the QDs in the polymer particles and two aspects were noteworthy: the QDs aggregated, but preserved their optical properties and the QDs were located at the edge of the polymer particles, namely at the interface of the particles and aqueous phase (Figure 1.11). Although the authors showed that fluorescent latexes were produced, they did not provide any information of the fluorescence during storage which might be affected by the location of the QDs in the vicinity of the aqueous phase.

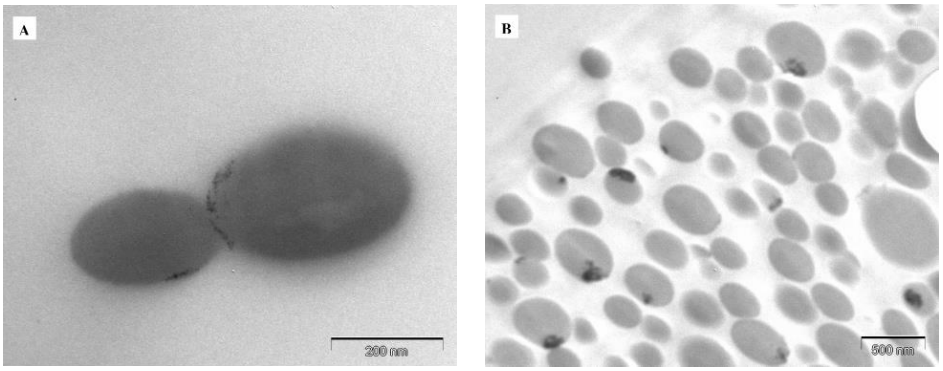

Figure 1.11 TEM micrographs of ultrathin sections showing the location of the TOPO coated CdSe/ZnS QDs in the polymer particles (Image taken from reference [62]).

More recently, Harun et al. used miniemulsion polymerization to encapsulate alkylated silicon quantum dots (Si-QD) in polymer nanoparticles composed of styrene and 4-vinylbenzaldehyde monomers[63]. The authors claimed encapsulation by measurements done by confocal microspectroscopy using Raman and luminescence spectra and by bright field optical images, but well-resolved TEM images were not obtained and hence neither the location nor the distribution of the Si-QDs within each polymer particles could be provided. Interestingly,

these authors analyzed the preservation of the luminescence of the latexes during time upon exposure to aqueous alkali medium (0.02M). They showed that bare Si-QDs lost their fluorescence intensity in 24 hours, whereas the hybrids lost in the same time 60% of the intensity. Unfortunately, the authors did not provide fluorescence information in longer time periods.

All the above reports indicated, not only that there is still a need to efficiently encapsulate fluorescent QDs in submicron colloidal particles, but also to preserve the fluorescence of the colloidal particles during storage, in order to have time to fabricate optical devices without jeopardizing the properties achieved right after the synthesis of the hybrid colloidal particles.

1.3. Applications

Taking advantage of the unique optical and electronic properties of quantum dots, they have been extensively investigated as perfect candidates for several applications. Encapsulated into polymer particles they are easily manipulated, they can be better dispersed in different mediums, they are better protected against damage of their surface and the environment is protected against their toxicity, they can improve the electronic transmission in electronic devices, such as light emission diodes[64–66] and solar cells[67–69], and the optical properties for example for biological assays as multiplexing and for bioimaging[42,70].

1.3.1. Biological applications

Regarding biological labelling, the small retard (ns) of quantum dots for emitting fluorescence in comparison with organic chromophores is an important advantage. Cellular components present autofluorescence during a short period of time, that coincide with the time during which organic dyes present their highest fluorescence, making difficult their detection by fluorescence. However, as QDs start emitting later, they avoid the overlapping of the signals distinguishing better the organelles of interest, and carrying out measurements during longer periods of time[71]. Taking into account the potential toxicity of QDs and their sensible surface, in most of the reported works they are coated with amphiphilic polymers, specially PEG. However, the encapsulation or coating of the QDs with polymers increases their size making difficult to introduce them into the cell. So, for cell labelling quantum dots are directly capped with terminal functional groups as thiols, carboxylic acids or amine, so they can be conjugated to diverse molecules such as proteins and DNA[72–74]. Both in vitro and in vivo labelling has been reported by different groups, taking into account the most appropriate functionalization depending on the desired binding, as well as the size of the resulting particle to be suitable for the labelling[39,75–80].

As presented above, quantum dots present a very narrow fluorescence emission peak and absorb light in a very wide range of wavelengths. Thanks to this, different quantum dots can be detected simultaneously using a single excitation wavelength and avoiding overlapping of the emission signals. This has been studied for the application of the nanocrystals in multiplexing assays[45–47,71,74,78,81]. Multiplexing assays are based on the encapsulation of different types of QDs into polymer particles and the posterior modification of the polymer

particles to make them compatible with biological systems. The recognition of the polymer particle by an analyte, and the already known fluorescence spectra corresponding to each polymer particle modification allows the identification of the analyte (Figure 1.12). A good stability of the hybrid polymer-QDs particles as well as a good dispersibility of the QDs into them is important in order to get good results.

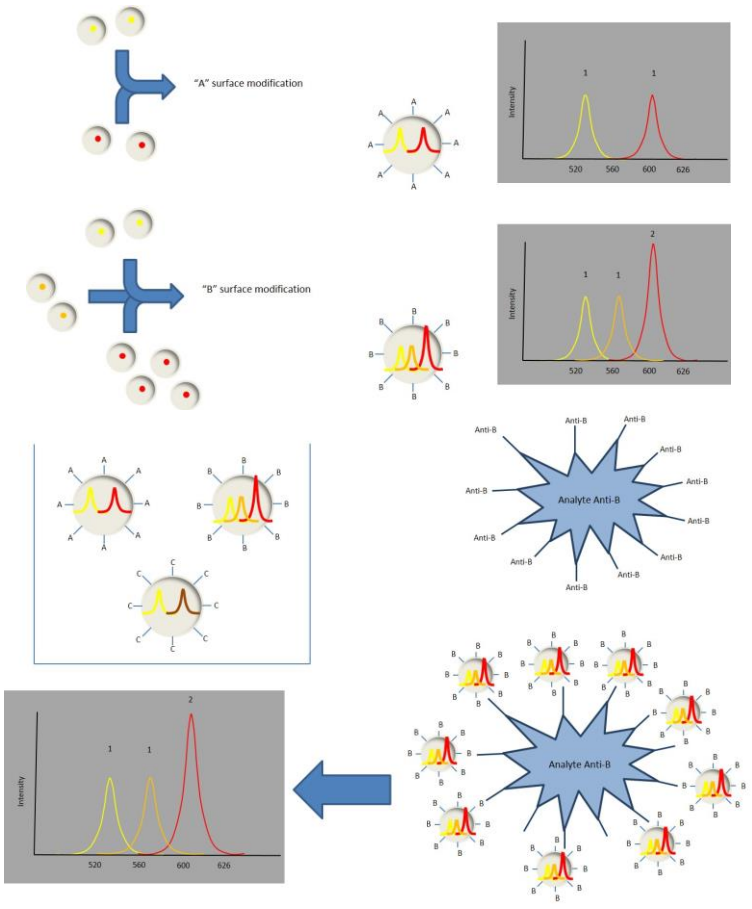

Figure 1.12 Scheme of a multiplexing assay.

1.3.2. Optoelectronics

The use of quantum dots in optoelectronic applications is another field that has been investigated in the last years. Combination of the nanocrystals with polymers in order to avoid aggregation and to keep their electronic and optical properties is also necessary in this case. However, an additional requirement is needed, the polymer used has to be able to conduct the charges generated by the nanocrystals through the material.

Solar cells transform solar energy in electronic current. For that, charges have to be efficiently transported to the electrodes. The rise of solar cell market has motivated the finding of a way for improving their efficiency exceeding the Shockley-Queissar[82] limit, which was calculated to be 31%, developing the third generation of solar cells. There are three ways described for the use of quantum dots in solar cells, metal-semiconductor or Schottkly junction, polymer-semiconductor junction and semiconductor sensitized solar cell or p-n junction[67,83] (Figure 1.13).

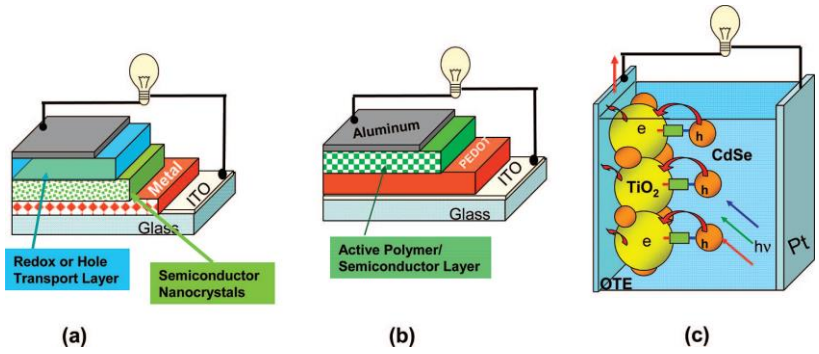

Figure 1.13 Types of solar cells using QDs in their structure (Image taken from reference [83]).

Metal-semiconductor junction is an electrical junction in which a semiconductor comes in contact with a metal undergoing Fermi level equilibration. Different cases of metal-semiconductor junctions using QDs have been investigated such as self-assembly with gold nanoparticles or infrared responsive photovoltaic devices. In the former case it has been observed that the union linker between the metal and the QD particles has an important effect in the charge transport[84–86]. In the latter case, most of the examples are based on the use of PbS derivatives quantum dots. A thin film of quantum dots is put on a treated indium tin oxide (ITO) substrate obtaining high efficiency devices[69,87,88].

Polymer-QDs or organic solar cells are another option in the synthesis of efficient solar cells[89,90]. Depending on the polymer used for such devices, different properties of the QDs are required, working as photosensitizer or as electron acceptor. When incorporating a small amount of QDs into a carrier-transporting polymer, such as poly(N-vinylcarbazole) (PVK), the matrix was sensitized, observing an enhancement of the photoinduced charge generation efficiency and an extension of the sensitivity range compared to the synthesis of blends[91,92]. On the other hand, semiconductor polymers have also been used (poly(3-hexylthiophene) (P3HT), phenyl-C61-butyric acid methyl ester (PCBM) or poly(p-phenylene vinylene) (PPV)) taking advantage of the electron acceptor properties of QDs as well as their high electron conductivity. The holes generated in the QDs are injected in the polymer, whereas the electrons remain in the nanocrystal. Incorporation of the QDs in the polymer matrix, blends of conjugated polymers and QDs[93–95], and grafting of polymers with QDs[96] are techniques studied for the improvement of efficiencies.

The last type of third generation solar cells is p-n junction systems. Those are based on the wide absorbance wavelength range of QDs using them as light harvesters for then transferring the electrons to TiO_2 nanoparticles that take part on the electrode[67,68,83], making this way a simpler device compared to the previous ones. Kamat[83] studied deeply the QDs/TiO_2 system, describing how fluorescence bleaching appears and depends on the QDs particle size when combining these two nanoparticles. This fact confirms the electron transfer from the QDs to TiO_2 nanoparticles.

Light emitting devices are based on the same principle as solar cells, quantum dots combined with functional polymers. The polymer is normally used as hole or electron transporting material to the QDs, while QDs absorb light in a wide range of wavelengths or emit at a specific wavelength depending on the size. QD-LEDs can be fabricated in different ways, incorporation of the QDs in the as-synthesized polymer, dispersion of the QDs in a polymer matrix, deposition of the QDs dispersion as films on the electrodes or polymerization of the matrix in the presence of the QDs[20,64–66,97,98,22,25].

1.3.3. Gas sensing applications

Apart from the most known applications for colloidal quantum dots such as biological labelling, biological assays and optoelectronic devices, quantum dots have also been used as gas sensors. Quantum dots can be combined with certain polymers in order to detect electrical conductivity changes in the presence of volatile organic compounds (VOCs)[99]. In this work, Tatavarty et al. dispersed TOPO and octadecylamine coated CdSe/ZnS quantum dots in

chloroform and mixed them with a solution of polystyrene and polystyrene-co maleic anhydride in N,N-dimethylformamide (DMF). Then, the mixture was vortexed and sonicated for producing nanofibers by electrospinning. Fluorescent and electrically conductive nanofibers were obtained. The detection of VOCs was carried out by exposing the nanofibers to tetrahydrofuran (THF), chloroform and DMF. For the three solvent vapors an increase in the electrical conductivity of the nanofibers was observed when increasing the concentration of vapor, concluding that the QD-PS-PSMA nanofibers could be used in gas sensing applications.

1.3.4. Catalysis

Quantum dots have also been used as photosensitizers in photocatalysis for water treatment, as well as for carbon dioxide reduction. In the case of water splitting, for example, QDs when excited are able to transfer a hole to a water oxidation catalysts or an electron to proton reduction catalyst, driving the water splitting reaction or synthesis of molecular hydrogen[100,101].

Recently, the use of QDs as carbon-carbon bond forming photocatalyst has been reported[102]. This has been done using a single size CdSe quantum dot as photoassisted redox catalysts that can replace several conventional photoredox catalysts.

1.4. Main objectives

As discussed in this introduction, quantum dots exhibit exceptional optical and electronic properties that are of great interest in different fields for several applications. Their size tunability, specific emission peak, absorbance at a very wide wavelength range, emission stability and brightness, leads to an improvement in imaging resolution, more reliable fluorescence assays (multiplexing) and an improvement in electronic transport. However, they are very sensitive nanoparticles and can easily loss their properties if their surface is not well protected. Electron loss through the defects of their surface is a major drawback in the use of quantum dots. Their difficult manipulation due to their small size and their composition, mainly heavy metals, are also key factors that have to be overcome.

In order to profit from the advantages that quantum dots provide, but taking into account their drawbacks, the first objective of this work was to efficiently encapsulate the quantum dot nanocrystals into polymer particles maintaining their optical properties during storage. Then, with the multiplexing application in mind, the combination of four different sizes of octadecylamine coated CdSe/ZnS quantum dots was studied. The synthesis of multifunctional polymer particles using quantum dots was also on the scope of this thesis. Thus, the combination of quantum dots with other inorganic nanoparticles, specifically with cerium oxide, was investigated. Finally, we explored potential applications for the waterborne hybrid dispersions with encapsulated QDs.

1.5. Outline

This thesis manuscript is divided in six chapters. **Chapter 1** is a general introduction about the synthesis, structure, encapsulation and applications of quantum dots.

In **Chapter 2** a complete description of the process of encapsulation of octadecylamine coated CdSe/ZnS quantum dots in polymer particles is shown. A two-step polymerization process is optimized to obtain hybrid polymer-QDs particles. In the first step, miniemulsion polymerization is the chosen technique for the synthesis of polystyrene and polystyrene-divinyl benzene hybrid polymer-QDs particles. The second step is a seeded semi-batch emulsion polymerization of MMA or MMA/DVB using as seed the polymer particles of the first step. Core-shell and cross-linked core-shell hybrid particles were synthesized. The morphology of the hybrid particles was studied by TEM and fluorescence was measured during storage.

In **Chapter 3** the encapsulation of quantum dots of different sizes into cross-linked core-shell PS/PMMA polymer particles is shown. First the synthesis of different QDs sizes is carried out in supercritical fluids. Then, the effect of the co-encapsulation of different QDs in the same polymer particle is studied by fluorescence. Additionally, a complete control of the fluorescence emission intensity of each type of quantum dot is achieved both in dispersion and blending latexes containing the different types of QDs.

The synthesis of multifunctional latexes and films by co-encapsulation of quantum dots with cerium oxide is addressed in **Chapter 4**. The effect of the incorporation of CeO_2 in the system on the optical properties of quantum dots is deeply analyzed by fluorescence emission

measurements during storage in the dark and at daylight. An enhancement of the fluorescence emission intensity both in the latexes and in the films during time is observed when co-encapsulating both nanoparticles and stored the material at daylight.

One potential applications of the hybrid waterborne dispersions containing QD nanoparticles synthesized is explained in **Chapter 5**. Nanofibres are produced by electrospinning out of hybrid polymer/quantum dots latexes and studied as optical and electrical gas sensors.

The most relevant conclusions on this Thesis are presented in **Chapter 6**.

Appendix I shows in more detail the experimental procedure and the techniques used during this work. Additionally, **Appendix II** shows additional experiments carried out during this PhD thesis.

1.6. References

(1) A.A.Onushchenko, a. I. E. Quantum Size Effect in Three-Dimensional Micorscopic Semiconductor Crystals. *Jetp Lett.* **1981**, *34* (6), 345–349.

(2) Rossetti, R.; Nakahara, S.; Brus, L. E. Quantum Size Effects in the Redox Potentials, Resonance Raman Spectra, and Electronic Spectra of CdS Crystallites in Aqueous Solution. *J. Chem. Phys.* **1983**, *79* (2), 1086–1087.

(3) Brus, L. E. Electron–electron and Electron-Hole Interactions in Small Semiconductor Crystallites: The Size Dependence of the Lowest Excited Electronic State. *J. Chem. Phys.* **1984**, *80* (9), 4403.

(4) Bawendi, M. G.; Steigerwald, M. L.; Brus, L. E. The Quantum Mechanics Of Larger Semiconductor Clusters. *Annu. Rev. Phys. Chem.* **1990**, *41* (4), 477–496.

(5) Brus, L.; Laboratories, T. B.; Hill, M. Quantum Crystallites and Nonlinear Optics. *Appl. Phys. A* **1991**, *74* (53), 465–474.

(6) Efros, A. L. R. M. The Electronic Structure of Semiconductor Nanocrystals. *Annu. Rev. Mater. Sci.* **2010**, *30*, 475–521.

(7) Kasfner, M. A. Artificial Atoms. *Phys. Today* **1993**, *46* (1), 24–31.

(8) Ashoori, R. C. Electrons in Artificial Atoms. *Nature* **1996**, *379* (6564), 413–419.

(9) Rajeshwar, K.; de Tacconi, N. R.; Chenthamarakshan, C. R. Semiconductor-Based Composite Materials: Preparation, Properties, and Performance. *Chem. Mater.* **2001**, *13* (9), 2765–2782.

(10) Trindade, T.; O'Brien, P.; Pickett, N. L. Nanocrystalline Semiconductors: Synthesis, Properties, and Perspectives. *Chem. Mater.* **2001**, *13* (11), 3843–3858.

(11) Chakrabarty, A.; Marre, S.; Landis, R. F.; Rotello, V. M.; Maitra, U.; Guerzo, A. Del; Aymonier, C. Continuous Synthesis of High Quality CdSe Quantum Dots in Supercritical Fluids. *J. Mater. Chem. C* **2015**, *3* (29), 7561–7566.

(12) Murray, C. B.; Norris, D.; Bawendi, M. G. Synthesis and Characterization of Nearly Monodisperse CdE (E= S, Se, Te) Semiconductor Nanocrystallites. *J. Am. Chem. Soc.* **1993**, *115* (4), 8706–8715.

(13) Hines, M. A.; Guyot-Sionnest, P. Synthesis and Characterization of Strongly Luminescing ZnS-Capped CdSe Nanocrystals. *J. Phys. Chem.* **1996**, *100* (2), 468–471.

(14) Alivisatos, A. P. Semiconductor Clusters, Nanocrystals, and Quantum Dots. *Science (80-.).* **1996**, *271* (5251), 933–937.

(15) Dabbousi, B. O.; Rodriguez-Viejo, J.; Mikulec, F. V.; Heine, J. R.; Mattoussi, H.; Ober, R.; Jensen, K. F.; Bawendi, M. G. (CdSe)ZnS Core−Shell Quantum Dots: Synthesis and Characterization of a Size Series of Highly Luminescent Nanocrystallites. *J. Phys. Chem. B* **1997**, *101* (46), 9463–9475.

(16) Reiss, P.; Protière, M.; Li, L. Core/Shell Semiconductor Nanocrystals. *Small* **2009**, *5* (2), 154–168.

(17) Marre, S.; Park, J.; Rempel, J.; Guan, J.; Bawendi, M. G.; Jensen, K. F. Supercritical Continuous-Microflow Synthesis of Narrow Size Distribution Quantum Dots. *Adv. Mater.* **2008**, *20* (24), 4830–4834.

(18) Balet, L. P.; Ivanov, S. A.; Piryatinski, A.; Achermann, M.; Klimov, V. I. Inverted Core/shell Nanocrystals Continuously Tunable between Type-I and Type-II Localization Regimes. *Nano Lett.* **2004**, *4* (8), 1485–1488.

(19) Kim, S.; Fisher, B.; Eisler, H. J.; Bawendi, M. Type-II Quantum Dots: CdTe/CdSe(core/shell) and CdSe/ZnTe(core/shell) Heterostructures. *J. Am. Chem. Soc.* **2003**, *125* (38), 11466–11467.

(20) Anc, M. J.; Pickett, N. L.; Gresty, N. C.; Harris, J. a.; Mishra, K. C. Progress in Non-Cd Quantum Dot Development for Lighting Applications. *ECS J. Solid State Sci. Technol.* **2012**, *2* (2), R3071–R3082.

(21) Ryu, E.; Kim, S.; Jang, E.; Jun, S.; Jang, H.; Kim, B.; Kim, S.-W. Step-Wise Synthesis of InP/ZnS Core−Shell Quantum Dots and the Role of Zinc Acetate. *Chem. Mater.* **2009**, *21* (4), 573–575.

(22) Kim, S.; Kim, T.; Kang, M.; Kwak, S. K.; Yoo, T. W.; Park, L. S.; Yang, I.; Hwang, S.; Lee, J. E.; Kim, S. K.; et al. Highly Luminescent InP/GaP/ZnS Nanocrystals and Their Application to White Light-Emitting Diodes. *J. Am. Chem. Soc.* **2012**, *134* (8), 3804–3809.

(23) Song, W. S.; Lee, H. S.; Lee, J. C.; Jang, D. S.; Choi, Y.; Choi, M.; Yang, H. Amine-Derived Synthetic Approach to Color-Tunable InP/ZnS Quantum Dots with High

Fluorescent Qualities. *J. Nanoparticle Res.* **2013**, *15* (6).

(24) Tessier, M. D.; Dupont, D.; De Nolf, K.; De Roo, J.; Hens, Z. Economic and Size-Tunable Synthesis of InP/ZnE (E = S,Se) Colloidal Quantum Dots. *Chem. Mater.* **2015**, *3*, 150611083950009.

(25) Yang, S. J.; Oh, J. H.; Kim, S.; Yang, H.; Do, Y. R. A. Realization of InP/ZnS Quantum Dots for Green, Amber and Red down-Converted LED and Their Color-Tunable, Four-Package White LEDs. *J. Mater. Chem. C* **2015**, *3*, 3582–3591.

(26) Altintas, Y.; Talpur, M. Y.; ??nl??, M.; Mutlug??n, E. Highly Efficient Cd-Free Alloyed Core/Shell Quantum Dots with Optimized Precursor Concentrations. *J. Phys. Chem. C* **2016**, *120* (14), 7885–7892.

(27) Li, L.; Reiss, P. One-Pot Synthesis of Highly Luminescent InP/ZnS Nanocrystals without Precursor Injection. *J. Am. Chem. Soc.* **2008**, *130* (35), 11588–11589.

(28) Giroire, B.; Marre, S.; Garcia, A.; Cardinal, T.; Aymonier, C. Continuous Supercritical Route for Quantum-Confined GaN Nanoparticles. *React. Chem. Eng.* **2016**, *1* (2), 151–155.

(29) Tomczak, N.; Jańczewski, D.; Han, M.; Vancso, G. J. Designer Polymer-Quantum Dot Architectures. *Prog. Polym. Sci.* **2009**, *34* (5), 393–430.

(30) Tomczak, N.; Liu, R.; Vancso, J. G. Polymer-Coated Quantum Dots. *Nanoscale* **2013**, *5* (24), 12018–12032.

(31) Hezinger, A. F. E.; Teßmar, J.; Göpferich, A. Polymer Coating of Quantum Dots - A Powerful Tool toward Diagnostics and Sensorics. *Eur. J. Pharm. Biopharm.* **2008**, *68* (1), 138–152.

(32) Wang, X.-S.; Dykstra, T. E.; Salvador, M. R.; Manners, I.; Scholes, G. D.; Winnik, M. A. Surface Passivation of Luminescent Colloidal Quantum Dots with Poly(dimethylaminoethyl Methacrylate) through a Ligand Exchange Process. *J. Am. Chem. Soc.* **2004**, *126* (25), 7784–7785.

(33) Querner, C.; Benedetto, A.; Demadrille, R.; Rannou, P.; Reiss, P. Carbodithioate-Containing Oligo- and Polythiophenes for Nanocrystals' Surface Functionalization. *Chem. Mater.* **2006**, *18* (20), 4817–4826.

(34) Skaff, H.; Emrick, T. The Use of 4-Substituted Pyridines to Afford Amphiphilic, Pegylated Cadmium Selenide Nanoparticles. *Chem. Commun.* **2003**, No. 1, 52–53.

(35) Skaff, H.; Ilker, M. F.; Coughlin, E. B.; Emrick, T. Preparation of Cadmium Selenide−Polyolefin Composites from Functional Phosphine Oxides and Ruthenium-Based Metathesis. *J. Am. Chem. Soc.* **2002**, *124* (20), 5729–5733.

(36) Lemon, B. I.; Crooks, R. M. Preparation and Characterization of Dendrimer-Encapsulated CdS Semiconductor Quantum Dots [12]. *J. Am. Chem. Soc.* **2000**, *122* (51), 12886–12887.

(37) Donners, J. J. J. M.; Hoogenboom, R.; Schenning, A. P. H. J.; Van Hal, P. A.; Nolte, R. J. M.; Meijer, E. W.; Sommerdijk, N. A. J. M. Fabrication of Organic-Inorganic Semiconductor Composites Utilizing the Different Aggregation States of a Single Amphiphilic Dendrimer. *Langmuir* **2002**, *18* (7), 2571–2576.

(38) Dubertret, B. In Vivo Imaging of Quantum Dots Encapsulated in Phospholipid Micelles. *Science (80-.).* **2002**, *298* (5599), 1759–1762.

(39) Gao, X.; Yang, L.; Petros, J. A.; Marshall, F. F.; Simons, J. W.; Nie, S. In Vivo Molecular and Cellular Imaging with Quantum Dots. *Curr. Opin. Biotechnol.* **2005**, *16* (1), 63–72.

(40) Yu, W. W.; Chang, E.; Falkner, J. C.; Zhang, J.; Al-Somali, A. M.; Sayes, C. M.; Johns, J.; Drezek, R.; Colvin, V. L. Forming Biocompatible and Nonaggregated Nanocrystals in Water Using Amphiphilic Polymers. *J. Am. Chem. Soc.* **2007**, *129* (10), 2871–2879.

(41) Chen, J.; Imam, P. Causes of Asset Shortages in Emerging Markets. *Rev. Dev. Financ.* **2013**, *3* (1), 22–40.

(42) Chan, W. C. W.; Nie, S. Quantum Dot Bioconjugates for Ultrasensitive Nonisotopic Detection. *Science (80-.).* **1998**, *281* (5385), 2016–2018.

(43) Leatherdale, C. a; Woo, W. K.; Mikulec, F. V; Bawendi, M. G. On the Absorption Cross Section of CdSe Nanocrystal Quantum Dots. *J. Phys. Chem. B* **2002**, *106*, 7619–7622.

(44) Bradley, M.; Bruno, N.; Vincent, B. Distribution of CdSe Quantum Dots within Swollen Polystyrene Microgel Particles Using Confocal Microscopy. *Langmuir* **2005**, *21* (7), 2750–2753.

(45) Han, M.; Gao, X.; Su, J. Z.; Nie, S. Quantum-Dot-Tagged Microbeads for Multiplexed Optical Coding of Biomolecules. *Nat. Biotechnol.* **2001**, *19* (7), 631–635.

(46) Li, M.; Zhang, H.; Zhang, J.; Wang, C.; Han, K.; Yang, B. Easy Preparation and Characterization of Highly Fluorescent Polymer Composite Microspheres from

Aqueous CdTe Nanocrystals. *J. Colloid Interface Sci.* **2006**, *300* (2), 564–568.

(47) Kuang, M.; Wang, D.; Bao, H.; Gao, M.; Möhwald, H.; Jiang, M. Fabrication of Multicolor-Encoded Microspheres by Tagging Semiconductor Nanocrystals to Hydrogel Spheres. *Adv. Mater.* **2005**, *17* (2), 267–270.

(48) Zhang, J.; Xu, S.; Kumacheva, E. Polymer Microgels: Reactors for Semiconductor, Metal, and Magnetic Nanoparticles. *J. Am. Chem. Soc.* **2004**, *126* (25), 7908–7914.

(49) Das, M.; Zhang, H.; Kumacheva, E. Microgels: Old Materials with New Applications. *Annu. Rev. Mater. Res.* **2006**, *36* (1), 117–142.

(50) O'Brien, P.; Cummins, S. S.; Darcy, D.; Dearden, A.; Masala, O.; Pickett, N. L.; Ryley, S.; Sutherland, A. J. Quantum Dot-Labelled Polymer Beads by Suspension Polymerisation. *Chem. Commun. (Camb).* **2003**, No. 1, 2532–2533.

(51) Sheng, W.; Kim, S.; Lee, J.; Kim, S.-W.; Jensen, K.; Bawendi, M. G. In-Situ Encapsulation of Quantum Dots into Polymer Microspheres. *Langmuir* **2006**, *22* (8), 3782–3790.

(52) Yang, X.; Zhang, Y. Encapsulation of Quantum Nanodots in Polystyrene and Silica Micro-/nanoparticles. *Langmuir* **2004**, *20* (14), 6071–6073.

(53) Sherman, R. L.; Ford, W. T. Semiconductor Nanoparticle / Polystyrene Latex Composite Materials. *Langmuir* **2005**, *21* (18), 5218–5222.

(54) Lee, B. H.; Kwon, K.-W.; Shim, M. Semiconductor Polymer Hybrid Colloidal Nanoparticles. *J. Mater. Chem.* **2007**, *17* (13), 1284–1291.

(55) Ugelstad, J. Emulsion Polymerization: Initiation of Polymerization in Monomer Droplets. *J. Polym.* **1973**, *11*, 503–513.

(56) Asua, J. M. Miniemulsion Polymerization. *Prog. Polym. Sci.* **2002**, *27* (7), 1283–1346.

(57) Asua, J. M. Mapping the Morphology of Polymer-Inorganic Nanocomposites Synthesized by Miniemulsion Polymerization. *Macromol. Chem. Phys.* **2014**, *215* (5), 458–464.

(58) Fleischhaker, F.; Zentel, R. Photonic Crystals from Core-Shell Colloids with Incorporated Highly Fluorescent Quantum Dots. *Chem. Mater.* **2005**, *17* (6), 1346–1351.

(59) Esteves, A. C.; Barros-Timmons, A.; Monteiro, T.; Trindade, T. Polymer Encapsulation of CdE (E = S, Se) Quantum Dot Ensembles via in-Situ Radical Polymerization in Miniemulsion. *J. Nanosci .Nanotechnol* **2005**, *5* (5), 766–771.

(60) Esteves, A. C. C. AGET ATRP in Miniemulsion from Functionalized CdS QD's Surface. *Polym. Prepr.* **2005**, *46* (2), 134.

(61) Esteves, A. C. C.; Bombalski, L.; Trindade, T.; Matyjaszewski, K.; Barros-Timmons, A. Polymer Grafting from CdS Quantum Dots via AGET ATRP in Miniemulsion. *Small* **2007**, *3* (7), 1230–1236.

(62) Joumaa, N.; Lansalot, M.; Théretz, A.; Elaissari, A.; Sukhanova, A.; Artemyev, M.; Nabiev, I.; Cohen, J. H. M. Synthesis of Quantum Dot-Tagged Submicrometer Polystyrene Particles by Miniemulsion Polymerization. *Langmuir* **2006**, *22* (4), 1810–1816.

(63) Harun, N. A.; Horrocks, B. R.; Fulton, D. a. A Miniemulsion Polymerization Technique for Encapsulation of Silicon Quantum Dots in Polymer Nanoparticles. *Nanoscale* **2011**, *3* (11), 4733–4741.

(64) Zhao, J.; Bardecker, J. A.; Munro, A. M.; Liu, M. S.; Niu, Y.; Ding, I.-K.; Luo, J.; Chen, B.; Jen, A. K.-Y.; Ginger, D. S. Efficient CdSe/CdS Quantum Dot Light-Emitting Diodes Using a Thermally Polymerized Hole Transport Layer. *Nano Lett.* **2006**, *6* (3), 463–467.

(65) Sun, Q.; Wang, Y. A.; Li, L. S.; Wang, D. Y.; Zhu, T.; Xu, J.; Yang, C. H.; Li, Y. F. Bright, Multicoloured Light-Emitting Diodes Based on Quantum Dots. *Nat. Photonics* **2007**, *1* (12), 717–722.

(66) Caruge, J. M.; Halpert, J. E.; Wood, V.; Bulović, V.; Bawendi, M. G.; Caruge, J. M.; Halpert, J. E.; Wood, V.; Bulovic, V. Colloidal Quantum-Dot Light-Emitting Diodes with Metal-Oxide Charge Transport Layers. *Nat. Photonics* **2008**, *2* (4), 247–250.

(67) Nozik, A. . Quantum Dot Solar Cells. *Phys. E Low-dimensional Syst. Nanostructures* **2002**, *14* (1–2), 115–120.

(68) Huynh, W. U. Hybrid Nanorod-Polymer Solar Cells. *Science (80-.).* **2002**, *295* (5564), 2425–2427.

(69) Nam, M.; Kim, S.; Kim, S.; Kim, S.-W.; Lee, K. Efficient Hybrid Solar Cells Using PbS(x)Se(1-X) Quantum Dots and Nanorods for Broad-Range Photon Absorption and Well-Assembled Charge Transfer Networks. *Nanoscale* **2013**, *5* (17), 8202–8209.

(70) Bruchez Jr., M.; Moronne, M.; Gin, P.; Weiss, S.; Alivisatos, A. P. Semiconductor Nanocrystals as Fluorescent Biological Labels. *Science (80-.).* **1998**, *281* (5385), 2013–2016.

(71) Jin, S.; Hu, Y.; Gu, Z.; Liu, L.; Wu, H.-C. Application of Quantum Dots in Biological Imaging. *J. Nanomater.* **2011**, *2011*, 1–13.

(72) Medintz, I. L.; Uyeda, H. T.; Goldman, E. R.; Mattoussi, H. Quantum Dot Bioconjugates for Imaging, Labelling and Sensing. *Nat. Mater.* **2005**, *4* (6), 435–446.

(73) Rosenthal, S. J.; Chang, J. C.; Kovtun, O.; McBride, J. R.; Tomlinson, I. D. Biocompatible Quantum Dots for Biological Applications. *Chem. Biol.* **2011**, *18* (1), 10–24.

(74) Kairdolf, B. A.; Smith, A. M.; Stokes, T. H.; Wang, M. D.; Young, A. N.; Nie, S. Semiconductor Quantum Dots for Bioimaging and Biodiagnostic Applications. *Annu. Rev. Anal. Chem.* **2013**, *6* (1), 143–162.

(75) Alivisatos, P. The Use of Nanocrystals in Biological Detection. *Nat. Biotechnol.* **2004**, *22* (1), 47–52.

(76) Gao, X.; Cui, Y.; Levenson, R. M.; Chung, L. W. K.; Nie, S. In Vivo Cancer Targeting and Imaging with Semiconductor Quantum Dots. *Nat. Biotechnol.* **2004**, *22* (8), 969–976.

(77) Bentzen, E. L.; Tomlinson, I. D.; Mason, J.; Gresch, P.; Warnement, M. R.; Wright, D.; Sanders-Bush, E.; Blakely, R.; Rosenthal, S. J. Surface Modification to Reduce Nonspecific Binding of Quantum Dots in Live Cell Assays. *Bioconjug. Chem.* **2005**, *16* (6), 1488–1494.

(78) Fu, A.; Gu, W.; Larabell, C.; Alivisatos, A. P. Semiconductor Nanocrystals for Biological Imaging. *Curr. Opin. Neurobiol.* **2005**, *15* (5), 568–575.

(79) Choi, H. S.; Liu, W.; Misra, P.; Tanaka, E.; Zimmer, J. P.; Ipe, B. I.; Bawendi, M. G.; Frangioni, J. V. Renal Clearance of Quantum Dots. *Nat. Biotechnol.* **2007**, *25* (10), 1165–1170.

(80) Wegner, K. D.; Hildebrandt, N. Quantum Dots: Bright and Versatile in Vitro and in Vivo Fluorescence Imaging Biosensors. *Chem. Soc. Rev.* **2015**, *44* (14), 4792–4834.

(81) Chan, W. C. W.; Maxwell, D. J.; Gao, X.; Bailey, R. E.; Han, M.; Nie, S. Luminescent Quantum Dots for Multiplexed Biological Detection and Imaging. *Curr. Opin.*

Biotechnol. **2002**, *13* (1), 40–46.

(82) Shockley, W.; Queisser, H. J. Detailed Balance Limit of Efficiency of P-N Junction Solar Cells. *J. Appl. Phys* **1961**, *32* (3), 510–519.

(83) Kamat, P. V. Quantum Dot Solar Cells. Semiconductor Nanocrystals as Light Harvesters. *J. Phys. Chem. C* **2008**, *112* (48), 18737–18753.

(84) Nakanishi, T.; Ohtani, B.; Uosaki, K. Fabrication and Characterization of CdS-Nanoparticle Mono- and Multilayers on a Self-Assembled Monolayer of Alkanedithiols on Gold. *J. Phys. Chem. B* **1998**, *102* (97), 1571–1577.

(85) Hens, Z.; Tallapin, D. V.; Weller, H.; Vanmaekelbergh, D. Breaking and Restoring a Molecularly Bridged Metal/quantum Dot Junction. *Appl. Phys. Lett.* **2002**, *81* (22), 4245–4247.

(86) Granot, E.; Patolsky, F.; Willner, I. Electrochemical Assembly of a CdS Semiconductor Nanoparticle Monolayer on Surfaces : Structural Properties and Photoelectrochemical Applications. *Power* **2004**, *250*, 5875–5881.

(87) Clifford, J. P.; Johnston, K. W.; Levina, L.; Sargent, E. H. Schottky Barriers to Colloidal Quantum Dot Films. *Appl. Phys. Lett.* **2007**, *91* (25).

(88) Johnston, K. W.; Pattantyus-Abraham, A. G.; Clifford, J. P.; Myrskog, S. H.; MacNeil, D. D.; Levina, L.; Sargent, E. H. Schottky-Quantum Dot Photovoltaics for Efficient Infrared Power Conversion. *Appl. Phys. Lett.* **2008**, *92* (15), 90–93.

(89) Günes, S.; Sariciftci, N. S. Hybrid Solar Cells. *Inorganica Chim. Acta* **2008**, *361* (3), 581–588.

(90) Saunders, B. R.; Turner, M. L. Nanoparticle-Polymer Photovoltaic Cells. *Adv. Colloid Interface Sci.* **2008**, *138* (1), 1–23.

(91) Wang, Y. Semiconductor Nanocrystals in Carrier-Transporting Polymers. Charge Generation and Charge Transport. *J. Lumin* **1996**, *70*, 48–59.

(92) Yang, C. L.; Wang, J. N.; Ge, W. K.; Wang, S. H.; Cheng, J. X.; Li, X. Y.; Yan, Y. J.; Yang, S. H. Significant Enhancement of Photoconductivity in Truly Two-Component and Chemically Hybridized CdS-poly(N-Vinylcarbazole) Nanocomposites. *Appl. Phys. Lett.* **2001**, *78* (6), 760–762.

(93) Han, L.; Donghuan, Q.; Jiang, X.; Liu, Y.; Wang, L.; Chen, J.; Cao, Y. Synthesis of High Quality Zinc-Blende CdSe Nanocrystals and Their Application in Hybrid Solar Cells. *Nanotechnology* **2006**, *17* (18), 4736–4742.

(94) Park, E.-K.; Kim, J.-H. J.-H.; Ji, I. A.; Choi, H. M.; Kim, J.-H. J.-H.; Lim, K.-T.; Bang, J. H.; Kim, Y.-S. Optimization of CdSe Quantum Dot Concentration in P3HT:PCBM Layer for the Improved Performance of Hybrid Solar Cells. *Microelectron. Eng.* **2014**, *119*, 169–173.

(95) Yin, J.; Kumar, M.; Lei, Q.; Ma, L.; Raavi, S. S. K.; Gurzadyan, G. G.; Soci, C. Small-Size Effects on Electron Transfer in P3HT/InP Quantum Dots. *J. Phys. Chem. C* **2015**, *119* (47), 26783–26792.

(96) Ren, S.; Chang, L.-Y.; Lim, S.-K.; Zhao, J.; Smith, M.; Zhao, N.; Bulović, V.; Bawendi, M.; Gradecak, S. Inorganic-Organic Hybrid Solar Cell: Bridging Quantum Dots to Conjugated Polymer Nanowires. *Nano Lett.* **2011**, *11* (9), 3998–4002.

(97) Xuan, Y.; Pan, D.; Zhao, N.; Ji, X.; Ma, D. White Electroluminescence from a poly(N-Vinylcarbazole) Layer Doped with CdSe/CdS Core–shell Quantum Dots. *Nanotechnology* **2006**, *17* (19), 4966–4969.

(98) Liu, J.; Xie, C.; Zhang, Y.; Hu, W.; Pickering, S.; You, G.; Wang, A. Y.; Xu, J. Degradation Studies of Colloidal Quantum Dot Light-Emitting Diodes. *MRS Proc.* **2011**, *1286*.

(99) Tatavarty, R.; Hwang, E. T.; Park, J. W.; Kwak, J. H.; Lee, J. O.; Gu, M. B. Conductive Quantum Dot-Encapsulated Electrospun Nanofibers from Polystyrene and Polystyrene-Co-Maleic Anhydride Copolymer Blend as Gas Sensors. *React. Funct. Polym.* **2011**, *71* (2), 104–108.

(100) Fernando, K. A. S.; Sahu, S.; Liu, Y.; Lewis, W. K.; Guliants, E. A.; Jafariyan, A.; Wang, P.; Bunker, C. E.; Sun, Y. P. Carbon Quantum Dots and Applications in Photocatalytic Energy Conversion. *ACS Appl. Mater. Interfaces* **2015**, *7* (16), 8363–8376.

(101) Rajabi, H. R. Photocatalytic Activity of Quantum Dots. In *Semiconductor Photocatalysis - Materials, Mechanisms and Applications*; Cao Mechanisms and Applications, W. B. T.-S. P.-M., Ed.; InTech, 2016; p Chapter 17.

(102) Caputo, J. A.; Frenette, L. C.; Zhao, N.; Sowers, K. L.; Krauss, T. D.; Weix, D. J. General and Efficient C-C Bond Forming Photoredox Catalysis With Semiconductor Quantum Dots. *J. Am. Chem. Soc.* **2017**, *139* (12), 4250–4253.

Chapter 2. Encapsulation of octadecylamine coated CdSe/ZnS quantum dots and assessment of their fluorescent properties

*****Part of this work has been published in Chemical Engineering Journal, 2017, 313, 261-269.

2.1. Introduction

As discussed in Chapter 1 many researchers have attempted the encapsulation of quantum dots into polymer particles[1–11] aiming at enhancing the compatibility of the nanocrystals in a given medium, to protect their surface, to protect the environment against their toxicity, and for an easier manipulation[12,13]. Nevertheless, a general approach has not been established yet. Likely the simplest and more general method to encapsulate QDs in hydrophobic submicron polymer particles is by means of miniemulsion polymerization; namely, by generating an aqueous dispersion of nanodroplets of a polymerizing monomer in which the surface coated QDs are compatible. The polymerization of the nanodroplet dispersion would then yield a dispersion of polymer nanoparticles that would contain quantum dots, provided that the QDs are also compatible with the polymer.

It is clear, not only that there is a need to encapsulate fluorescent QDs in submicron colloidal particles, but also to preserve the fluorescence of the colloidal particles during storage in order to have time to fabricate optical devices without jeopardizing the properties achieved after the synthesis of the hybrid colloidal particles. This Chapter reports the research carried out to obtain an efficient encapsulation and fixation of octadecylamine coated CdSe/ZnS QDs into colloidal polymer particles and the study of the stability of their fluorescent properties over time.

In this study, the synthesis of hybrid polystyrene/quantum dots polymer particles by batch miniemulsion polymerization was first considered. These hybrid polymer particles produced did not preserve the fluorescence and this was attributed to the location of the QDs

at the polymer particle/aqueous phase interface. In order to avoid the lack of stability of the fluorescence emission intensity, PS/PMMA core-shell and cross-linked PS-DVB/PMMA-DVB core-shell morphology hybrid particles were produced by seeded semi-batch emulsion polymerization. The cross-linked core-shell hybrid particles presented the best optical properties.

2.2. Experimental part

2.2.1. Characterization of octadecylamine coated CdSe/ZnS quantum dots

The main properties of octadecylamine coated CdSe/ZnS core-shell quantum dots (Ocean NanoTech) were characterized in toluene dispersions. In order to measure their particle size distribution (PSD) they were dispersed in toluene at a concentration of 0.03 wt%. The PSD was calculated by measuring 500 particles from TEM images. A representative TEM image is shown in Figure 2.1a, from which a number average particle size of 7 nm was determined (Figure 2.1b).

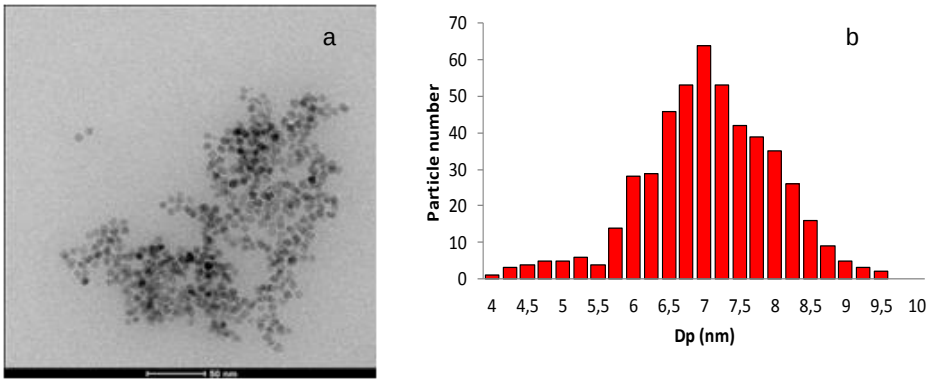

Figure 2.1 a) TEM image of octadecylamine coated CdSe/ZnS quantum dots dispersed in toluene (0.03 wt%) and b) Particle size distribution obtained after counting 500 particles in TEM images.

Dispersions of QDs in toluene at different concentrations were prepared to study the effect of the QDs load on the fluorescence emission intensity. Figure 2.2a shows that the fluorescence emission intensity strongly depends on the amount of quantum dots added; the higher the load of QDs, the higher the fluorescence emission intensity. As seen in Figure 2.2b, this increase tends to level off as the concentration of QDs increases.

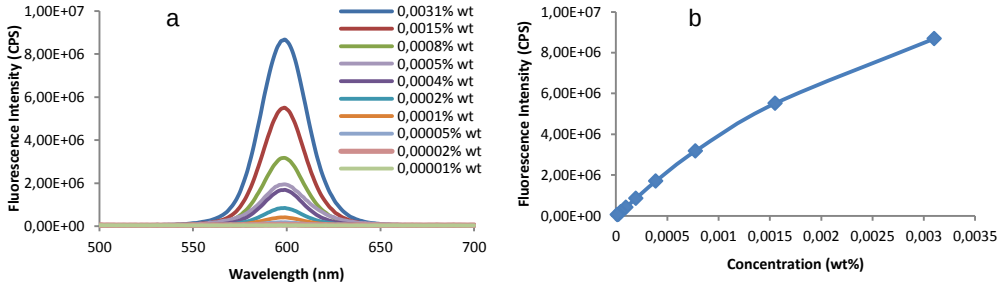

Figure 2.2 a) Fluorescence emission spectrum of QDs toluene dispersions at different concentrations. b) Intensity vs concentration plot for QDs dispersions in toluene.

In order to assess the dispersibility of quantum dots in monomer, styrene and methyl methacrylate were chosen as representative monomers.

When dispersing the QD nanoparticles in styrene (S) a completely transparent dispersion was obtained independently of the concentration of quantum dots, indicating a good compatibility between this monomer and the octadecylamine coated CdSe/ZnS quantum dots (Figure 2.3a and b). This dispersion was stable for several months at ambient temperature without losing any optical properties (Figure 2.3c) or evidencing any sedimentation of the quantum dots at the bottom of the vial. In contrast, if the quantum dots were dispersed in methyl methacrylate (MMA), a turbid dispersion was obtained, observing the sedimentation of the nanocrystals at the bottom of the vial 40 minutes after stopping the stirring (Figure 2.4). Therefore, the octadecylamine coated QDs used in this study were not compatible with MMA.

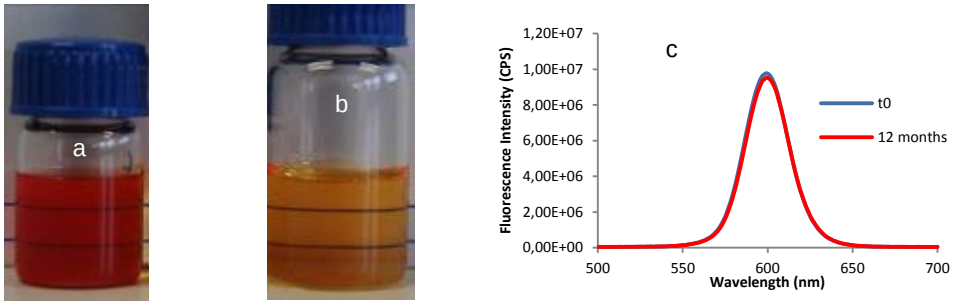

Figure 2.3 Dispersion of quantum dots in styrene at two different concentrations a) 0.81 wt% and b) 0.008 wt% and c) fluorescence emission intensity of a toluene dispersion of QDs over time.

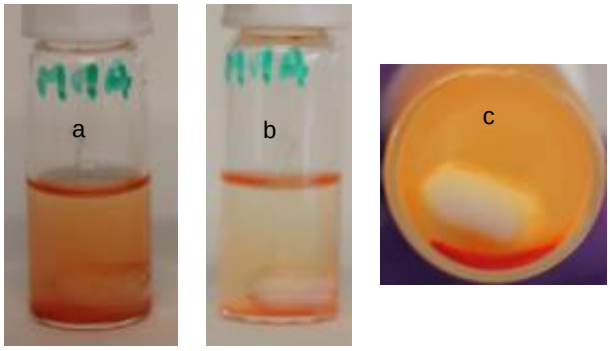

Figure 2.4 CdSe/ZnS quantum dots dispersed in methyl methacrylate 0.03 wt% a) Just after stirring, b) 40 minutes after stirring, c) bottom of the vial 40 minutes after stopping the stirring.

2.2.1.1. Study of the degradation of the quantum dots fluorescence

As water based miniemulsion polymerizations were carried out to encapsulate QD nanoparticles, the effect of water and free radicals on the fluorescence properties of QDs was studied. For this purpose, two different dispersions of QD nanoparticles in styrene were prepared by adding water to one of them and an aqueous solution of KPS to the other one. These dispersions were kept under vigorous magnetic agitation and the fluorescence emission was measured during time. A first measurement was done right after adding the aqueous solution, and then measurements were repeated after several days. The results are presented in Figure 2.5a for the QDs dispersion with water and Figure 2.7b for QDs dispersion with a KPS solution. In both cases fluorescence emission is lost upon mixing with pure water or a KPS aqueous solution. The fluorescence loss seems faster for the later. Therefore, in order to avoid

the degradation of QDs, there is a strong incentive for an efficient encapsulation of QDs into polymer particles.

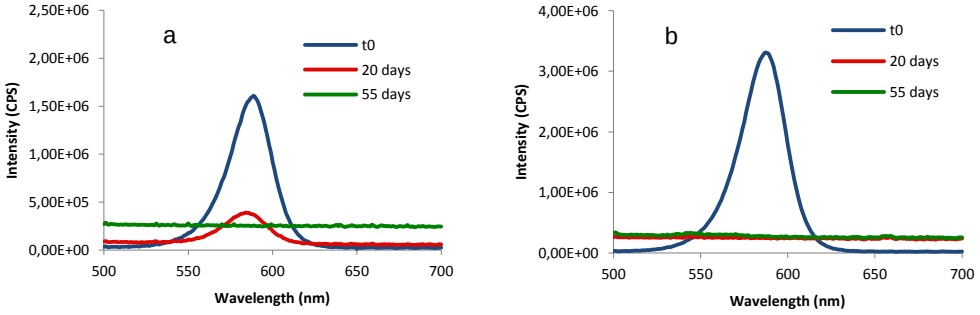

Figure 2.5 Fluorescence emission evolution for a dispersion of QDs in styrene a) in contact with water, b) in contact with an aqueous solution of KPS.

2.2.2. Synthesis of hybrid polystyrene/quantum dots and hybrid polystyrene-divinyl benzene/quantum dots latexes

Hybrid polystyrene-(DVB)/quantum dots latexes with 5% final solids content (S.C.) were synthesized by batch miniemulsion polymerization following the formulation presented in Table 2.1. On one hand, an organic phase was prepared by mixing the monomer (styrene, S), the co-stabilizer (hexadecane, HD), the cross-linker (divinyl benzene, DVB), in the case of cross-linked PS particles, and the octadecylamine coated quantum dots for 10 minutes. The aqueous phase was obtained by dissolving the emulsifier (SDS) and the buffer ($NaHCO_3$) in water. Then, both phases were mixed together for 20 minutes under vigorous stirring and the miniemulsion was obtained by sonicating for 4 minutes using a Hielscher sonicator (operating

at 80% amplitude and 100% cycle) in an ice bath under magnetic stirring. To stabilize the monomer droplets, an additional 1% weight based on monomer (wbm%) SDS was added to the so formed miniemulsion. This 5% S.C. miniemulsion was polymerized in batch in a 25 ml round bottom flask with a nitrogen inlet under magnetic stirring. When the desired temperature (75ºC) was reached, the initiator KPS (0.5 wbm%) was added to the miniemulsion in a shot. The polymerization was carried out for 6 hours.

Table 2.1 Formulation used to prepare 5% S.C. PS-(DVB)/QDs hybrid latexes.

	Component	wt%
Organic phase	Styrene	5
	Hexadecane*	4
	Divinyl benzene*	0-1
	CdSe/ZnS* (PS/QDs)	0-0.41
	CdSe/ZnS* (PS-DVB/QDs)	0-1.53
Aqueous phase	SDS*	2
	$NaHCO_3$*	1
	Deionized water	60
Post-addition	SDS*	1
	Deionized water	25
Initiator	KPS*	0.5
	Deionized water	10

*With respect to the monomer

2.2.2.1. Miniemulsion stability

To achieve an efficient droplet nucleation during miniemulsion polymerization the miniemulsion should be stable, at least, during the polymerization reaction time.

Two miniemulsions were prepared, a blank (S+HD) and a hybrid one (S+HD+QDs), and their stability was measured by using the Turbiscan equipment (see Appendix I for more information). Backscattering measurements were carried out during six hours at 60ºC to assess the stability of the as prepared miniemulsions. Figure 2.6 shows that the percentage of backscattered light (measured every 60 minutes) for both miniemulsions remained almost unchanged for six hours, which is an indication of a stable miniemulsion.

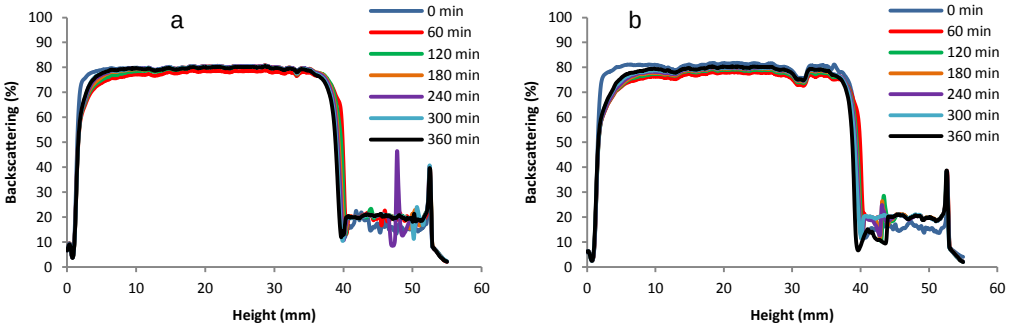

Figure 2.6 Backscattered light of a) blank miniemulsion and b) hybrid styrene-quantum dots (0.30 wbm%) miniemulsion.

2.2.3. Synthesis of hybrid core-shell latexes

Core-shell PS/QDs/PMMA and core-shell cross-linked PS-DVB/QDs/PMMA-DVB latexes were synthesized by seeded semi-batch emulsion polymerization. The polymer shell was produced on the previously synthesized core used as seed (PS/QDs or PS-DVB/QDs). The seed was placed into a round bottom flask with a nitrogen inlet. At the desired temperature (75ºC), the initiator (KPS 0.5 wbm %) was added in a shot and the monomer (MMA) or the monomer mixture (MMA+DVB) was fed into the reactor using a syringe pump at a feeding rate of 0.12 g/min (Figure 2.7). The amount of monomer needed to obtain a certain shell thickness was calculated from the size of the seed particles assuming absence of secondary nucleation (see Appendix I for detailed calculations). When the feeding was finished, the latex was kept at 75ºC for 3 hours. Table 2.2 presents a typical formulation used to produce a PS-DVB/QDs/PMMA-DVB composite hybrid latex of a shell thickness of 25 nm.

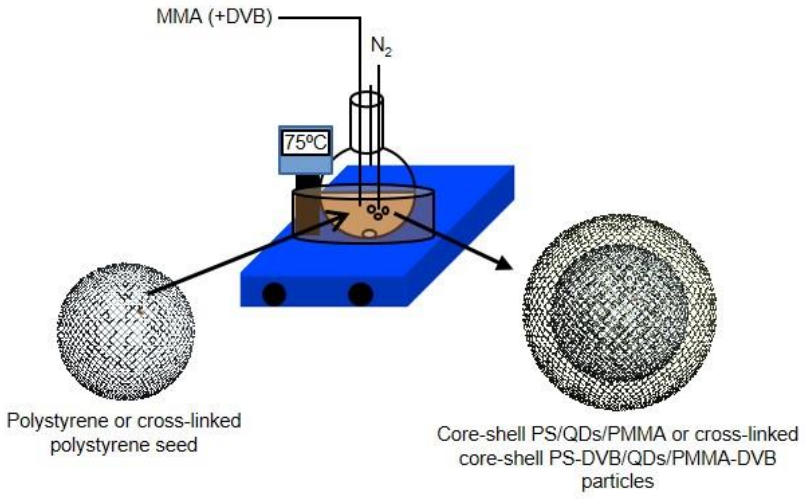

Figure 2.7 Schematic representation of seeded semi-batch emulsion polymerization of hybrid core-shell polymer particles.

Table 2.2. Formulation used to prepare a core-shell latex with a shell thickness of 25 nm.

	Component	wt%
Initial charge	Seed	57
	KPS	0.5*
	Water	34
Feed	MMA	9
	DVB	1*

*Weight based on MMA

2.3. Synthesis of hybrid core-shell polymer-quantum dots particles

2.3.1. Synthesis of hybrid polystyrene/quantum dots nanoparticles

Batch polymerizations with different concentrations of quantum dots were carried out following the procedure explained in section 2.2.2. Miniemulsion polymerization of styrene in the presence of quantum dots was carried out obtaining hybrid latexes at 5% S.C. In order to characterize the different latexes synthesized, final conversion, droplet size and final particle size were measured for each case and compared to each other. Also, the theoretical number of QDs per particle was calculated based on the amount of QDs added, the number average particle size of the QDs, the number average polymer particle size measured and the polymer and QDs density (see Appendix I for the detailed calculations). Table 2.3 summarizes the results in terms of the conversion, droplet size and final particle sizes achieved in the polymerization as well as the theoretical number of QD per particle for the experiments carried out with different concentrations of QDs. Neither the final conversion nor the final particle size were affected by the number of nanocrystals used in the polymerization reaction, and the

theoretical number of QDs per particle depended both on the concentration of nanocrystals and on the final polymer particle size obtained.

Table 2.3 Characterization of hybrid polystyrene/QDs latexes in terms of QDs loading, conversion calculated by gravimetry, monomer droplet size and polymer particle size.

Sample	CdSe/ZnS (%wbm)	Conversion (%)	Dd (nm)	Dp (nm)	Theoretical number of QDs per particle*
Run C1	0	97	87	93	-
Run C2	0.25	100	77	104	0.7
Run C3	0.32	93	89	87	0.5
Run C4	0.38	96	95	106	1.1
Run C5	0.41	90	85	106	1.2

*Calculated based on the amount of QDs added, the number average particle size of QDs, the average polymer particle size provided in this table and the polymer and QDs density (ρ_{pol} = 1.04 g/mL; ρ_{QD} = 5.82 g/mL).

During the polymerization of the hybrid styrene/QDs miniemulsions, samples were withdrawn from the reactor to determine the evolution of both the conversion and the particle size. As it can be seen in Figure 2.8 the evolution was affected by the concentration of QDs but without a clear trend, reaching high final conversion for all the cases and obtaining particles sizes between 87 nm and 106 nm.

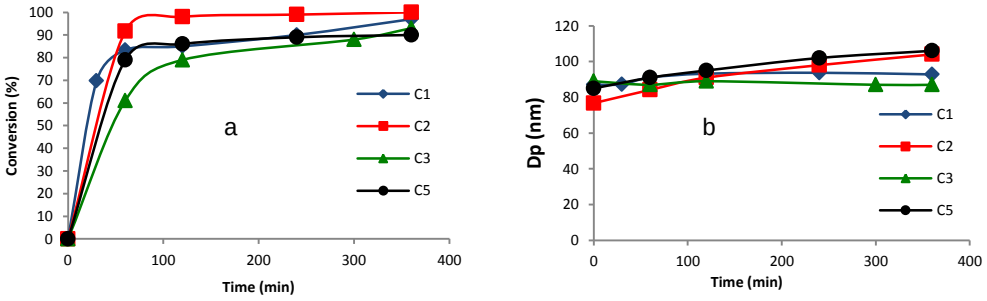

Figure 2.8 a) Time evolution of the conversion of the miniemulsion polymerizations carried out with different QDs loads. b) Time evolution of the particle size measured by DLS.

Apart from the characterizations shown above in terms of polymer particle size, conversion and theoretical number of quantum dots per polymer particle, Run C2 and Run C5 were also characterized by TEM. Figure 2.9 shows TEM micrographs of the resulting latexes. Quantum dots (the black spots marked with the red arrows) were placed in the polymer particles, but really close to the polymer particle-aqueous phase interface. This morphology has been observed by other authors for miniemulsion polymerizations using QDs[9] and for other inorganic nanoparticles[14]. This hemispherical morphology can be explained by the interfacial surface tensions of the polymer-water, inorganic particle-water and inorganic particle-polymer[15,16]. Regarding their distribution, it is observed that most of the particles having QDs contained just one, and in the cases in which more than one nanocrystal is present in the same polymer particle, no aggregation is observed between them.

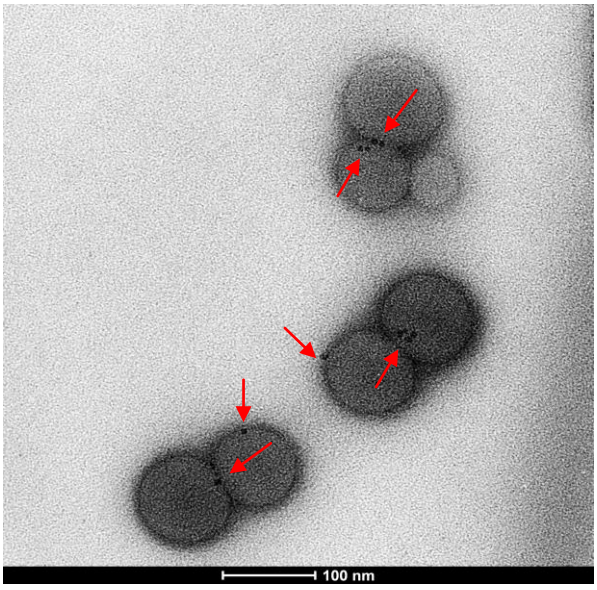

Run 2

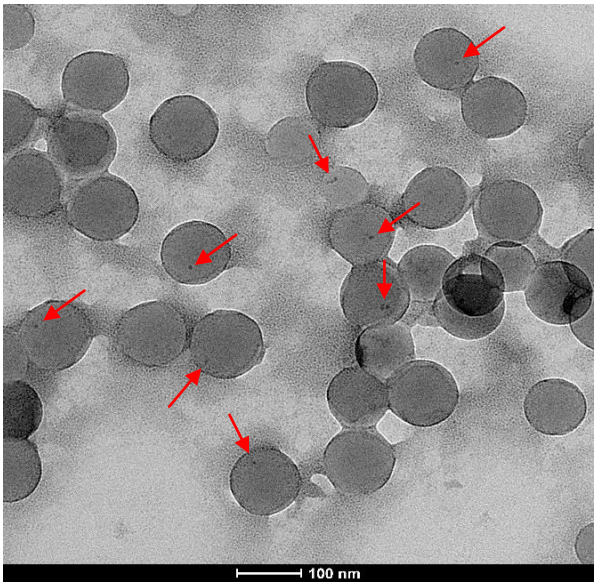

Run 5

Figure 2.9 TEM micrographs corresponding to hybrid polystyrene/QDs Runs C2 (0.25 %wbm) and C5 (0.41 %wbm).

Based on the TEM micrographs of Run C2, the distribution of the quantum dots in the polymer particles was obtained counting 225 polymer particles. In Figure 2.10 the number distribution of QDs per polymer particle is shown, observing that around 40% of the polymer particles contained quantum dots, and from them most of the particles contained just one QD (22%). From this distribution, the experimental average number of QD per particle was obtained (0.56 QDs/polymer particle). After the polymerization reaction QDs were observed stuck on the magnetic bar, meaning that during the reaction some QDs diffuse out of the polymer particles explaining the difference between the experimental and the theoretical average number of QDs per polymer particle for Run C2 (0.7 QDs/polymer particle).

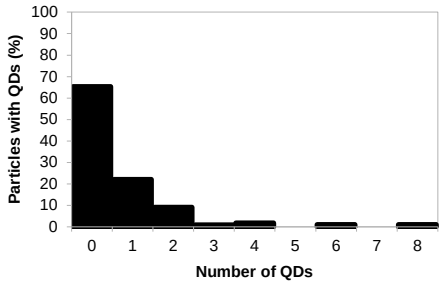

Figure 2.10 Number distribution of QDs in hybrid polystyrene/QDs particles for Run C2 (0.25 %wbm).

Fluorescence analysis were also carried out measuring the fluorescence emission intensity during storage of latex C4. As it can be observed in Figure 2.11 the intensity decreased 80% during the first three weeks, then maintaining this intensity during the next weeks. This decrease of the fluorescence emission intensity with time, is likely related to the degradation of the QDs that might occur if they get in contact with water as shown above. According to Figure 2.9 QD nanoparticles are at the polymer particle-aqueous phase interface and hence degradation by getting in contact with water is likely, (either by the nanoparticles diffusing to the outer side of the polymer particles or by contact with water that penetrates into the polymer particles).

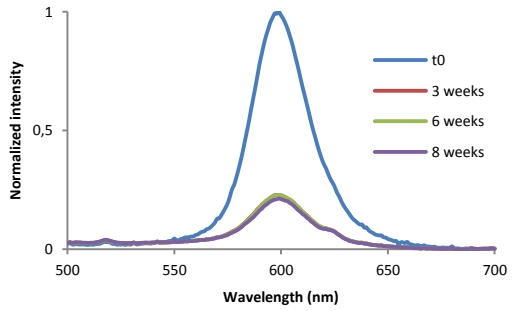

Figure 2.11 Fluorescence emission intensity evolution of Run C4 PS/QDs latex over time.

2.3.2. Synthesis of hybrid core-shell polymer/quantum dots particles

As explained in Chapter 1, quantum dots remain sensitive upon manipulation, which may damage their unique properties, and furthermore they are toxic for the environment. Therefore, an efficient incorporation into colloidal polymer particles is a must. In section 2.5.1 it has been demonstrated that the encapsulation of quantum dots into polystyrene particles was not efficient because fluorescence emission was lost over time. Therefore, a new approach was adopted to improve the efficiency of the encapsulation in order to better protect the QDs from the environment.

Seeded semi-batch emulsion polymerization was carried out using the polystyrene/quantum dot hybrid particles as seed. Methyl methacrylate was the chosen monomer for the production of the shell because polymethyl methacrylate is more hydrophilic than polystyrene and hence the most likely expected equilibrium morphology is core-shell, although hemispherical morphology can be obtained depending on the initiator and emulsifiers employed in the polymerization[17]. Additionally, the wettability of the octadecylamine coated QDs in MMA was poor, and consequently we also expected that QDs will not be compatible with PMMA and they will not leave out from the polymer particles. Table 2.4 shows the characterization of two different runs carried out to produce hybrid core-shell particles.

The theoretical final particle size was targeted to be 125 nm for Run CS2 and 150 nm for Run CS4. The targeted final particle size was almost achieved in both experiments, not observing secondary nucleation or the presence of a bimodal distribution in DLS and in TEM

analysis. Therefore, the theoretical number of quantum dots per polymer particle was the same than for the core hybrid polymer particles.

Table 2.4 Characterization of hybrid core-shell latexes in terms of monomer used for the production of the shell, QDs loading, conversion and final polymer particle size.

Sample	Seed	Shell monomer	CdSe/ZnS (%wbm)[#]	Conversion (%)	Dp (nm)	Theoretical number of QDs per particle
Run CS2	Run C2	MMA	0.25	92	128	0.7
Run CS4	Run C4	MMA	0.32	90	148	1.1

Weight based on total monomer (S+MMA).

The position of the QDs into the synthesized PS/PMMA polymer particles of Run CS2 was studied by TEM (Figure 2.12). In most of the polymer particles containing QDs (marked with red arrows), they were observed at the edge of the darker area, that corresponds to the polystyrene phase, and none in the lighter part (PMMA). Therefore, QDs were not diffusing through the PMMA phase. Regarding their distribution into the polymer particles, some of the polymer particles contained more than one QD, nevertheless no aggregation was observed, as in the case of hybrid polystyrene/QDs polymer particles. Thus, the introduction of MMA did not affect the QDs behavior into the polymer particles.

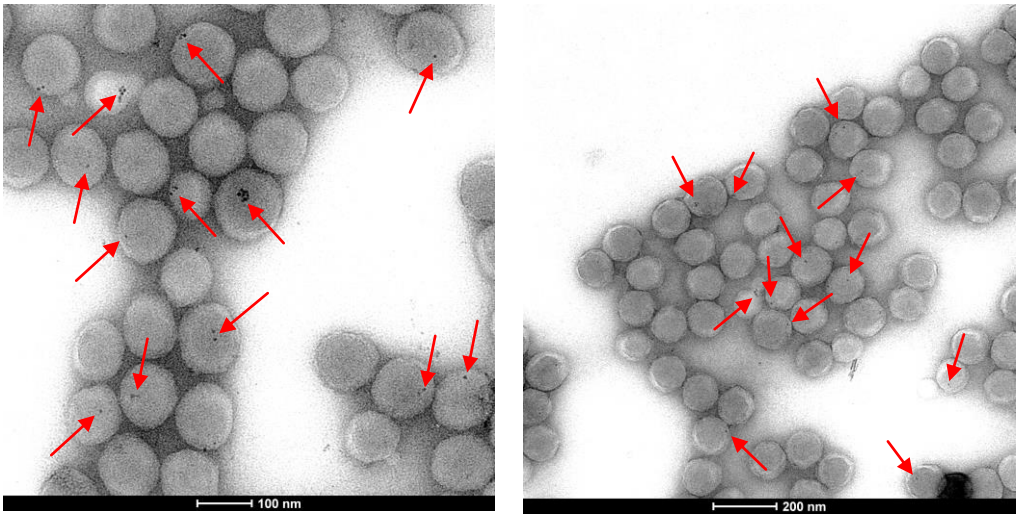

Figure 2.12 TEM micrograph of hybrid PS-QD/PMMA polymer particles of Run CS2.

In order to increase the contrast between PMMA and PS phases in TEM, new sample grids were prepared by using hydroxyethyl cellulose (HEC) to embed the latex particles. A solution of 0.06 wt% HEC was added to the latexes and a drop of this mixture was deposited in a TEM grid and let it dry at room temperature. The grids were observed in TEM and the images are shown in Figure 2.13. According to these images the PS cores were not completely covered by the PMMA polymer, not observing a pure core-shell morphology.

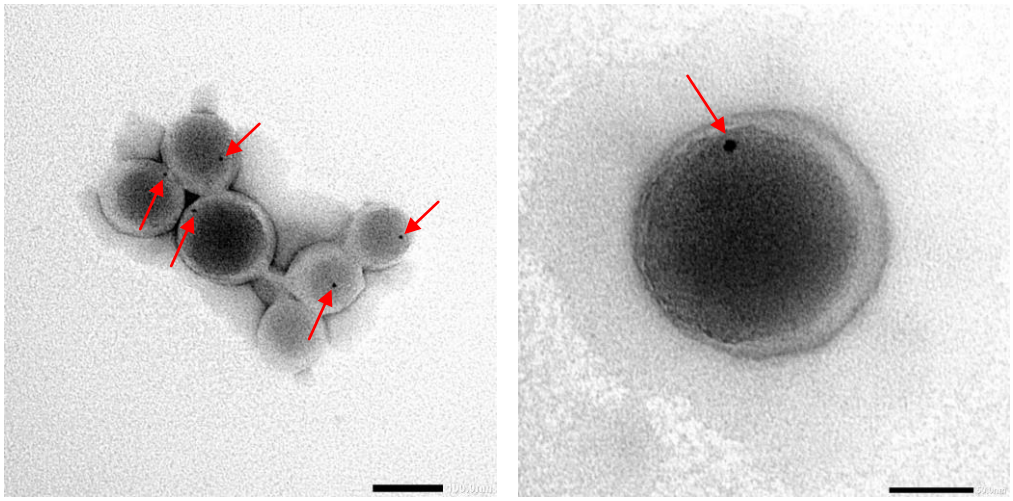

Figure 2.13 High contrast TEM micrographs of polystyrene/QDs/polymethyl methacrylate hybrid polymer particles of CS4 run after mixing with HEC.

Figure 2.14 shows the equilibrium morphology mapping for a two phase system predicted by González-Ortíz and Asua[18]. As it can be observed, the final morphology depends on the interfacial tension between phase 1 (PS) and phase 2 (PMMA) (σ_{12}) and between phase 1 (PS) with phase 3 (H_2O) (σ_{13}) and phase 2 (PMMA) with phase 3 (H_2O) (σ_{23}). For the system presented here, polystyrene is more hydrophobic than polymethyl methacrylate; therefore, interfacial tension σ_{13} is higher than σ_{23}. Regarding the interfacial tension between the polymers (σ_{12}) it is high as they are not compatible. According to some reports[19,17], σ_{23} is bigger than σ_{12}. Thus, $\sigma_{12}/\sigma_{23} < 1$ and $\left|\frac{\sigma_{23}-\sigma_{12}}{\sigma_{13}}\right| < 1$. Without having more accurate data for the interfacial tensions, one can only predict that the equilibrium morphology lies between a core-shell and hemispherical as indicated by the red square drawn in Figure 2.14. The morphology of Figure 2.13 is in agreement with this prediction.

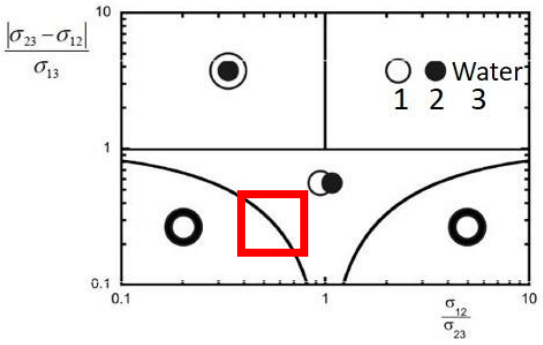

Figure 2.14 Equilibrium morphologies of a two phase system predicted by the minimization of the surface energy of the system (image taken from reference [18]), and location for the PS/PMMA system highlighted with a red square.

In order to see if this morphology could lead to a preservation of the optical properties of the QDs, fluorescence emission measurements during storage were carried out for Run CS4. As done for the polystyrene/QDs core, fluorescence was followed during storage at dark and room temperature noticing a decrease of 40% after eight weeks (Figure 2.15). However, this decrease was lower than in the case of the core hybrid particles (Figure 2.11), meaning that the introduction of PMMA in the system reduces, up to some extent, the contact of the QDs with water.

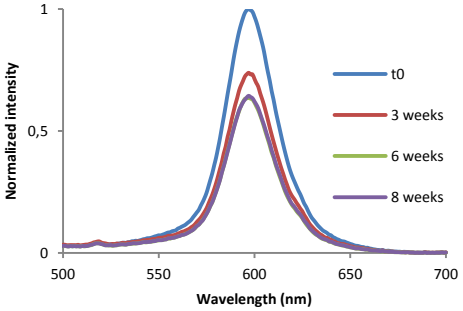

Figure 2.15 Fluorescence emission intensity evolution of PS/QDs/PMMA latex over time.

The decrease of the fluorescence emission intensity observed might be caused by the fraction of composite particles with hemispherical morphology. As PS particles are not completely covered by a PMMA shell, a fraction of quantum dots are not entirely confined into the polystyrene core particles, so some might migrate to the polymer particle/aqueous phase interface and degrade explaining the loss of fluorescence during storage. The polystyrene/QDs and polystyrene/QDs/polymethyl methacrylate latexes, synthesized in section 2.5 did not succeed in the efficient encapsulation of QD nanoparticles and hence in the preservation of the optical properties of the QDs. Therefore, new approaches were pursued to increase the encapsulation efficiency as well as the optical properties.

2.4. Synthesis of cross-linked core-shell particles with encapsulated QDs

In order to better anchor the QDs in the polymer particles and avoid their migration to the aqueous phase, the cross-linking of both the core and the shell of the polymer particles was envisaged.

2.4.1. Synthesis and characterization of hybrid cross-linked cores

First the position of the quantum dots into the monomer droplets in the miniemulsion was analyzed. For this cryo-TEM was used (extended explanation of the sample preparation can be found in Appendix I). Figure 2.16 shows cryo-TEM micrographs of the hybrid styrene/DVB/QDs monomer miniemulsion (0.32%wbm). According to these images all the

quantum dots were in the monomer nanodroplets, some of them near the edge of the droplets, but there were not quantum dots in the aqueous phase. It is also important to point out that some droplets contained several QDs, but interestingly they did not aggregate. Also noticeable was the shape of the monomer droplets, which was not spherical in all the cases and likely it was caused by the preparation method used in the cryo-TEM analysis.

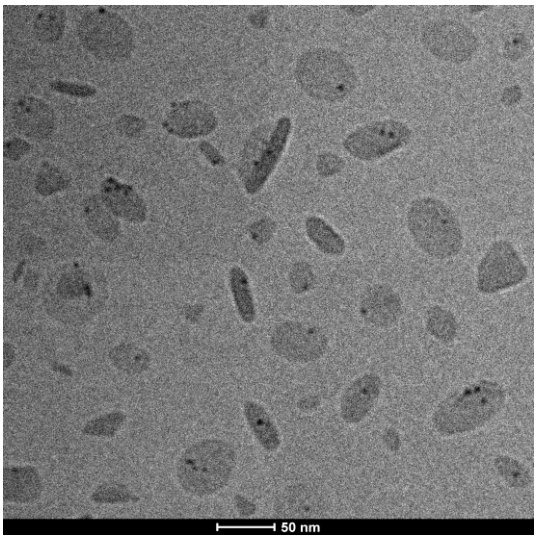

Figure 2.16 Cryo-TEM micrograph of styrene/DVB monomer miniemulsion droplets containing QDs (0.32% wbm).

Table 2.5 presents the results obtained for five representative reactions carried out to obtain the cross-linked hybrid PS/QDs cores with different loads of quantum dots. During the polymerization of the hybrid styrene/DVB/QDs miniemulsion, samples were withdrawn from the reactor to determine the evolution of both the instantaneous conversion and the particle size (Figure 2.17). It was observed that, as for the case of hybrid polystyrene/QDs particles

described in Section 2.5.2, neither the conversion nor the particle size were substantially affected by the concentration of quantum dots in the formulation.

Table 2.5 Characterization of the cross-linked hybrid polystyrene/QDs seeds in terms of QDs loading, conversion calculated by gravimetry, monomer droplet size and polymer particle size.

Sample	QDs (wbm%)	Conversion (%)	Dd (nm)	Dp (nm)	Theoretical number of QDs/particle*
Run XC1	0	98	78	94	0
Run XC2	0.27	100	86	104	0.7
Run XC3	0.36	96	108	96	0.8
Run XC4	0.81	95	76	101	2
Run XC5	1.53	94	75	99	4

*Calculated based on the amount of QDs added, the number average particle size of the QDs (7.2 nm), the average particle size provided in this table and the polymer and QDs density.

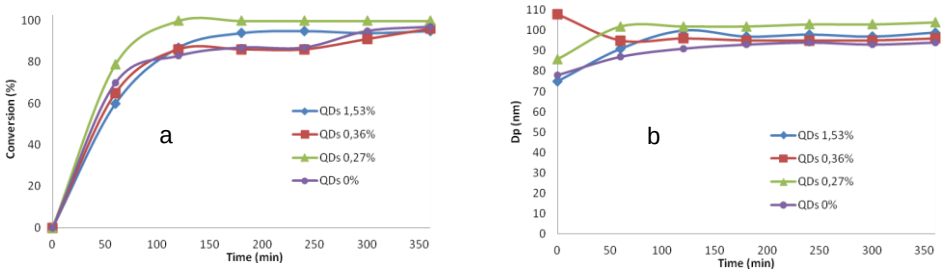

Figure 2.17 a) Time evolution of the conversion of the seeds for different QDs loads. b) Time evolution of the particle size of the seeds measured by DLS.

Regarding their optical appearance, these latexes, as well as the ones previously described, were pinkish at the end of the polymerizations (except for Run XC1), showing a more intense color while increasing the concentration of nanocrystals in the latex.

Figure 2.18a presents the TEM image of one of these hybrid seeds (Run XC2, 0.27% wbm). As for the hybrid miniemulsion, all the QDs were located in polymer particles, none being found in the water phase and proving high incorporation efficiency. In order to quantify the number of particles containing quantum dots and their distribution, 500 particles were counted in the TEM micrographs obtaining the distribution shown in Figure 2.18b.

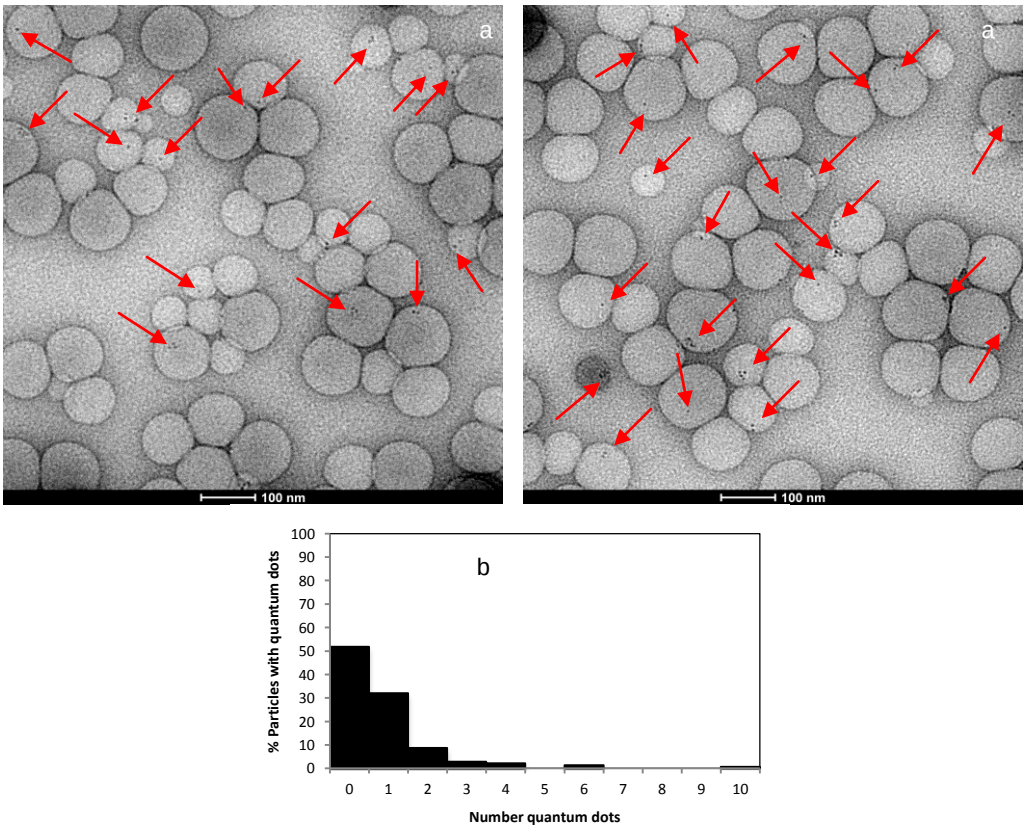

Figure 2.18 a) TEM micrographs of cross-linked polystyrene Run XC2 (0.27% wbm QDs). b) Number distribution of QDs in the cross-linked polystyrene polymer particles for Run XC2.

According to this analysis, around half of the polymer particles contained QDs (48%). It is worth to point out that most of the particles containing QDs contained just one (30%) and the particles with more than one nanocrystal did not present aggregation between them; namely, QDs could be well differentiated from each other. From this distribution, the average number of QDs/particle could be calculated. A value of 0.65 was obtained, which is in good agreement with the theoretical value of 0.7 presented in Table 2.5, demonstrating the statistical distribution of the QDs in the polymer particles and the absence of QDs in the aqueous phase. Comparing this distribution with the one obtained for Run C2 (non-cross-linked polystyrene hybrid polymer particles) having the same theoretical number of QDs per polymer particle, it was observed that the number of particles non-containing QDs decreased. Therefore, the increase of the internal viscosity of the polymer particles because of the cross-linking of the PS chains makes more difficult the diffusion of QDs.

In order to shed light on the encapsulation of the quantum dots in the polymer particles, electron tomography TEM was carried out. The cross-linked polystyrene/QDs sample was characterized using tilt series of micrographs and their subsequent 3D reconstruction. The tilt series was obtained tilting the sample from +60º to -60º taking pictures every 2º with a pixel size of 0.22 nm/pixel. Figure 2.19a shows the 0º TEM micrograph of Run XC2 sample analyzed by tomography. One of the polymer particles of the specimen considered contained two quantum dots (QD1 and QD2), whose position was studied individually by cutting the reconstructed volume (XYZ) by two planes, OXY and OYZ (see Figure 2.19b for the XYZ axis identification).

As shown in Figure 2.19c and Figure 2.19d, the orthogonal cuts done to this reconstructed area for each quantum dot showed that both nanocrystals were surrounded by polymer in all the directions. From this analysis, it can be concluded that QDs were successfully encapsulated into cross-linked polystyrene particles, even if they were relatively close to the edge of the polymer particles.

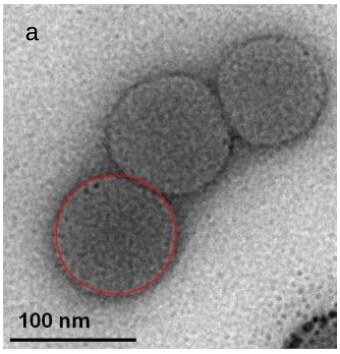

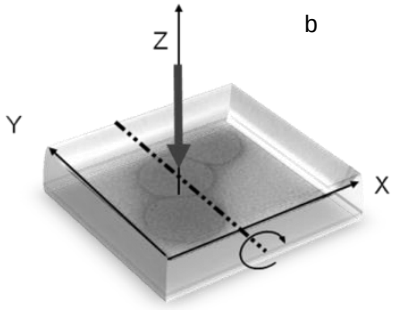

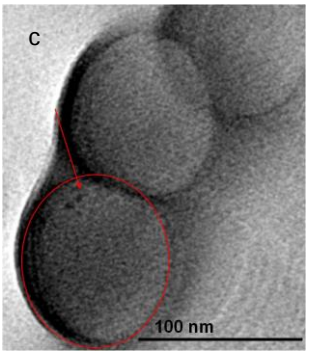

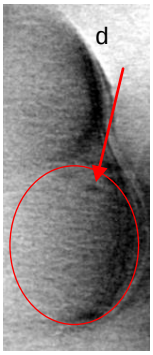

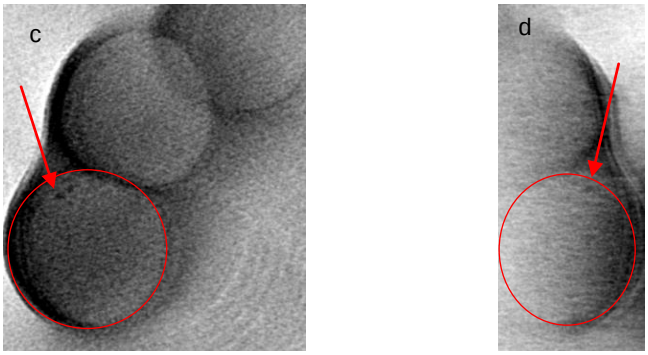

Figure 2.19 Electron tomography TEM of Run XC2. a) Original 2D-TEM micrograph showing the area of interest. b) Tomographic reconstruction of the sample. c), d) OXY and OYZ orthogonal sections for QD1 and QD2 in the region of reconstructed volume, respectively.

The evolution of the position of the quantum dots in the polymer particles was studied by comparing TEM micrographs of Run XC2 during storage (after 10 months, Figure 2.20a). As it can be seen, the amount of polymer particles containing quantum dots had notably decreased. Figure 2.20b shows the distribution of the QDs into the polymer particles after this time. Clearly the number of polymer particles without QDs increased up to 90%. This means that the quantum dots either diffuse out of the polymer particles during storage or that water penetrated into the particles and degraded the QDs. Then, the effect of the cross-linking on the fluorescence properties was analyzed.

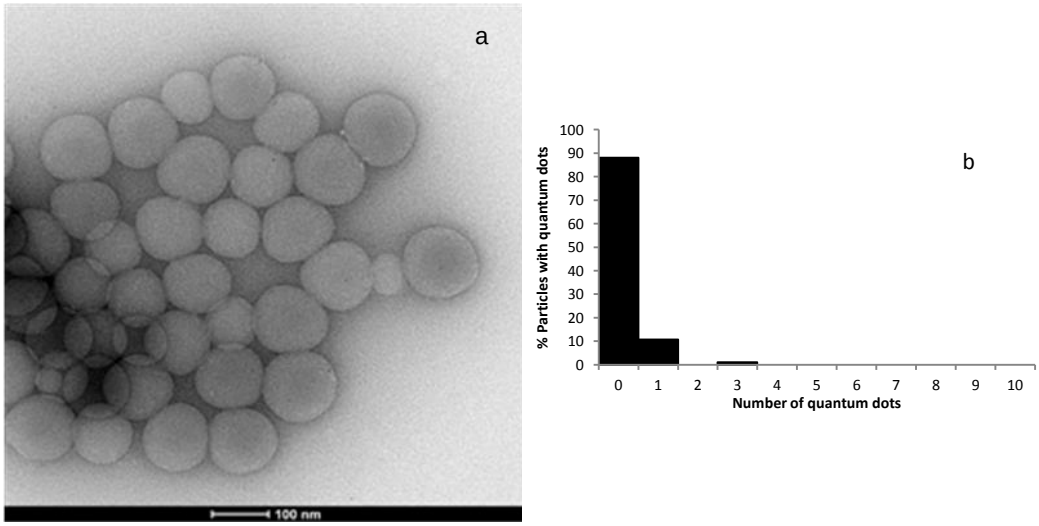

Figure 2.20 a) TEM micrograph of Run XC2 sample ten months after the synthesis. b) Number distribution of QDs in the polymer particles after ten months' storage of the hybrid Run XC2.

The evolution of the fluorescence intensity during storage was assessed. As a representative example, the fluorescence of Run XC4 latex (0.81% wbm QDs) was studied during 8 weeks. The sample was measured right after the polymerization and then kept at dark measuring again after 3, 6 and 8 weeks withdrawing the sample to be analyzed from the top of the vial. As it can be seen in Figure 2.21, the fluorescence intensity for the latex decreased to less than half of the original one after 3 weeks. After week 6 it got to a minimum value that was kept almost constant after 8 weeks. In order to check if fluorescence loss was due to sedimentation of the polymer particles containing quantum dots in the bottom of the vial, in week 6, this was agitated vigorously and fluorescence was measured again in the same conditions resulting in a small increase of the emission intensity, but not enough to recover the original value. Nonetheless, it is important to point out that during storage, the emission

wavelength was maintained; namely, the encapsulated quantum dots did not suffer any change in their size. The decrease in the fluorescence was likely due to the migration of the QDs from the edge of the polymer particles to the aqueous-polymer particle interface and degradation of the QDs surface or to the reaction of the QDs with the water that penetrates in the polymer particles. Fleischaker and Zentel also found loss of fluorescence in hybrid latexes prepared with CdSe/Zns QDs and attributed the degradation to incomplete coverage by the ZnS shell layer. As explained in Section 2.4, it was observed that the contact of QDs with water or an aqueous solution of KPS degrades their surface and affects their fluorescence. This hypothesis is in agreement with the TEM observation of Figure 2.18a and Figure 2.20b (taken right after the synthesis of the latex and after several months respectively) that indicated a substantial reduction of the number of polymer particles containing QDs.

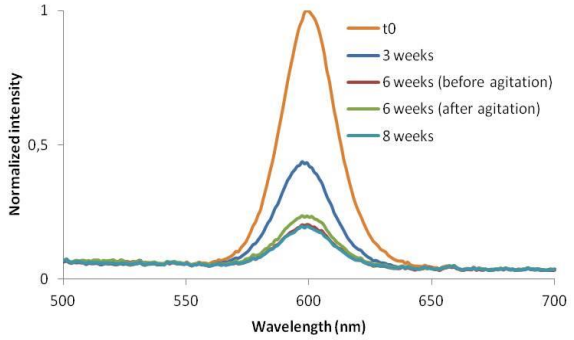

Figure 2.21 Evolution of the fluorescence emission intensity with time for Run XC4.

2.4.2. Synthesis and characterization of hybrid core-shell particles

As seen in the previous section, the cross-linking of the polystyrene particles did not avoid the loss of fluorescence during storage of the hybrid latexes. Taking into account that when including methyl methacrylate in the formulation (Section 2.3.2) the decrease in the fluorescence emission intensity was attenuated but not avoided, it was thought that a potential way to definitely avoid the migration of the QDs from the polystyrene particle surface was to produce a highly cross-linked MMA shell on top of the cross-linked polystyrene cores. This was done by feeding a MMA/DVB mixture to the cross-linked polystyrene seed using a syringe pump at low feeding rate (0.12 g/min) to avoid secondary nucleation. Table 2.6 summarizes the seeded semi-batch emulsion polymerizations carried out varying the amounts of MMA in order to control the thickness of the shell.

Table 2.6 Characterization of core-shell latexes in terms of conversion, seed particle size, final particle size and PMMA/DVB shell thickness.

Sample	Seed	QDs (%wbm)[#]	Conversion (%)	Dp seed (nm)	Dp final (nm)	Shell thickness (nm)
Run XCS1	XC1	0	83	95	131	18
Run XCS2	XC2	0.19	97	104	146	21
Run XCS2*	XC2*	0.24	90	105	121	8
Run XCS2**	XC2*	0.23	93	105	128	12
Run XCS2***	XC2*	0.20	95	105	136	16
Run XCS3	XC3	0.17	95	96	170	37
Run XCS4	XC4	0.46	75	101	166	33
Run XCS5	XC5	1.03	96	99	154	28

Weight based on total monomer (S+MMA+DVB).

Figure 2.22 shows a TEM micrograph of a latex with a clear core-shell morphology (Run XCS3) in contrast to the non-cross-linked PS/PMMA polymer particles. The darkest regions

correspond to the cross-linked polystyrene cores and the lighter regions to cross-linked polymethyl methacrylate shell. In one of the core-shell particles it is also clearly distinguished the presence of two QDs nanoparticles located at the edge of the PS core (see arrows).

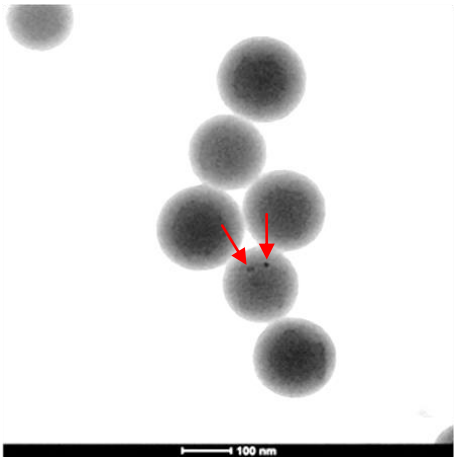

Figure 2.22 TEM micrograph of cross-linked core-shell polystyrene/QDs/polymethyl methacrylate (Run XCS3) hybrid polymer particles.

The analysis of the morphology obtained for these particles was done with the help of the equilibrium morphology map showed in Figure 2.23. Regarding the interfacial tensions, and as in the case of non-cross-linked PS/PMMA polymer particles, σ_{12} represents the interfacial tension between the polymers (cross-linked PS and cross-linked PMMA), σ_{13} is the interfacial tension between the cross-linked PS and water and σ_{23} is the interfacial tension between the cross-linked PMMA and water. Unlike the non-cross-linked PS/PMMA polymer particles, in this case the PS-DVB phase and the PMMA-DVB phase are more compatible, leading to a decrease of σ_{12}, and the cross-linked PMMA phase is more hydrophobic, increasing the value of σ_{23}. This way σ_{12}/σ_{23} is lower than one, and smaller than for the non cross-linked core-shell

particles $|\sigma_{23}- \sigma_{12}| / \sigma_{13}$ is also lower than one being slightly larger than in the case of non-cross-linked particles. This makes the equilibrium morphology to be most likely core-shell, as marked in the equilibrium map.

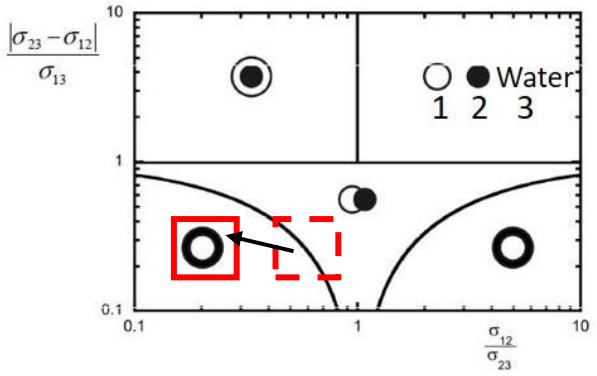

Figure 2.23 Equilibrium morphologies of a two phase system predicted by the minimization of the surface energy of the system (image taken from reference [18]), and location for the cross-linked PS/PMMA system (continuous red square) respect to the location for the non cross-linked PS/PMMA system (dashed red square).

Electron tomography TEM was used to determine more accurately the position of the QDs into the cross-linked core-shell polymer particles. In this case the sample was tilted from -55º to +71º taking TEM pictures every 2º. Figure 2.24a presents the reconstructed area and Figure 2.24b the rotational axis (Y), the direction of the electron beam (Z) and the planar axis (X). In this TEM picture two core-shell polymer particles with one quantum dot each (QD3 and QD4) (black spots in the image) were analyzed. For both nanocrystals, orthogonal cross-sections OXY and OYZ were done (Figure 2.24c and Figure 2.24d), in which it was clearly observed that the particles were surrounded by polymer in all the directions, and in a more centered position into the polymer particles than in the case of the QDs encapsulated in the core particles. The TEM analysis confirms that when adding a shell of cross-linked PMMA to

the seed particles, the QDs are further from the aqueous phase/polymer particle interface and hence they are less prone to suffer degradation. In principle, they should preserve better their optical properties.

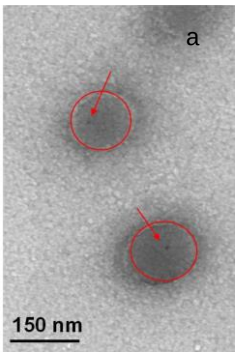

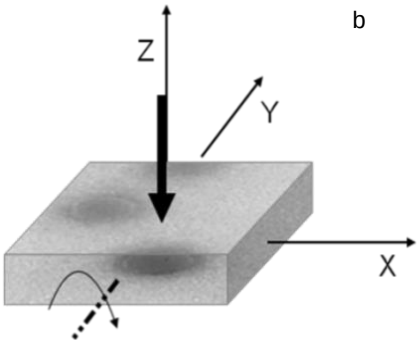

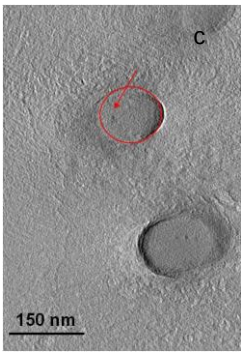

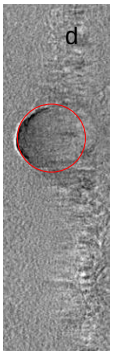

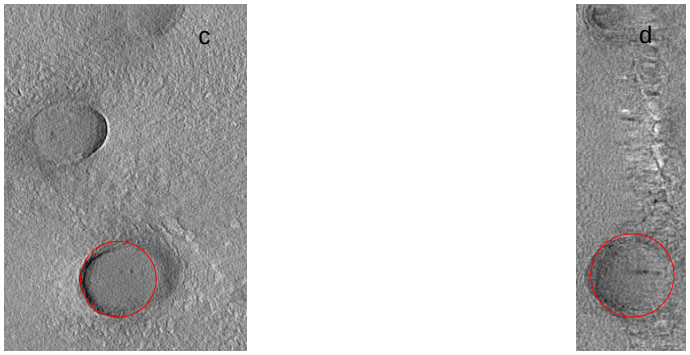

Figure 2.24 Run XCS2 electron tomography TEM. a) Original 2D-TEM micrograph showing the area of interest. b) Tomography reconstruction of the sample. c), d) OXY, OYZ orthogonal sections for QD3 and QD4 in the region of reconstructed volume.

Several TEM images (as the one shown in Figure 2.22) were used to calculate the distribution of the quantum dots in the polymer particles after the synthesis of the shell. On one hand, Figure 2.25a shows the distribution of the quantum dots in the polymer particles for Run XCS2 (0.19%wbm), which was very similar to Run XC2. Indeed, a resembling number of QDs/polymer particle was determined 0.62, which, as in the case of the cross-linked hybrid core, is very close to the theoretical 0.7 QDs/polymer particle. In addition, the distribution for the latex with the highest concentration of QDs synthesized and presenting an average theoretical number of QDs per polymer particle of 4 (Run XC5) was also obtained (Figure 2.25b). A decrease on the number of particles non-containing QDs was observed, as well as a broadening of the distribution (observing some polymer particles containing up to 60 QDs). Therefore, when increasing the concentration of QDs, the percentage of polymer particles containing QDs substantially increased, from 48% for Run XC2 to 57% for Run XC5. Moreover, an experimental average number of QDs per polymer particle of 1.3 for Run XC5 was calculated.

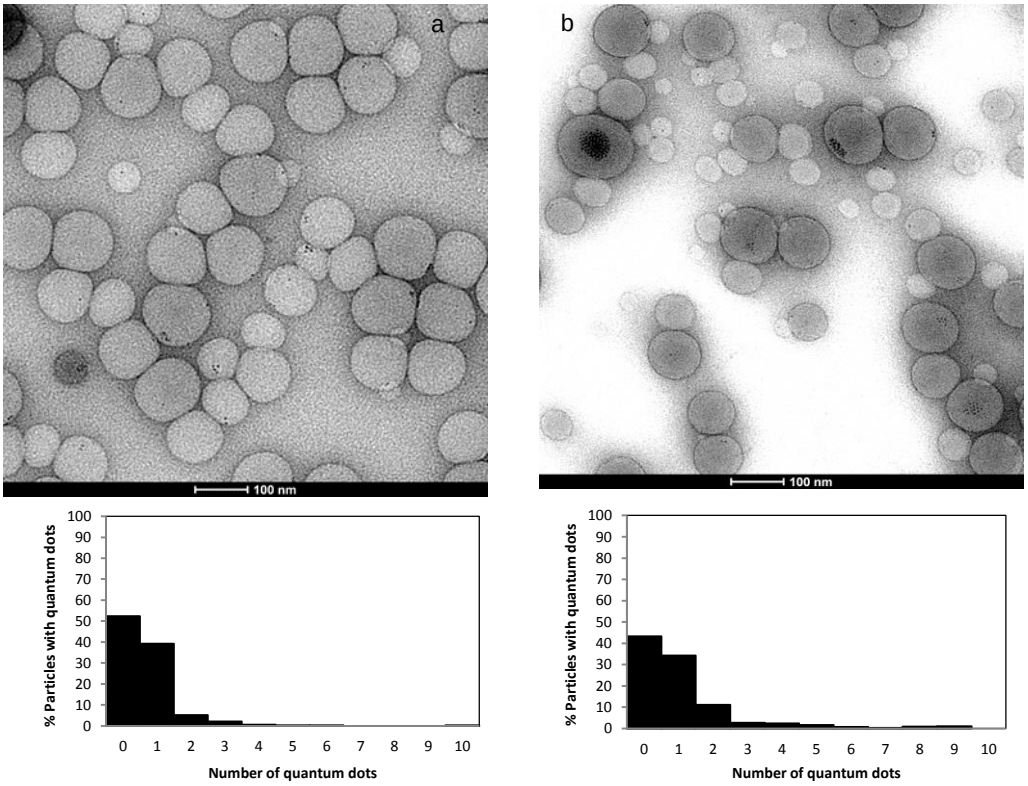

Figure 2.25 QDs particle number distribution in the core-shell polymer particles for a) Run XCS2 and b) Run XCS5.

Regarding the optical properties, when comparing the fluorescence emission spectra of the hybrid cores and the hybrid core-shell particles, the same intensity and emission wavelength was observed (Figure 2.26a), showing that octadecylamine coated CdSe/ZnS QDs were not affected by the synthesis of the cross-linked shell.

The efficiency of the encapsulation was also proven by assessing fluorescence during storage. As presented in Figure 2.21, fluorescence intensity of Run XC4 decreased during storage; the emission intensity decreased to less than half in 6 weeks. Thus, fluorescence of

the Run XCS4 core-shell latex (synthesized from Run XC4) was also studied during several months. The first measurement was done right after the polymerization and the vial was kept at dark measuring again after 3, 6, 8 and 46 weeks. As it can be seen in Figure 2.26b, fluorescence intensity decreased a bit in the first weeks, but afterwards it remained constant, indicating that quantum dots were well encapsulated into the polymer particles preserving their optical properties over time. Different PMMA-DVB shell thicknesses were synthesized (see Table 2.6), and its effect on the fluorescence stability of the samples during storage was studied. Although the shell thickness did not have an effect on the initial fluorescence emission intensity, it was observed that for shell thicknesses lower than 12 nm the fluorescence decreased over time. This is shown for Run XCS2*, for which fluorescence emission intensity during storage was measured over time observing a fast decrease of the intensity (Figure 2.26c). Thus, there is a minimum PMMA shell thickness required to preserve the optical properties of the final material avoiding the migration of the quantum dots out of the polymer particles.

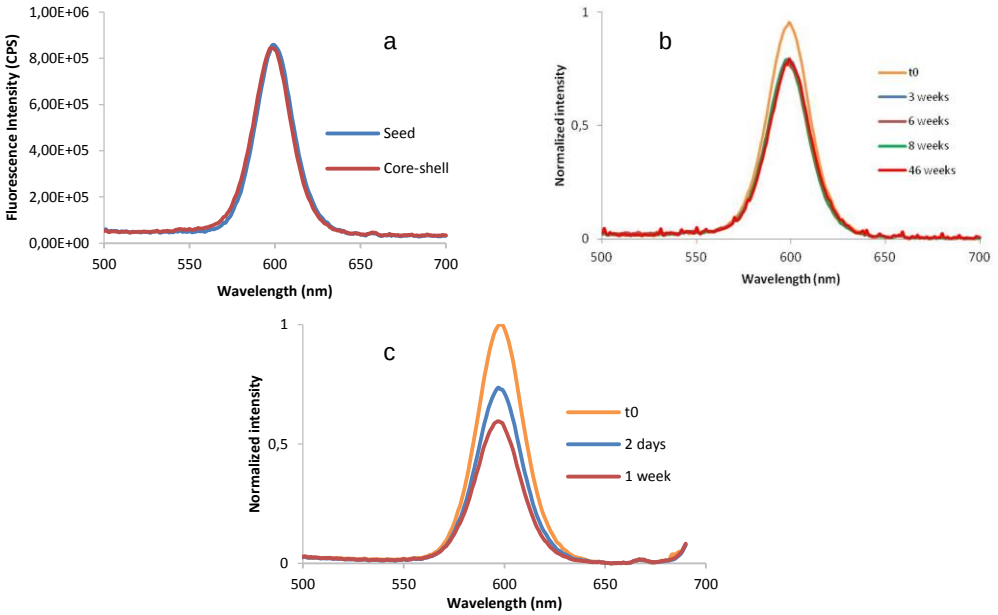

Figure 2.26 a) Fluorescence emission intensity comparison of cross-linked core and core-shell latex b) Fluorescence emission intensity evolution with time for Run XCS4 hybrid core-shell latex c) Fluorescence emission intensity evolution with time for Run XCS2* hybrid core-shell latex.

2.5. Conclusions

Octadecylamine coated CdSe/ZnS quantum dots dispersed well in styrene, being the dispersion stable during months and maintaining their optical properties unvaried. However, quantum dots were degraded losing their fluorescence emission when contacted with water during 55 days and faster if KPS was present. Thus, different strategies to protect the nanocrystals from degradation were investigated in this Chapter.

Hybrid PS/QDs latexes at 5% S.C varying the concentration of QDs from 0.25 to 0.41% wbm were synthesized by miniemulsion polymerization. By TEM analysis it was found that the nanocrystals were located at the edge of the polymer particles. To improve their encapsulation, hybrid polystyrene/QDs/polymethyl methacrylate polymer particles were synthesized using the hybrid PS/QD latexes as seed expecting core-shell morphology to avoid the degradation of QDs. The morphology of these hybrid particles was carefully studied observing a substantial fraction of the composite particle presenting morphologies between hemispherical and core-shell and the quantum dots placed at the aqueous phase-polymer particles interface. Fluorescence properties of both PS-QDs and PS-QDs/PMMA particles were studied over time, observing that the emission intensity decreased during storage indicating that quantum dots degraded.

Therefore, the synthesis of hybrid cross-linked core-shell polystyrene-polymethyl methacrylate polymer particles was attempted. Different loadings of nanocrystals (up to 1.03% wbm) were used without noticing any influence on the reaction kinetics. The encapsulation of the nanocrystals was proved by 3D-TEM analyses, showing that CdSe/ZnS nanoparticles were close to the polymer particle/aqueous phase interface in the seed polystyrene-DVB particles, but were better encapsulated (inner regions) in the core-shell particles.

Moreover, fluorescence studies were done to the synthesized cross-linked core-shell latexes in order to control and optimize the optical properties of the final material. First, the influence of the concentration of QDs in the latex had on the fluorescence emission intensity was investigated. Increasing the amount of quantum dots used fluorescence emission intensity increased.

The evolution of the fluorescence emission intensity during storage time was also analyzed both for cross-linked core and core-shell latexes. For the first case, and because of the position of the QDs close to the polymer particle/aqueous phase interface, the nanocrystals were degraded by the aqueous phase in few weeks. However, when the cores were coated with PMMA/DVB shell the QDs were better encapsulated avoiding their migration or contact with water. The fluorescence of the core/shell latexes was not affected in 46 weeks.

Finally, the effect that the cross-linked shell thickness had on the fluorescence of the final material was also studied. It was found that a minimum PMMA shell thickness of 12 nm was needed to preserve the optical properties of the QDs over time.

2.6. References

(1) Han, M.; Gao, X.; Su, J. Z.; Nie, S. Quantum-Dot-Tagged Microbeads for Multiplexed Optical Coding of Biomolecules. *Nat. Biotechnol.* **2001**, *19* (7), 631–635.

(2) O'Brien, P.; Cummins, S. S.; Darcy, D.; Dearden, A.; Masala, O.; Pickett, N. L.; Ryley, S.; Sutherland, A. J. Quantum Dot-Labelled Polymer Beads by Suspension Polymerisation. *Chem. Commun. (Camb).* **2003**, No. 1, 2532–2533.

(3) Xu, S.; Zhang, J.; Paquet, C.; Lin, Y.; Kumacheva, E. From Hybrid Microgels to Photonic Crystals. *Adv. Funct. Mater.* **2003**, *13* (6), 468–472.

(4) Zhang, H.; Zhou, Z.; Liu, K.; Wang, R.; Yang, B. Controlled Assembly of Fluorescent Multilayers from an Aqueous Solution of CdTe Nanocrystals and Nonionic Carbazole-Containing Copolymers. *J. Mater. Chem.* **2003**, *13* (6), 1356–1361.

(5) Fleischhaker, F.; Zentel, R. Photonic Crystals from Core-Shell Colloids with Incorporated Highly Fluorescent Quantum Dots. *Chem. Mater.* **2005**, *17* (6), 1346–1351.

(6) Esteves, A. C.; Barros-Timmons, A.; Monteiro, T.; Trindade, T. Polymer Encapsulation of CdE (E = S, Se) Quantum Dot Ensembles via in-Situ Radical Polymerization in Miniemulsion. *J. Nanosci .Nanotechnol* **2005**, *5* (5), 766–771.

(7) Esteves, A. C. C. AGET ATRP in Miniemulsion from Functionalized CdS QD's Surface. *Polym. Prepr.* **2005**, *46* (2), 134.

(8) Kuang, M.; Wang, D.; Bao, H.; Gao, M.; Möhwald, H.; Jiang, M. Fabrication of Multicolor-Encoded Microspheres by Tagging Semiconductor Nanocrystals to Hydrogel Spheres. *Adv. Mater.* **2005**, *17* (2), 267–270.

(9) Joumaa, N.; Lansalot, M.; Théretz, A.; Elaissari, A.; Sukhanova, A.; Artemyev, M.; Nabiev, I.; Cohen, J. H. M. Synthesis of Quantum Dot-Tagged Submicrometer Polystyrene Particles by Miniemulsion Polymerization. *Langmuir* **2006**, *22* (4), 1810–1816.

(10) Esteves, A. C. C.; Bombalski, L.; Trindade, T.; Matyjaszewski, K.; Barros-Timmons, A. Polymer Grafting from CdS Quantum Dots via AGET ATRP in Miniemulsion. *Small* **2007**, *3* (7), 1230–1236.

(11) Harun, N. A.; Horrocks, B. R.; Fulton, D. a. A Miniemulsion Polymerization Technique for Encapsulation of Silicon Quantum Dots in Polymer Nanoparticles. *Nanoscale* **2011**, *3* (11), 4733–4741.

(12) Yang, Y.; Tu, C.; Gao, M. A General Approach for Encapsulating Aqueous Colloidal Particles into Polymeric Microbeads. *J. Mater. Chem.* **2007**, *17* (28), 2930–2935.

(13) Gao, Y.; Reischmann, S.; Huber, J.; Hanke, T.; Bratschitsch, R.; Leitenstorfer, A.; Mecking, S. Encapsulating of Single Quantum Dots Into Polymer Particles. *Colloid Polym. Sci.* **2008**, *286*, 1329–1334.

(14) Aguirre, M.; Paulis, M.; Barrado, M.; Iturrondobeitia, M.; Okariz, A.; Guraya, T.; Ibarretxe, J.; Leiza, J. R. Evolution of Particle Morphology during the Synthesis of Hybrid acrylic/CeO2 Nanocomposites by Miniemulsion Polymerization. *J. Polym. Sci. Part A Polym. Chem.* **2014**, *53* (6), 792–799.

(15) Asua, J. M. Mapping the Morphology of Polymer-Inorganic Nanocomposites Synthesized by Miniemulsion Polymerization. *Macromol. Chem. Phys.* **2014**, *215* (5), 458–464.

(16) Reyes, Y.; Paulis, M.; Leiza, J. R. Modeling the Equilibrium Morphology of Nanodroplets in the Presence of Nanofillers. *J. Colloid Interface Sci.* **2010**, *352* (2), 359–365.

(17) Herrera, V.; Pirri, R.; Asua, J. M.; Leiza, J. R. Morphology Control in Polystyrene/Poly(methyl Methacrylate) Composite Latex Particles. *J. Polym. Sci. Part A Polym. Chem.* **2006**, *45*, 2484–2493.

(18) Gonzalez-Ortiz, L. J.; Asua, J. M. Development of Particle Morphology in Emulsion Polymerization. 1. Cluster Dynamics. *Macromolecules* **1995**, *28* (9), 3135–3145.

(19) Wu, S. Polymer Interface and Adhesion. *M. Dekker* **1982**.

Chapter 3. Encapsulation of multiple quantum dots in colloidal polymer particles.

Part of this work was carried out during the internship at Group 7 at ICMCB in Bordeaux under the supervision of Professor Cyril Aymonier.

3.1. Introduction

A way of efficiently encapsulating octadecylamine coated CdSe/ZnS quantum dots was presented in Chapter 2. The aim of this Chapter is the encapsulation in polymer particles of different types of quantum dots, in order to create a sort of barcode to open the door to imaging detection assays. For this purpose, quantum dots with good optical properties and narrow emission peaks are needed (to avoid overlapping of the emission peaks when combining them).

The synthesis of CdSe/CdS quantum dots of different sizes using supercritical fluid technology was investigated.

Supercritical fluid technology is a powerful technique for the synthesis of nanoparticles, such as quantum dots, in a continuous way[1–3]. It has several advantages over the synthesis in solution as, for example, an enhancement of the mass and heat transfer, and a good control of the residence time that leads to a good control of both the final size and the growth of the particles. This way very narrow particle size distributions can be obtained and therefore, very specific fluorescence emission peaks. In any case, the reaction parameters have to be carefully selected because the nanocrystal structure depends on the reaction temperature, and the morphology of the final nanoparticles can be tuned obtaining spheres, nanorods…

Even if this technique provides flexibility in terms of control during the synthesis of the nanoparticles, the amount of solvents available for this process is limited. The solvent chosen should be able to solubilize all the precursors and ligands at ambient temperature and to stay

in liquid form during all the process. Normally, the solvents that accomplish these requirements are too viscous leading to mixing problems. Nevertheless, taking advantage of the supercritical regime these problems can be overcome, increasing the number of compatible solvents and reagents allowing the synthesis of a wide range of nanoparticles[4–7].

The second part of the Chapter presents the use of QDs with different sizes in the production of hybrid latexes with a characteristic emission spectrum. Two approaches were pursued to accomplish the goal. In the first one quantum dots of different particle size were co-encapsulated in polymer particles following the approach presented in Chapter 2. In a second approach, several latexes each one containing a single type of quantum dot were blended.

3.2. Synthesis of quantum dots using supercritical fluid technology

The synthesis of core-shell CdSe/CdS quantum dots was carried out in supercritical hexane. Figure 3.1 shows the phase diagram for hexane. The critical point for hexane is at a temperature of 234ºC and a pressure of 3MPa.

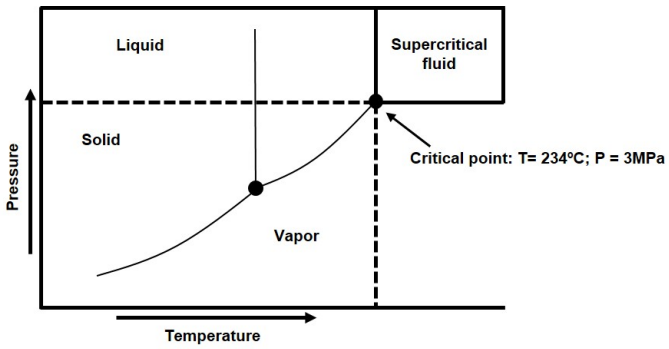

Figure 3.1 Phase diagram highlighting the supercritical point of hexane.

A two-step synthesis procedure was employed for the synthesis of CdSe/CdS quantum dots. First, the synthesis of CdSe core quantum dots modified in their surface with oleylamine was carried out. Then, trioctyphosphine oxide-hexadecylamine (TOPO-HDA) coated CdSe/CdS core-shell quantum dots were synthesized also in supercritical hexane. The materials, the set-up, the synthetic route followed and the results obtained are explained in the following sections.

3.2.1. Materials

The following reagents were used for the synthesis of TOPO/hexadecylamine coated CdSe/CdS quantum dots in supercritical conditions: cadmium deoxycholate [$Cd(DCh)_2$], previously synthesized in the lab, elemental selenium (Se, Sigma Aldrich), elemental sulfur (S, Sigma Aldrich) and trioctyl phosphine (TOP, Sigma Aldrich, technical grade 90%) were used for the synthesis of the cadmium, selenium and sulfur precursors. Oleylamine (OA, Sigma Aldrich, technical grade 70%) was used as surface modifier for CdSe quantum dots. Trioctyl phosphine oxide (TOPO, Stem Chemicals, 90%) and hexadecylamine (HDA, Sigma Aldrich)

were used as surface modifiers in the synthesis of CdSe/CdS QDs. Hexane (Sigma Aldrich, anhydrous 95%) was used as solvent in the preparation of the precursors and as supercritical fluid during the synthesis. All the mentioned reagents were used without further treatment.

3.2.2. Experimental set up

The experimental set up used (Figure 3.2) comprises two high pressure syringe pumps (Harvard Apparatus, PHD 2000), each of them containing a stainless steel syringe, a temperature controller (Eurotherm) and a back pressure regulator (JASCO BP-2080).

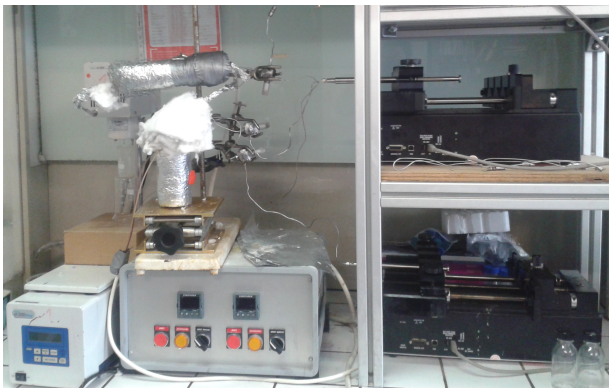

Figure 3.2 Picture of the experimental set up used for the synthesis of CdSe core and CdSe/CdS core-shell quantum dots.

In the case of the synthesis of the CdSe core QDs the syringes used were filled with the cadmium precursor (OA-TOP-Cd) in hexane and with the selenium precursor (TOP-Se) in hexane respectively. The syringes were connected by microtubes (1 m length and internal diameter of 400 μm) to a stainless steel tubular reactor (1/32" scrolled around a cylindrical heating cartridge) connected to the temperature controller (set at 250ºC or 310ºC) that

determines the final QDs morphology. In order to control the flow of the precursors in the microtubes, a three way valve was placed at the syringes´ exit. At the outlet of the reactor the back pressure regulator (BPR) was placed to control the pressure used in the process (10 MPa). At the outlet of the back pressure regulator the QDs dispersion was recovered at room temperature (Figure 3.3).

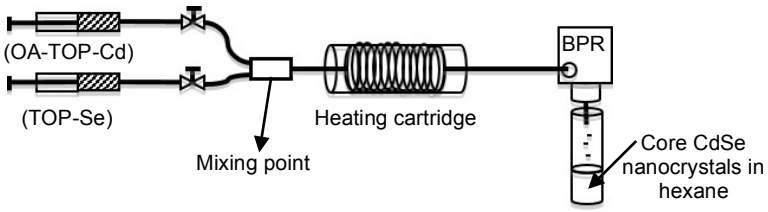

Figure 3.3 Scheme of the set-up used for the synthesis of oleylamine coated CdSe QDs

For the synthesis of the core-shell CdSe/CdS quantum dots the experimental set-up described above was slightly modified. An additional stainless steel tubular reactor 1/32" was scrolled around a second heating cartridge connected to the temperature controller. The cadmium precursor (HDA-TOPO-Cd in hexane) was connected to a heat exchange unit (the configuration of the heat exchanger is equal to the reactor used in the first set up) to condition the Cd precursor to 250ºC and avoid clogging of the microtubes. On the other hand, the sulfur precursor (TOP-S in hexane) was mixed with the CdSe nanocrystals dispersed in hexane and the mixture let to the reactor at room temperature. Both precursor streams were mixed prior entering to the reactor. The reactor temperature was set at 285ºC to produce the CdS shell. The reactor was connected to the back pressure regulator set at 10 MPa through stainless steel microtubes of 1/32" diameter. After releasing the pressure and cooling down, the final core-shell quantum dots are collected as a dispersion in hexane (Figure 3.4).

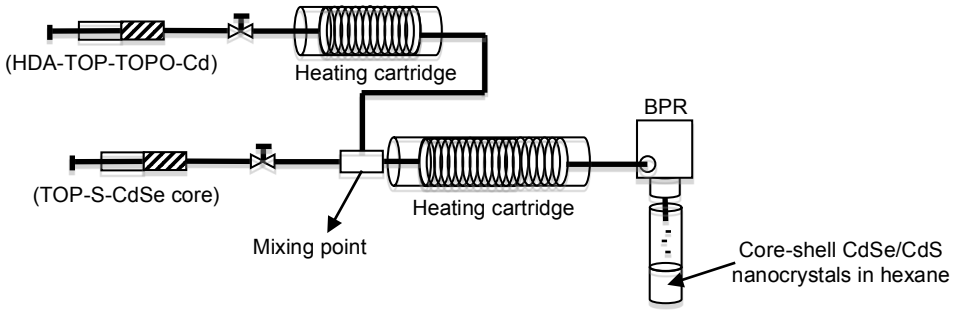

Figure 3.4 Scheme of the set-up used for the synthesis of TOPO-HDA coated CdSe/CdS QDs

The growing of the nanocrystals depends on the temperature and on the residence time. The residence time (Rt) depends on the flow rate of the syringe pumps (Q_{tot} [$\mu m^3/s$]), the reactor volume ($V_{reactor}$ [μm^3]) and the density of the fluid both before increasing the temperature (ρ_{before} [kg/m^3]) and at reaction temperature ($\rho_{reaction}$ [kg/m^3]), but both at high pressure (Equation 3.1).

$$\mathbf{Rt} = \frac{\mathbf{Vreactor}}{\mathbf{Qtot}} \times \frac{\boldsymbol{\rho}\ \mathbf{reaction}}{\boldsymbol{\rho}\ \mathbf{before}} \qquad \textbf{(Equation 3.1)}$$

The experimental set-up described above was used for all the synthesis described in the following sections, both for the synthesis of core CdSe or core-shell CdSe/CdS of different sizes.

3.2.3. Synthesis of CdSe core quantum dots

The first step in the synthesis of CdSe nanocrystals was the preparation of the cadmium and selenium precursors. Based on previous reports, cadmium deoxycholate [$(Cd(DCh)_2$] was used as cadmium precursor because it is highly thermally stable and inexpensive[8]. This salt (225 mg) was mixed together with 0.5 ml of oleylamine (OA) and 1.5 ml of trioctylphosphine (TOP) used as surfactants, in a round bottom flask heated up to 80ºC in a silicon bath. A clear solution was obtained after 15 minutes and it was diluted in 8 ml of hexane, as this was the chosen solvent for the synthesis of the nanoparticles.

On the other hand, the selenium precursor was prepared by mixing 30 mg of selenium powder with 1 ml of trioctylphosphine (TOP) also at 80ºC until complete solution of selenium. This precursor was also diluted in 9 ml of hexane to get a final volume equal to the one of the cadmium precursor.

In order to avoid problems with oxygen during the synthesis of the nanocrystals in the microfluidic system, both precursors were degassed using argon. Protection against light was also needed to keep them away from degradation issues.

In the literature it has been reported that depending on the process temperature, two different crystal structures can be obtained for CdSe nanocrystals[6]. At 250ºC zinc blend structure was produced whereas at 310ºC würtzite structure nanocrystals were synthesized.

Previous to the injection of the precursors the reactor was purged with hexane, at the reaction conditions (250ºC or 310ºC and 10 MPa). In order to maintain the reactor pressure, valves were closed while charging the precursors in the syringes.

Afterwards, the feeding rate of each syringe pump was set depending on the desired residence time, and hence the desired final particle size. The relationship between the residence time and the flow rate for reaction temperatures of 250ºC and 310ºC calculated from (Equation 3.1) for a reactor volume of $1.96*10^{11}$ μm^3 is summarized in Table 3.1.

Table 3.1 Relationship between retention time and the syringe pumps flow rate depending on the temperature for a reactor volume of $1.96*10^{11}$ μm^3.

	Residence time (s)	Flow rate (µl/min)		Residence time (s)	Flow rate (µl/min)
250ºC	5	769	310ºC	5	604
	10	384		10	302
	20	192		20	151
	30	128		30	101
	40	96		40	75
	50	77		50	60
	60	64		60	50

The nanocrystals dispersed in hexane were collected at room temperature at the back pressure regulator outlet. Taking advantage of the characteristic emission color of the quantum dots depending on their size, the sample coming out the back pressure regulator was irradiated with a UV lamp for ensuring the recovery of the desired QDs´ size. When the synthesis was

finished, the set up was cleaned with ethanol at the same supercritical conditions in order to pull out all the remaining reactants as well as to unclog the microtubing, if necessary.

One of the advantages of this synthesis method, apart from being continuous and having the possibility of collecting large amounts of product, is that the flow rate can be changed during the reaction. This way different sizes can be synthesized in a single run taking into account the residence time of the desired CdSe size, discarding the grade transition product between steady states.

3.2.4. Synthesis of CdSe/CdS core-shell quantum dots

Cadmium sulfide presents a similar crystal lattice to the one of cadmium selenide, expecting this way a better coating of the CdSe surface in order to achieve a good preservation of the optical properties by covering the surface defects of the nanocrystal. It is important to point out that due to this good compatibility between the core and the shell crystal lattices, electrons are not confined to the CdSe core but delocalized between both structures. This affects the final emission wavelength in the sense that when growing a CdS shell on the top of the core, the emission wavelength will suffer a red shift[9,10]. The thicker the shell the bigger the shift.

Prior to the preparation of the cadmium and sulfur precursors, the CdSe core quantum dots had to be purified to remove the excess of surfactant that was not bonded to the surface of the nanocrystals. For this, the procedure below was followed:

- 4 ml of CdSe sample were placed into a 50 ml centrifuge tube

- 31 ml of acetone were added to the centrifuge tube
- Centrifugation for 30 minutes at 11000 r.p.m was carried out.
- After the centrifugation, the supernatant was discarded and the CdSe pellet was washed with acetone two times.
- The CdSe pellet was then redispersed in 4 ml of hexane.

Then, the cadmium and sulfur precursors were prepared for the synthesis of TOPO-HDA coated CdSe/CdS quantum dots. In contrast to common core-shell QDs synthesis, two organic compounds were used in this case for the surface modification of the QDs. On one hand, trioctylphosphine oxide (TOPO) leads to high quantum yields of the final nanocrystals. On the other hand, hexadecylamine (HDA) maintains the spherical morphology of the quantum dots.

The preparation of the precursors was based on the number of monolayers sought, and on the Cd:S molar ratio, which for the synthesis carried out was set at 1:5. Several reports in literature explain the importance of controlling the reagents molar ratio in order to get nanoparticles with good optical properties, especially high quantum yields and control of their size[11,12]. Some examples in literature show that a minimum shell thickness is required in order, not only to preserve the optical properties of the CdSe nanocrystals, but also to avoid blinking (fluorescence intermittency)[9,13,14] of the quantum dots. The CdS shell was synthesized by producing sequential monolayers on the top of the nanocrystals, being each monolayer 0.337 nm thick, which corresponds to half the würtzite structure cell unit c-axis dimension[10]. At first, the number of monolayers sought in this work was 7, in order to preserve the optical properties of the quantum dots by avoiding the electron leaks that can appear because of defects in the

CdSe nanocrystal structure. However, due to the characteristics of the synthesis, that is in continuous, it was not possible to produce seven monolayers of CdS as the residence time needed would be much longer than possible with this set-up. Therefore, the number of monolayers to be synthesized was set to 4, maintaining their thickness. Finally, and also in order to avoid clogging problems in the supercritical fluid system, bigger particles were synthesized in three steps obtaining core-shell-shell nanocrystals.

The preparation of the cadmium and sulfur precursors was done as follows, taking into account the number of CdS monolayers and the CdSe core size. First, the adequate amount of [$(Cd(DCh)_2$] salt for the core size used and 2 g of TOPO were solubilized in 1.5 ml of TOP in a 25 ml round bottom flask at 80ºC during 15 minutes obtaining a clear solution. Meanwhile, 0.367 g of HDA were solubilized in 6.5 ml of hexane using an ultrasound bath. Finally, both solutions were mixed obtaining this way the cadmium precursor. In the case of the sulfur precursor, elemental sulfur (S) was dissolved in 1 ml of trioctylphosphine (TOP) in a round bottom flask at 80ºC. Once sulfur was completely dissolved, the solution was cooled down to room temperature and 3 ml of the previously purified CdSe quantum dots dispersed in hexane were added to it. More hexane was added in order to have the same volume as for the cadmium precursor (6 ml). Both precursors were purged with argon before use to avoid problems with oxygen during the synthesis of the core-shell nanocrystals.

3.2.5. Morphological characterization of the obtained quantum dots

High resolution transmission electron microscopy (HRTEM) was used for the characterization of both CdSe core and CdSe/CdS core-shell quantum dots. With this technique, apart from the morphology and the size of the nanocrystals, also their crystalline structure could be observed, seeing the lattice planes of each particle.

Figure 3.5 shows HRTEM micrographs of some representative examples, the CdSe core nanoparticles synthesized at 250ºC and a residence time of 60s (C_250_60), the subsequent CdSe/CdS nanocrystals (CS_250_60) and the growing of those nanoparticles by the production of an extra CdS shell (CSS_250_60).

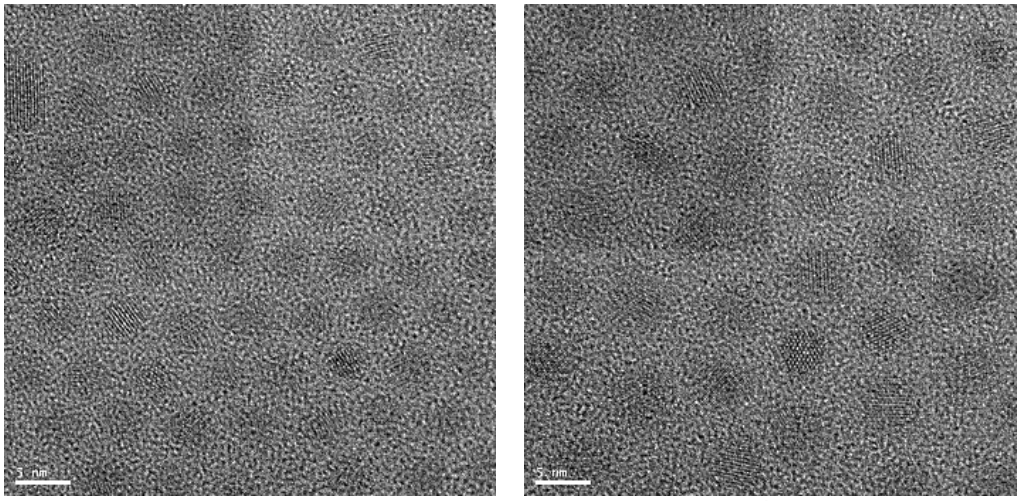

a b

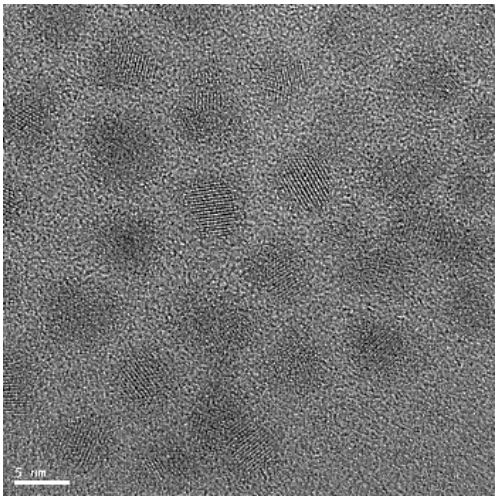

c

Figure 3.5 HRTEM micrographs of a) C_250_60, b) CS_250_60 and c) CSS_250_60 synthesized QDs

This morphology slightly changed while increasing the size of the nanoparticles, being spherical in the case of the CdSe cores and noticing the appearance of some sharp edges specially in the case of the CdSe/CdS/CdS core-shell-shell quantum dots. The change in size has a great influence on the morphology of the final particles.

Particle size distributions for each case were obtained from the HRTEM pictures. As shown in Figure 3.6, an increase in the particle size from the core to the core-shell and core-shell-shell nanocrystals was achieved, meaning that the synthesis of the CdS shell was successful. From these distributions, the average size for each case was calculated obtaining the following data: 3.8 nm for the CdSe core, 5.5 nm for the CdSe/CdS core-shell and 6.6 for the CdSe/CdS/CdS core-shell-shell nanocrystals. The size of the core resulted to be bigger than expected (3 nm), whereas the size of the core-shell and core-shell-shell nanocrystals resulted smaller than calculated from a 3 nm core (5.7 nm for the core-shell and 8.4 nm for the

core-shell-shell). If adjusting the calculations of the theoretical particle size for the core-shell and core-shell-shell particles to the real CdSe core particle size, this difference between the calculated sizes and the real ones results to be even higher (theoretical particle size for CdSe/CdS CS_250_60 = 6.5 nm; theoretical particle size for CdSe/CdS/CdS CSS_250_60 = 9.2 nm).

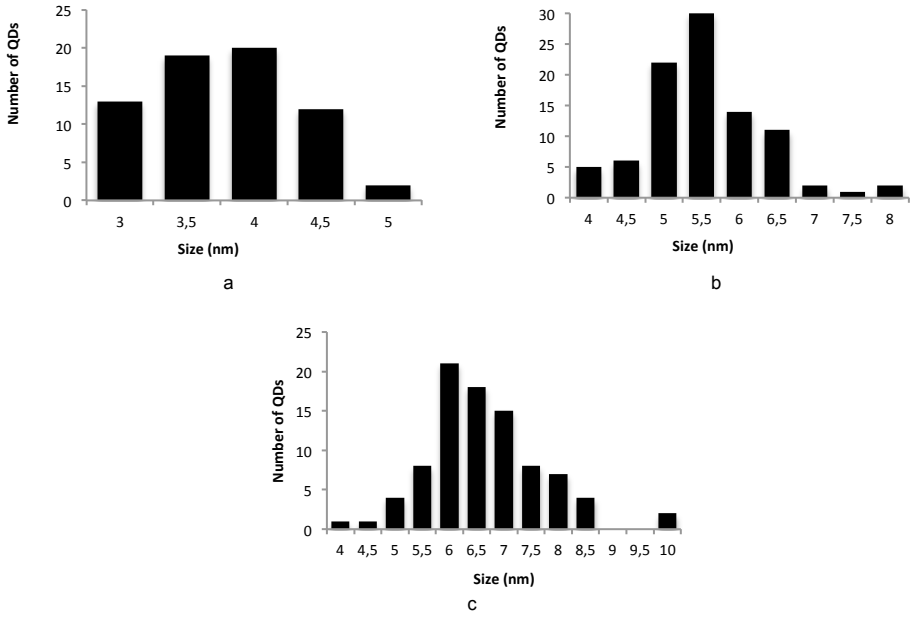

Figure 3.6 Particle size distribution for a) C_250_60, b) CS_250_60 and c) CSS_250_60 obtained from the HRTEM micrographs

This shows that, as explained above, the number of CdS monolayers that can be synthesized with this method is limited, as the residence times needed for such particle growth cannot be safely achieved in the experimental set-up used in this work. Longer residence times

would be needed. However, at longer times clogging of the microtubing occurs due to the solidification of TOPO and HDA at room temperature.

3.2.6. Fluorescence measurements of quantum dots dispersions

The quality of the synthesized quantum dots (CdSe, CdSe/CdS and CdSe/CdS/CdS) was checked by measuring their fluorescence. Fluorescence is the most important characteristic of QDs as it gives information about the size of the nanocrystals and about how specific the emission of the nanocrystals is. Therefore, it is a very useful information to forecast the combinations that can be prepared between them in future applications as multiplexing. The position of the main emission peak is related to the particle size, the longer the wavelength the bigger the particle size. The intensity of the emission gives information on the concentration of the sample, and the shape of the peaks gives information about the quality of the sample, the broadening of the peaks indicating a mixture of different sizes present in the sample and sharper peaks accounting for more monomodal PSD of QDs.

Before measuring the fluorescence of the synthesized nanocrystals, the optimum excitation wavelength for each sample was determined. The optimum excitation wavelength is the one at which the emission intensity reaches its maximum. This excitation wavelength normally is not far from the main absorbance peak wavelength, however, real time control measurements were done for each sample. This means doing a wavelength sweep of the excitation wavelength while observing the variation in the emission intensity and finding the maximum value. Quantum dots present more than one excitation wavelength that correspond

to their different excitation states. Therefore, the value was carefully chosen, being this the one corresponding to the first excitation state of each quantum dot size.

Figure 3.7 presents the fluorescence emission spectra obtained for the CdSe core QDs synthesized at 250ºC (a) and at 310ºC (b). According to the results, it can be concluded that the synthesis worked out better at 250ºC than at 310ºC. The peaks obtained are sharper for all residence times at this temperature (250ºC). In the case of würtzite CdSe quantum dots (reaction temperature 310ºC), a shoulder showed up in the emission spectrum, even for the shorter residence time, observing also big differences in intensity. This shoulder indicates the presence of several QDs sizes for the same residence time.

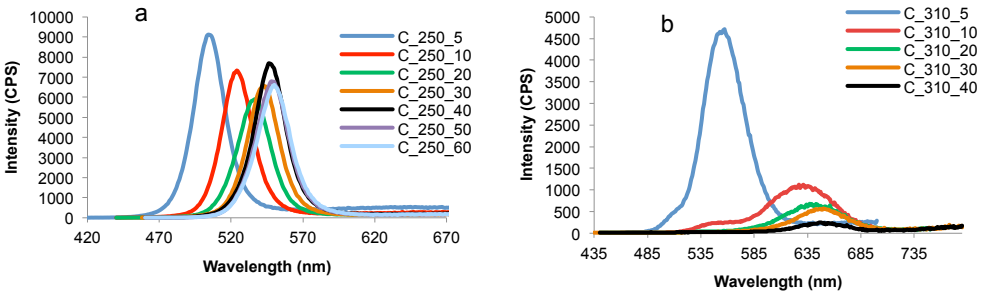

Figure 3.7 Photoluminiscence spectra of core CdSe QDs synthesized at a) 250ºC and b) 310ºC

Full width at half maximum (FWHM) of the photoluminescence spectra was calculated for the CdSe nanoparticles obtained at each residence time and at both temperatures. Table 3.2 summarizes the values obtained for each case together with their fluorescence emission wavelength.

Table 3.2 Fluorescence emission wavelength and full width at half maximum of the photoluminescence spectra for the different CdSe QDs synthesized at different residence times and at 250ºC and 310ºC.

	Name	λ_{em} (nm)	FWHM (nm)		Name	λ_{em} (nm)	FWHM (nm)
250ºC	C_250_5	504	23	310ºC	C_310_5	557	42
	C_250_10	524	25		C_310_10	631	71
	C_250_20	537	28		C_310_20	637	64
	C_250_30	542	26		C_310_30	646	58
	C_250_40	546	26		C_310_40	647	56
	C_250_50	548	27			-	-
	C_250_60	550	27			-	-

Table 3.2 shows the effect of the residence time and the reaction temperature on the emission wavelength of the CdSe quantum dots. On one hand, independently from the temperature, while increasing the residence time the emission wavelength of the QDs increased. This increase tends to level off, for both temperatures, from 30s of residence time observing smaller differences between the wavelengths obtained at longer residence times. On the other hand, an increase in the reaction temperature also derives on an increase on the emission wavelength at the same residence times. For example, at a residence time of 5s an emission wavelength of 504 nm is obtained at 250ºC and of 557 nm at 310ºC. Regarding the FWHM, interestingly at 250ºC increases at low residence times but it remained almost the same at high residence times. However, CdSe QDs synthesized at 310ºC presented higher FWHM values, indicating the obtaining of a mixture of QD sizes at this temperature.

Fluorescence emission was also measured for the CdSe/CdS core-shell (CS) quantum dots synthesized following the procedure explained in Section 3.2.4. Figure 3.8 shows the fluorescence spectra for the synthesized core-shell (a) and core-shell-shell (b) QDs. For the core-shell nanocrystals, when increasing the size of the CdSe core, so increasing the residence time, the emission peaks shifted to longer wavelengths. This shift was also noticed for the core-shell-shell (Figure 3.8b) quantum dots indicating a successful growing of the nanocrystals. (Note that the nomenclature used from now on to describe the core-shell and core-shell-shell QDs works as follows: core-shell (CS) or core-shell-shell (CSS)_reaction temperature for the core synthesis_residence time for the core synthesis.)

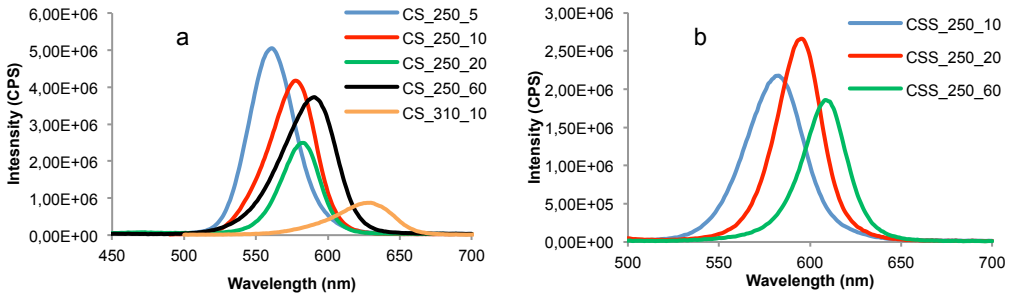

Figure 3.8 Fluorescence emission spectra of a) CdSe/CdS core-shell and b) CdSe/CdS/CdS core-shell-shell quantum dots.

Table 3.3 summarizes the emission wavelength of the CdSe/CdS core-shell (CS) and core-shell-shell (CSS) quantum dots synthesized.

Table 3.3 Emission wavelength for CdSe/CdS and CdSe/CdS/CdS core-shell and core-shell-shell nanocrystals synthesized from the CdSe core quantum dots.

CS		CSS	
Name	λ_{em} (nm)	Name	λ_{em} (nm)
CS_250_5	564	CSS_250_10	583
CS_250_10	578	CSS_250_20	595
CS_250_20	583	CSS_250_60	608
CS_250_60	591		
CS_310_10	630		

Fluorescence emission comparisons between some representative core and core-shell quantum dots are shown in Figure 3.9. In Figure 3.9a the shift between the C_250_5 core (λ_{em} 504 nm) and the corresponding CS_250_5 core-shell (λ_{em} 564 nm) is shown, and in Figure 3.9b the fluorescence emission of the series C_250_60 core (λ_{em} 550 nm), core-shell (λ_{em} 591 nm) and core-shell-shell (λ_{em} 608 nm) nanocrystals is presented. In both cases a shift of the emission peak from the core to the core-shell was observed. Additionally, in Figure 3.9b a shift from the core-shell to the core-shell-shell emission peak occurred showing the growth of CdS monolayers on the top of both the core and the core-shell nanocrystals. Regarding the differences in emission intensity, especially in Figure 3.9b, this is due to the different QDs concentrations used when doing the fluorescence measurements.

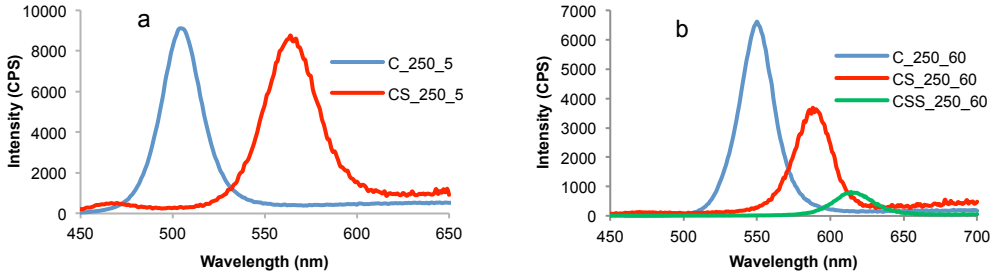

Figure 3.9 a) Fluorescence emission of CdSe core C_250_5 and CdSe/CdS core-shell CS_250_5 QDs. b) Fluorescence emission of CdSe core C_250_60, CdSe/CdS core-shell CS_250_60 and CdSe/CdS/CdS core-shell-shell CSS_250_60.

According to the FWHM values obtained, in both cases good quality QDs were synthesized, with narrow particle size distributions and good optical properties when dispersed in hexane and chloroform.

3.3. Encapsulation of the synthesized CdSe/CdS quantum dots into colloidal polymer particles

Taking advantage of the synthesis of different QDs sizes, different combinations can be made taking into account the emission wavelength and the full width at half maximum for each case in order to be able to distinguish the fluorescence emission peaks. Figure 3.10 shows the fluorescence spectrum of a dispersion in styrene of QDs of three different sizes in a ratio 1:1:1 in weight, in which the emission maxima are clearly differentiated. Combination of these QDs with the encapsulation technique reported in Chapter 2, that ensures stability of the optical properties of the nanocrystals during storage, waterborne dispersions of polymer particles containing QDs of different sizes were produced.

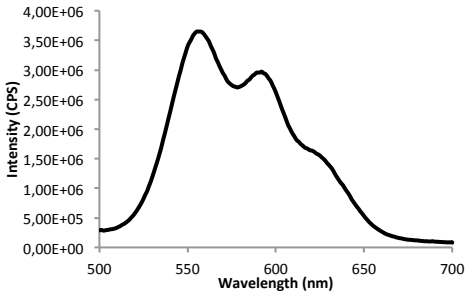

Figure 3.10 Fluorescence spectra of three different QDs, in a ratio 1:1:1 in weight, dispersed in styrene before their encapsulation.

The as-synthesized TOPO-hexadecylamine coated CdSe/CdS quantum dots were pretreated prior to their encapsulation into polymer particles. On the one hand quantum dots had to be purified in order to remove the excess of organic modifiers in the dispersion. Acetone was added to the nanoparticles dispersion and centrifuged for 30 minutes at 11.000 r.p.m. This procedure was done three times discarding the acetone after each centrifugation. After the last centrifugation, the obtained pellet was redispersed in a suitable solvent, in this case toluene, in order to facilitate the transport from the laboratory in Bordeaux to the laboratory at Polymat. The solvent was removed prior to the encapsulation of the QDs into polymer particles.

3.3.1. Synthesis of hybrid core-shell polymer/QDs particles

The synthesized CdSe/CdS quantum dots presented a good compatibility with styrene, being easily dispersible in this monomer, therefore, the encapsulation strategy followed was the one explained in Chapter 2 for the encapsulation of octadecylamine coated CdSe/ZnS quantum dots. Briefly, an organic phase composed by QDs, styrene as monomer, hexadecane (HD) as costabilizer and divinyl benzene (DVB) as cross-linker, and an aqueous phase containing sodium dodecyl sulfate (SDS) as surfactant, sodium bicarbonate ($NaHCO_3$) as buffer and water, were prepared separately. After 10 minutes of mixing each phase, they were brought together and mixed under vigorous stirring for 20 minutes. Then, the miniemulsion was produced using a Hielscher sonicator (operating at 80% amplitude and 100% cycle) sonicating during 4 minutes in an ice bath under magnetic stirring. The obtained monomer droplets were stabilized by doing a post-addition of SDS 1% wbm to the so formed miniemulsion. A 5% S.C monomer miniemulsion was obtained and polymerized in batch in a 25 ml round bottom flask with a nitrogen inlet under magnetic stirring. Potassium persulfate (KPS) was used as thermal

initiator, which was added when the temperature reached 75ºC. Polymerization was carried out for 6 hours and hybrid cross-linked polystyrene/quantum dots particles were obtained. Then, the production of the cross-linked polymethyl methacrylate shell by seeded semi-batch emulsion polymerization was carried out. The cross-linked PS/QDs seed was placed into a round bottom flask, which was inmersed in a silicon bath, with a nitrogen inlet. The temperature of the bath was increased up to 75ºC and then the initiator (KPS) was added in a shot and the mixture MMA+DVB was fed into the reactor using a syringe pump at a flow rate of 0.12 g/min. When the feeding was finished, the polymerization was kept during 3 more hours at the same temperature. Finally, hybrid cross-linked core-shell PS/QDs/PMMA hybrid polymer particles were obtained.

Three latexes containing one, two and three different types of CdSe/CdS QDs were synthesized. Table 3.4 summarizes the most relevant properties of these latexes as well as the type and the ratio (in weight) of QDs used in each Run.

Table 3.4 Characteristics of hybrid cross-linked core-shell PS/QDs/PMMA latexes in terms of conversion, droplet size, particle size of the seed and final particle size.

Sample	CdSe/CdS type	CdSe/CdS weight ratio	Conversion (%)	Dd (nm)	Dp seed (nm)	Dp core-shell (nm)
Run 1	CS_250_20s	1	90	95	113	156
Run 2	CS_250_10s + CSS_250_60s	1:1	96	92	112	162
Run 3	CS_250_5s + CS_250_20s + CSS_310_10s	1:1:1	75	86	101	131

3.3.2. Fluorescence properties

Fluorescence of the resulting hybrid colloidal polymer particles was studied. For this, latexes were diluted in water (0.1 g/ml) in order to avoid backscattering while measuring.

Figure 3.11 shows the fluorescence spectrum of the core cross-linked polystyrene/QDs latex containing CS_250_20s CdSe/CdS quantum dots and the fluorescence spectrum of Run 1, the corresponding core-shell latex. This type of QDs presents a fluorescence emission peak at around 583 nm, which is distinguished in the spectrum corresponding to the hybrid PS/QDs core polymer particles. However, this peak was not present for Run 1, that is, in the hybrid core-shell cross-linked PS/QD/PMMA polymer particles. Therefore, the synthesized HDA-TOPO coated CdSe/CdS quantum dots were degraded during the seeded semi-batch emulsion polymerization step.

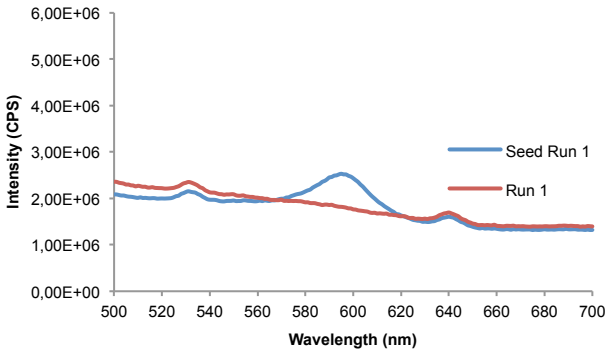

Figure 3.11 Comparison of fluorescence spectra after the synthesis of the hybrid seed (seed Run 1) and of the cross-linked core-shell PS/QD/PMMA polymer particles (Run 1).

In order to shed light on the fluorescence degradation of the QDs, the fluorescence emission intensity was monitored by withdrawing samples from the reaction during the synthesis of Run 3 (Figure 3.12). The fluorescence emission spectra corresponding to the styrene dispersion of the three different types of QDs used in Run 3 was already shown in Figure 3.10, in which the maximum fluorescence emission peaks of each QD were well differentiated. However, when producing the miniemulsion, the fluorescence emission spectrum only showed the emission peak corresponding to the bigger size QDs (CSS_250_20s). The disappearance of the fluorescence emission peaks of the smaller size QDs (CS_250_5s, CS_310_10s) shows a faster degradation of the QDs when decreasing their size. Samples were withdrawn during the polymerization and fluorescence was measured observing that the shape of the spectrum was maintained during the reaction. In contrast to Run 1 (Figure 3.11), in this case the fluorescence of the bigger QDs (CSS_250_20s) was maintained after the synthesis of the cross-linked PMMA shell. The QDs used for this reaction were bigger than the ones used for Run 1 and they contained an additional CdS shell. Therefore, the difference in the final result is probably related to a better coverage of the surface that slows down the degradation of the nanocrystals, and hence the loss of fluorescence.

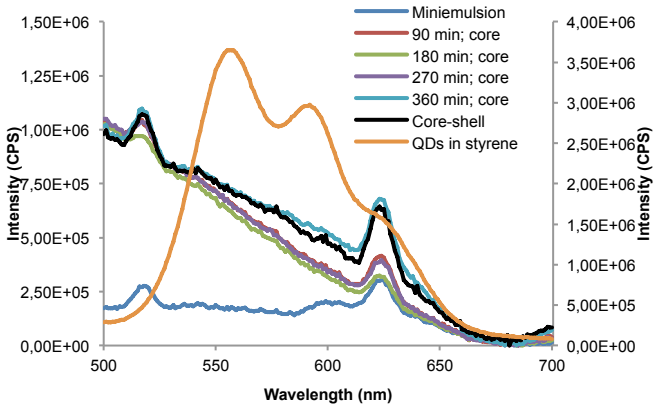

Figure 3.12 Fluorescence evolution during the polymerization reaction.

As reported in Chapter 2, commercial octadecylamine coated CdSe/ZnS quantum dots were degraded in contact with aqueous solutions. The QDs synthesized in this Chapter degraded too, but at a much faster rate than the commercial ones. Furthermore, it can be concluded that the smaller the QDs the faster the degradation. The faster degradation is likely related to a weaker protection shell resulting from the synthesis and purification strategies employed. On one hand, it is worth noting that independently of the residence times employed for the synthesis of the CdSe core, the amount of hexadecylamine and TOPO used to protect the surface of the CdSe/CdS nanocrystals was the same. Therefore, the surface coverage of the nanocrystals decreased as the nanocrystal size decreased as the number of nanoparticles obtained increased. That is, the amount of surface modifiers used would not be enough to efficiently cover the smaller QDs surface leading to less protected QDs. On the other hand, the continuous strategy used to produce the CdS shell on the CdSe nanocrystals did not ensure a minimum number of CdS layers to be produced and hence the QDs were only weakly protected. Finally, during the purification step prior to the synthesis of CdSe/CdS QDs, the

modifier molecules weakly adsorbed to the QDs surface would be released reducing the protection of the QDs´ surface. This would affect all the QDs´ sizes but with a greater impact in the ones less protected from the beginning.

Although the continuous synthesis of CdSe/CdS QDs under supercritical conditions of hexane in tubular microreactors is a versatile and robust approach to produce dispersions of QDs of tunable sizes, the process conditions used in this work did not guarantee their stability when contacting with aqueous solutions, as required in the strategy presented in Chapter 2. Even though the continuous synthesis approach can be optimized to increase the stability of the QDs dispersions, such attempt was not pursued in this PhD due to the lack of time. Instead, commercial QDs used in Chapter 2 were acquired in different sizes to attempt their simultaneous encapsulation into colloidal polymer particles.

3.4. Encapsulation of multiple commercial CdSe/ZnS QDs in colloidal polymer particles.

As described above, the synthesized TOPO-hexadecylamine coated CdSe/CdS quantum dots were not suitable for their encapsulation into colloidal polymer particles due to their loss of fluorescence when being in contact with the aqueous phase in the miniemulsification step. Therefore, octadecylamine coated CdSe/ZnS quantum dots of four different sizes were purchased from Ocean NanoTech for this purpose. The same encapsulation strategy described in Chapter 2 Section 2.7 was followed to encapsulate different QDs sizes into the same cross-linked core-shell PS/PMMA polymer particles.

3.4.1. Characterization of CdSe/ZnS of different sizes

Prior to the encapsulation, quantum dots were characterized in terms of size and fluorescence properties by preparing toluene dispersions of the four quantum dots purchased (QD520, QD560, QD600, QD626). Toluene dispersions of different concentrations were prepared for each quantum dot size. First, the most suitable excitation wavelength for each QD was checked maintaining it for all the measurements of each series. Taking into account the saturation and detection limit of the equipment, the slit was chosen and fixed at 2 nm for all the measurements independently from the type of QD.

Regarding the evolution of the fluorescence emission intensity with the QDs size, it was observed that, when increasing the size of the nanocrystals the emission wavelength shifted to the right (to longer wavelengths) and the fluorescence emission intensity decreased for the same concentration in weight of QDs (g/ml) (Figure 3.13a). Figure 3.13b shows the calibration curve for the four types of commercial QDs dispersed in toluene, in which the difference in emission intensity for each QD type at each concentration is clearly noticed. Based on these results, it was concluded that the number of particles and not the concentration in weight determines the fluorescence emission intensity of the quantum dots. As a result, the size of the nanocrystals had to be accurately determined in order to be able to calculate the number of QDs for each case, and hence to control the fluorescence emission intensity when combining different quantum dot sizes.

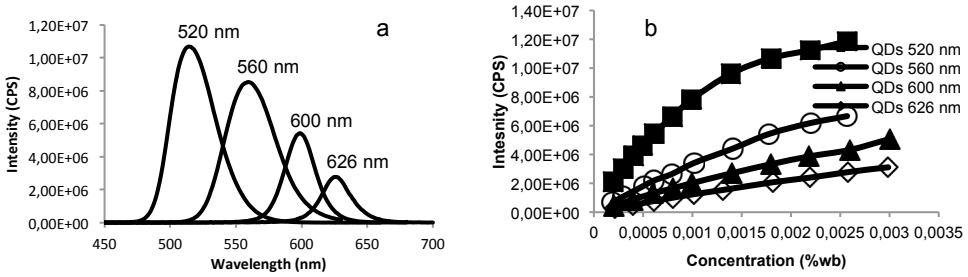

Figure 3.13 a) Fluorescence emission spectra for the different QDs at the same weight concentration. b) Fluorescence emission intensity calibration curves for the different types of QDs.

TEM micrographs of a toluene dispersion of each quantum dot were taken in order to obtain their particle size. Around 500 particles were measured to determine the distribution and the average particle sizes (Figure 3.14).

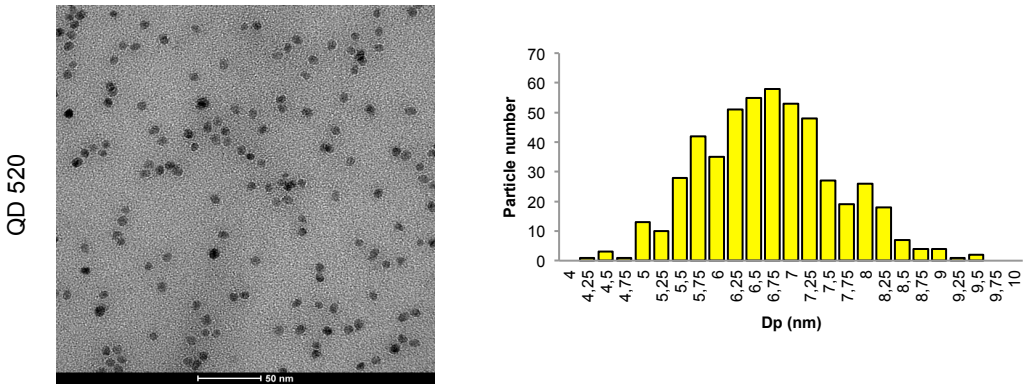

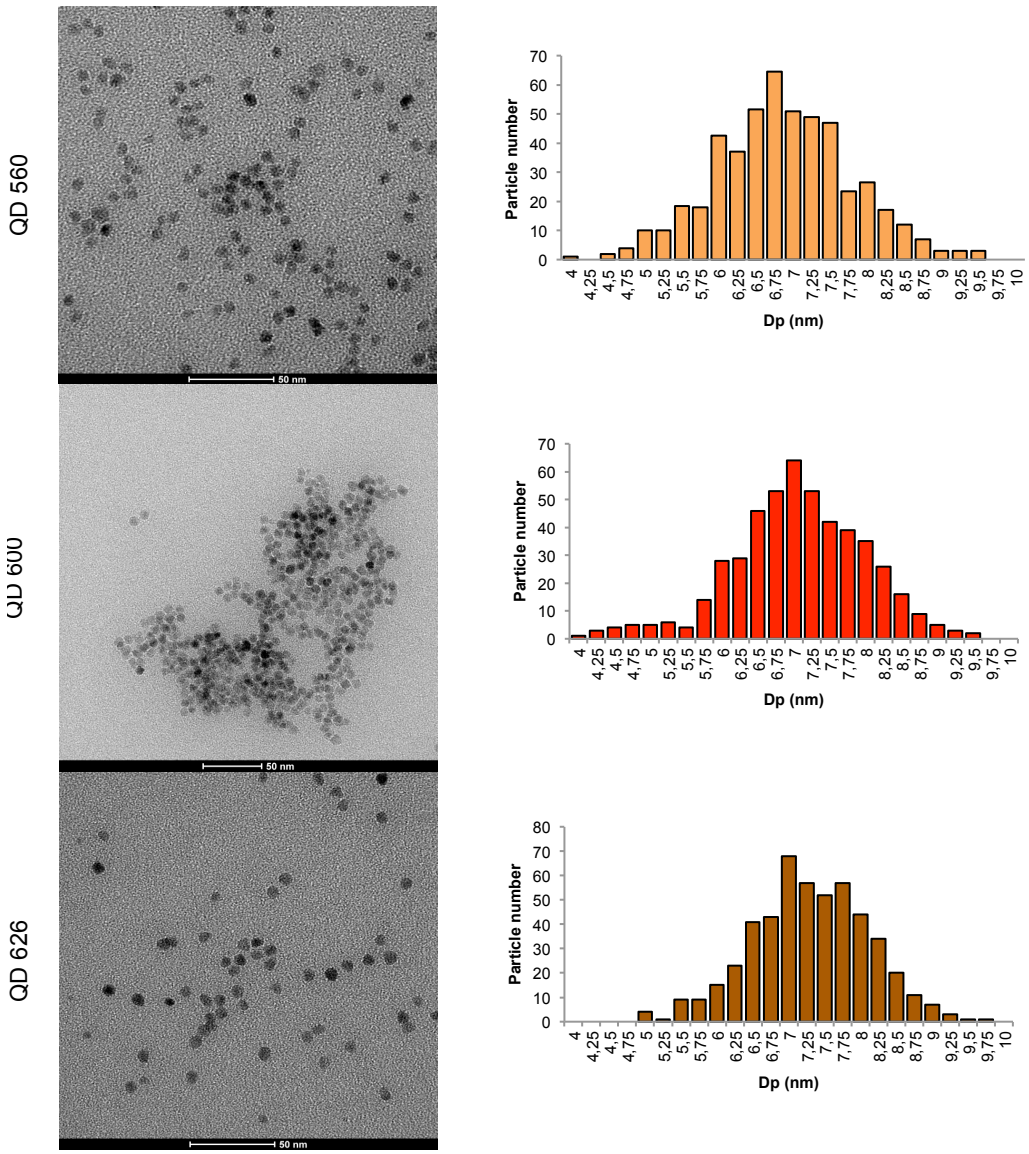

Figure 3.14 TEM micrographs of the four types of QDs and the particle size distribution obtained for each of them.

The TEM micrographs show that the quantum dots could be differentiated as individuals in all the cases, however dependent on the concentration they tend to be more or less close to each other. Table 3.5 shows the volume, number and weight particle size obtained for each QD, as well as the particle size distribution (Dw/Dn) and the full width at half maximum calculated from the fluorescence emission spectra. Interestingly, the particle size distributions were identical for the three smallest QDs, slightly decreasing for the bigger ones, indicating a good homogeneity on the particle size independently from their size. However, according to the FWHM values obtained from the emission spectra, a mixture of sizes would be present for the two smallest QD sizes as high values were obtained. Nevertheless, for the two bigger sizes a small full width at half maximum was obtained, showing homogeneity of the sample. This shows that for QDs very small differences in size have a great impact on their optical properties.

Table 3.5 Summary of the emission wavelength, calculated volume, number and weight particle size, particle size distribution and full width at half maximum of the emission peak for each QD.

Emission wavelength (nm)	Dv (nm)	Dn (nm)	Dw (nm)	PDI	FWHM (nm)
520	6.8	6.7	7	1.05	40
560	7.0	6.9	7.2	1.05	45
600	7.2	7.0	7.4	1.05	27
626	7.4	7.3	7.5	1.04	27

Knowing the particle size, the number of particles for a certain concentration, and vice versa, can be calculated using (Equation 3.2). Therefore, dispersions of multiple QDs sizes in solvent with known number of each size of QD can be readily prepared.

$$Np = \frac{6 * m_{QD}}{\pi * \rho * Dpv^3} \quad \textbf{(Equation 3.2)}$$

Where,

N_p = number of particles

m_{QD} = mass of quantum dots in the dispersion (g)

ρ = density of CdSe/ZnS = 5.82 g/cm^3

D_{pv} = QD volume average particle size (cm)

Two mixtures with different ratios of nanoparticles were prepared in order to analyze the influence of one type of quantum dot on the fluorescence properties of the other. For this, two types of quantum dots with well differentiated emission peaks (520 nm and 600 nm) were dispersed in toluene. Figure 3.15 shows the fluorescence emission spectra obtained when 1:1 and 1:2 ratios, in number of particles, were prepared. As it can be seen, the emission intensities were in close agreement with the ratio of number of particles. Furthermore, no influence on the fluorescence emission of none of the nanoparticles was observed, meaning that, besides the wide absorbance spectra that quantum dots show, none of them absorbed the light that the other emitted.

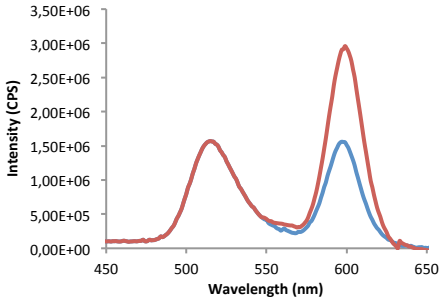

Figure 3.15 Fluorescence emission spectra for a mixture of QD520 and QD600 in ratios 1:1 (blue) and 1:2 (red) dispersed in toluene

After this thorough characterization of the four sizes of quantum dots, it was concluded that the simultaneous encapsulation of QDs into cross-linked core-shell PS/PMMA polymer particles controlling the final fluorescence emission intensity was possible taking into account that:

- The fluorescence emission intensity of the quantum dots is directly proportional to the number concentration.
- Quantum dots presenting well differentiated emission spectra are needed in order to differentiate the emission signals from each other.

3.4.2. Encapsulation results

Quantum dots emitting fluorescence at 520 nm (QD520) and 600 nm (QD600) were the chosen nanoparticles to be encapsulated into cross-linked core-shell polystyrene/polymethyl methacrylate polymer particles following the procedure described in Chapter 2.

First the concentration of QD600 was fixed at 0.31% wbm, as it was previously calculated that this concentration gives a theoretical distribution of one QD600 per polymer particle for polystyrene/DVB particles of 100 nm size. The number of QD particles corresponding to this concentration was calculated using (Equation 3.2). As the desired fluorescence ratio for this reaction was 1:1, the number of particles for the smaller QDs (QD520) should be the same. The amount of small QDs was thus calculated as follows:

$$Np_{QD600} = \frac{6 * 0.0031g}{\pi * 5.82g/cm^3 * 10^{-21} * (7.2nm)^3} = 2.7255 * 10^{15}$$

$$m_{QD520} = \frac{2.7255 * 10^{15} * \pi * 5.82g/cm^3 * 10^{-21} * (6.8nm)^3}{6} = 0.0026g$$

For comparative reasons, and prior to their encapsulation, fluorescence emission intensity of the mixture of both quantum dots dispersed in styrene was measured observing that, as expected, the emission intensity of both quantum dots was similar (Figure 3.16).

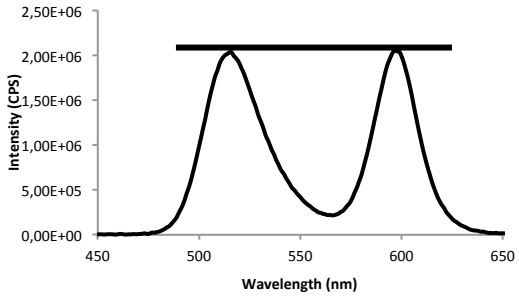

Figure 3.16 Fluorescence emission spectrum of a mixture 1:1 QD520:QD600 dispersed in styrene before the polymerization reaction.

Then, the polymerization reaction using the calculated concentrations of QDs was carried out following the procedure described in Chapter 2. Fluorescence of the core-shell latex was measured right after the polymerization and compared to the one of the styrene dispersion (Figure 3.17), noticing a big change in the fluorescence intensity ratio of both QDs. In fact, the 1:1 ratio was lost during the reaction. Moreover, the emission peak corresponding to QD520 suffered a broadening and a red shift with respect to the one obtained for the styrene dispersion. It is also noticeable that the intensity emission peak corresponding to QD600 was higher than the one for QD520, maintaining, for QD600, the maximum emission wavelength and its full width at half maximum. Note that the intensities of the spectra obtained in the styrene dispersion and in the core-shell latex cannot be compared because the concentrations of QDs are different.

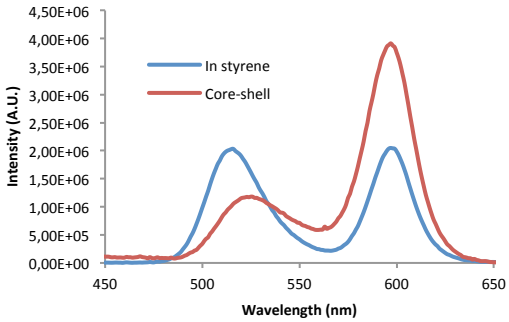

Figure 3.17 Comparison of fluorescence spectrum between the styrene dispersion and the core-shell final latex for a mixture 1:1 QD520:QD600.

A different hybrid latex containing quantum dots emitting at 560 nm and 626 nm was synthesized to study if the fluorescence emission spectrum was altered during the synthesis process (miniemulsion, seed and final core-shell latex). Calculations of the amount of QDs used were done to get a ratio 1:1 between the fluorescence emission peaks of both QDs.

According to Figure 3.18, after the miniemulsion the fluorescence ratio was still maintained, but after the synthesis of the hybrid seed this ratio changed. The fluorescence emission intensity of the smaller nanocrystals (QD560) was lower than the one of the bigger quantum dots (QD626). Furthermore, after the synthesis of the PMMA shell the fluorescence emission intensity difference between both peaks increased. The ratio between the maximum intensity values of both peaks for the core and the core-shell was calculated obtaining a value of 1.6 in the case of the seed and of 2.6 for the core-shell hybrid latex. This indicates a decrease in the fluorescence emission intensity of the smaller QDs during the polymerization reaction.

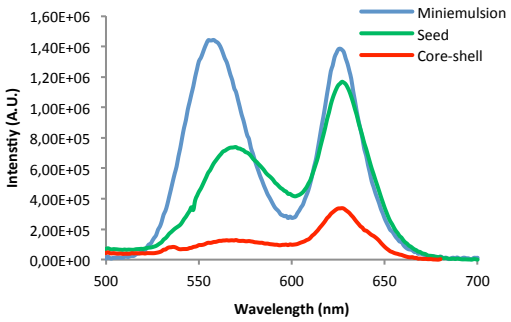

Figure 3.18 Comparison between the fluorescence obtained for the miniemulsion and the resulting core and core-shell latex for a mixture 1:1 QD560:QD626

The two examples of co-encapsulation of two different quantum dots in polymer particles presented the same fluorescence emission behavior. A large emission intensity decrease for the smaller QDs was observed in both cases, independently of the size of the nanocrystals. This fact is probably due to an absorption-emission process between the QDs of different sizes being placed close to each other. Quantum dots show a wide absorption spectrum, so when co-encapsulating different QDs sizes into the same polymer particles, the

bigger QDs can absorb the light that the smaller ones emit, which did not occur when the QDs were dispersed in toluene, much further away from each other.

Based on the results obtained, and although it was possible to control fluorescence in toluene and styrene dispersions controlling the number of quantum dots particles, this was not possible when co-encapsulating different QD sizes in the same polymer particles. Therefore, a new strategy was necessary in order to achieve a good control of the fluorescence emission intensity when combining different QDs, in order to open the door to detection applications.

3.5. Blends of waterborne hybrid polymer/QD dispersion with different QD nanoparticle sizes.

An alternative way of producing a waterborne hybrid polymer/QD dispersion with a characteristic spectrum corresponding to more than one QD size is the production of dispersions with a single QD size and then blending them. This approach, although more time consuming, might prevent the absorption-emission interactions between the QDs of different sizes.

Therefore, the synthesis of four latexes with a single quantum dot type (of different size) each was pursued. Latexes were synthesized following the same strategy as in the previous examples; first hybrid PS-DVB/QDs particles were obtained by miniemulsion polymerization, and then seeded semi-batch emulsion polymerization was carried out to obtain the final core-shell cross-linked PS/QDs/PMMA polymer particles. Table 3.6 summarizes the most relevant

properties of the four latexes obtained with each QDs size, QDs fluorescence emission wavelength and final polymer particle size. In all the cases, complete conversion was obtained.

Table 3.6 Summary of the particle size and fluorescence emission wavelength for each QD and final polymer particle size for each latex synthesized.

$Dp_{v\ QD}$ (nm)	λ_{QD} (nm)	Dp polymer particle (nm)
6.8	520	175
7.0	560	183
7.2	600	178
7.4	626	185

Here again the number of quantum dots was the key factor to control the fluorescence intensity and the proportion between the emission peaks of the different quantum dots when blending the latexes. That is, assuming that the encapsulation efficiency was the same in all the latexes, the number of quantum dots for a specific amount of latex was calculated and from it and depending on the proportion required, the quantity of the other latex or latexes was obtained.

This way, several blends were prepared combining two and three types of QDs with well separated emission peaks, avoiding overlapping and facilitating the recognition of the signal and analysis of the final spectrum. The following combinations were done:

- QD520 + QD600 (1:1, 1:2, 2:1)
- QD560 + QD600 (1:1)
- QD560 + QD626 (1:1)
- QD600 + QD626 (1:1)

- QD560 + QD600 + QD626 (1:1:1)

Fluorescence emission was measured fixing the most suitable excitation wavelength for each case. Figure 3.19 shows the spectra obtained for each blend in which the peaks could be perfectly distinguished and measured when blending two and three latexes. Unlike what happened with the latexes with two types of quantum dots encapsulated in the same polymer particle dispersion, this time fluorescence intensity ratio followed the number of particles ratio used in the blend.

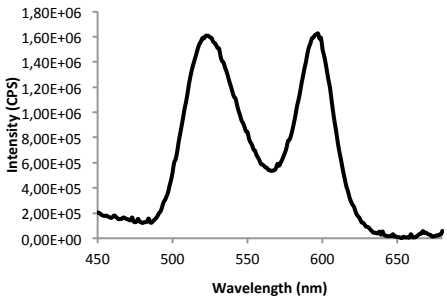

QD520 + QD600 1:1

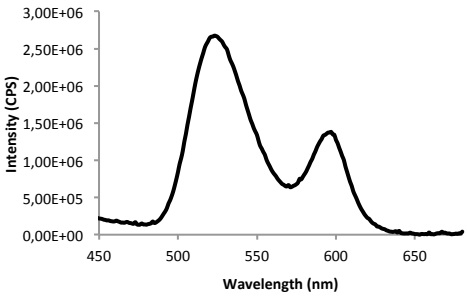

QD520 + QD600 2:1

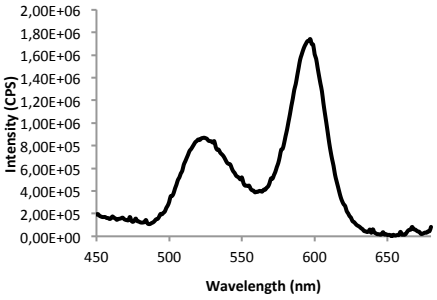

QD520 + QD600 1:2

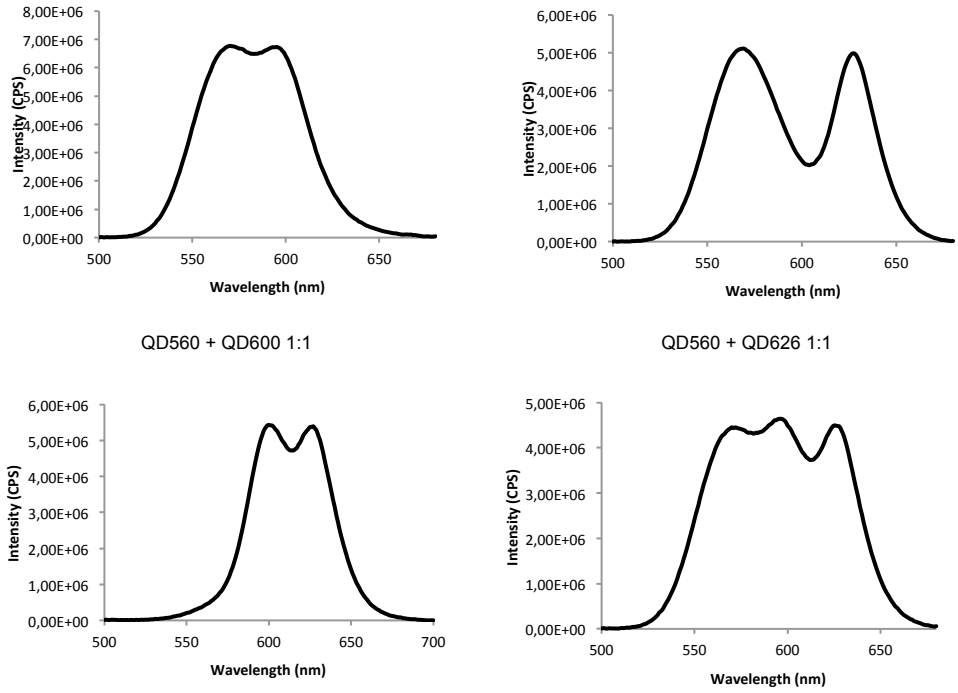

Figure 3.19 Fluorescence emission spectra for the blends prepared with different ratios of particles containing QDs of different sizes.

Therefore, it was demonstrated that blending different latexes, in which a good encapsulation efficiency of the quantum dots in the polymer particles was achieved, a high control of the fluorescence spectra can be accomplished. This way fluorescence spectra can be modulated at will allowing a large number of combinations by choosing the most suitable nanocrystals.

3.6. Application of the latex blends containing commercial QDs

In the previous section, it has been demonstrated that fluorescence spectra can be modulated at will by blending latexes containing commercial CdSe/ZnS QDs. This control of the fluorescence emission intensity and the demonstrated efficient encapsulation of the QDs into cross-linked core-shell PS/PMMA opens the door to multiplexing application.

The first step after the fluorescence characterization of different blends, would be the functionalization of the surface of the polymer particles of one blend with the same reactive group. This functionalization should be different for each blend so they could be differentiated during the detection process. That is, for example, the polymer particles of a blend containing QD520 and QD600 in a ratio 1:1 functionalized with A, and the polymer particles of a blend with QD560 and QD626 in a ratio 2:1 functionalized with B. Then, these blends would be mixed and put in contact with an analyte anti-B. This way only the particles modified with B would react and would be attached to the analyte, discarding the others. Measuring the fluorescence spectrum of the resulting sample, and as the spectra corresponding to the different blends were previously characterized, the analyte can be fast and easily identified (Figure 3.20).

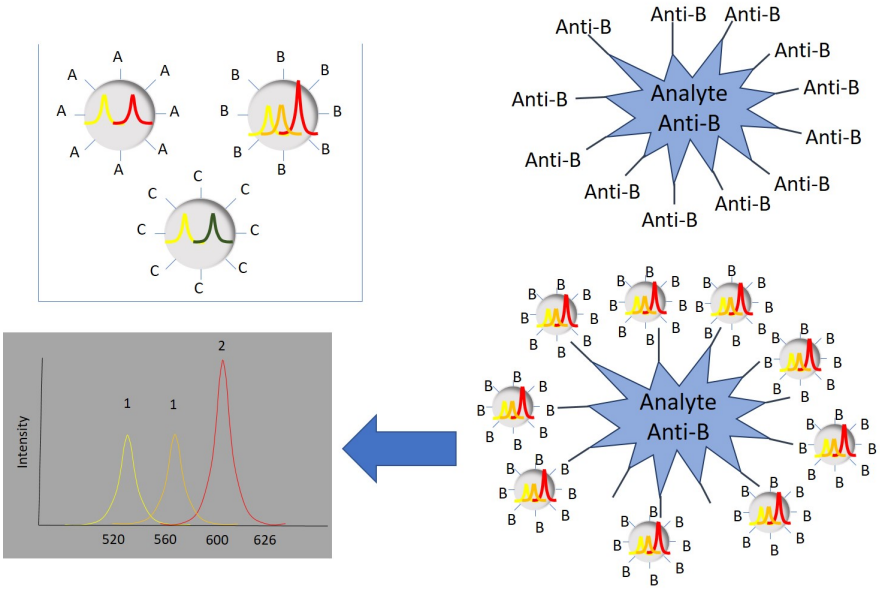

Figure 3.20 Schematic representation of a multiplexing assay.

A potential application of this work could be to functionalize the surface of the cross-linked core-shell PS/QDs/PMMA hybrid polymer particles with L-lysine. As shown previously by Holzapfel et al[15]., the surface of the polymer particles has to be firstly functionalized with carboxylic acid groups for then activating them and successfully coupling the lysine[15].

3.7. Conclusions

Trioctylphosphine oxide-hexadecylamine coated CdSe/CdS quantum dots were synthesized in supercritical hexane obtaining nanocrystals of different sizes and good optical properties, stable when dispersed in organic solvents. The aim was to encapsulate quantum

dots of different sizes in the polymer particles dispersion and to control the final fluorescence spectra. However, when carrying out the first step of the encapsulation by miniemulsion polymerization, fluorescence of the quantum dots was lost right after being in contact with the aqueous phase.

Therefore, commercial octadecylamine coated CdSe/ZnS quantum dots of four different sizes were used for the encapsulation of multiple quantum dots maintaining good optical properties in the final latex. The four of them were characterized both by fluorescence measurements and by TEM to calculate their size. It was determined that the fluorescence intensity of a QD dispersion (of any size) in solvent was proportional to the number concentration rather than the weight concentration. Thus, is was possible to prepare QD dispersions in solvents with the desired fluorescence spectrum by combination of the appropriate number of QDs of different sizes. Furthermore, it was observed that the absorption of the different QDs did not affect the emission intensity of the others present in the dispersion.

According to the results obtained in toluene dispersion, different QDs with wide enough separation of their fluorescence peaks were encapsulated together into cross-linked core-shell polystyrene/polymethyl methacrylate polymer particles. Two trials were done using the same number of particles for two different pairs of quantum dots with the idea of obtaining a fluorescence emission intensity ratio 1:1. Although the fluorescence ratio was the desired one in the miniemulsion, after the synthesis of the core-shell polymer particles this was lost obtaining a higher emission intensity for the bigger QDs. This happened no matter the combination of QDs used, probably because of an absorption-emission process occurring

between the quantum dot nanocrystals placed close enough to each other in the polymer particles.

To overcome this drawback waterborne polymer/dispersions using single size of QD were synthesized by the method developed in Chapter 2. Then, blends of dispersions containing different QD sizes were prepared. As in the previous case, different combinations were done taking into account both the number of QD particles to obtain the desired ratio, and the fluorescence emission peaks for each QD. Thus, a good control of the final fluorescence was achieved. This method opens the possibility to prepare dispersions with targeted fluorescence spectra by the combination of different hybrid latex dispersions.

3.8. References

(1) Cansell, F.; Aymonier, C.; Loppinet-Serani, A. Review on Materials Science and Supercritical Fluids. *Curr. Opin. Solid State Mater. Sci.* **2003**, *7* (2003), 331–340.

(2) Aymonier, C.; Loppinet-Serani, A.; Reverón, H.; Garrabos, Y.; Cansell, F. Review of Supercritical Fluids in Inorganic Materials Science. *J. Supercrit. Fluids* **2006**, *38* (2), 242–251.

(3) Cansell, F.; Aymonier, C. Design of Functional Nanostructured Materials Using Supercritical Fluids. *J. Supercrit. Fluids* **2009**, *47* (3), 508–516.

(4) Marre, S.; Park, J.; Rempel, J.; Guan, J.; Bawendi, M. G.; Jensen, K. F. Supercritical Continuous-Microflow Synthesis of Narrow Size Distribution Quantum Dots. *Adv. Mater.* **2008**, *20* (24), 4830–4834.

(5) Marre, S.; Baek, J.; Park, J.; Bawendi, M. G.; Jensen, K. F. High-Pressure/High-Temperature Microreactors for Nanostructure Synthesis. *JALA - J. Assoc. Lab. Autom.* **2009**, *14* (6), 367–373.

(6) Chakrabarty, A.; Marre, S.; Landis, R. F.; Rotello, V. M.; Maitra, U.; Guerzo, A. Del; Aymonier, C. Continuous Synthesis of High Quality CdSe Quantum Dots in Supercritical Fluids. *J. Mater. Chem. C* **2015**, *3* (29), 7561–7566.

(7) Giroire, B.; Marre, S.; Garcia, A.; Cardinal, T.; Aymonier, C. Continuous Supercritical

Route for Quantum-Confined GaN Nanoparticles. *React. Chem. Eng.* **2016**, *1* (2), 151–155.

(8) Chakrabarty, A.; Chatterjee, S.; Maitra, U. Cadmium Deoxycholate: A New and Efficient Precursor for Highly Luminescent CdSe Nanocrystals. *J. Mater. Chem. C* **2013**, *1* (11), 2136.

(9) Spinicelli, P.; Buil, S.; Quélin, X.; Mahler, B.; Dubertret, B.; Hermier, J. P. Bright and Grey States in CdSe-CdS Nanocrystals Exhibiting Strongly Reduced Blinking. *Phys. Rev. Lett.* **2009**, *102* (13).

(10) Greytak, A. B.; Allen, P. M.; Liu, W.; Zhao, J.; Young, E. R.; Popović, Z.; Walker, B.; Nocera, D. G.; Bawendi, M. G. Alternating Layer Addition Approach to CdSe/CdS Core/shell Quantum Dots with near-Unity Quantum Yield and High on-Time Fractions. *Chem. Sci.* **2012**, *3* (6), 2028–2034.

(11) Qu, L.; Peng, X. Control of Photoluminescence Properties of CdSe Nanocrystals in Growth. *J. Am. Chem. Soc.* **2002**, *124* (9), 2049–2055.

(12) Winter, J. O.; Gomez, N.; Gatzert, S.; Schmidt, C. E.; Korgel, B. A. Variation of Cadmium Sulfide Nanoparticle Size and Photoluminescence Intensity with Altered Aqueous Synthesis Conditions. *Colloids Surfaces A Physicochem. Eng. Asp.* **2005**, *254* (1–3), 147–157.

(13) Chen, Y.; Vela, J.; Htoon, H.; Casson, J. L.; Werder, D. J.; Bussian, D. A.; Klimov, V. I.;

Hollingsworth, J. A. “Giant” multishell CdSe Nanocrystal Quantum Dots with Suppressed Blinking. *J. Am. Chem. Soc.* **2008**, *130* (15), 5026–5027.

(14) Mahler, B.; Spinicelli, P.; Buil, S.; Quelin, X.; Hermier, J.-P.; Dubertret, B. Towards Non-Blinking Colloidal Quantum Dots. *Nat. Mater.* **2008**, *7* (8), 659–664.

(15) Holzapfel, V.; Lorenz, M.; Weiss, C. K.; Schrezenmeier, H.; Landfester, K.; Mailänder, V. Synthesis and Biomedical Applications of Functionalized Fluorescent and Magnetic Dual Reporter Nanoparticles as Obtained in the Miniemulsion Process. *J. Phys. Condens. Matter* **2006**, *18*, 2581–2594.

Chapter 4. Polymer particles containing CdSe/ZnS quantum dots and CeO_2 nanoparticles

*Part of this work has been accepted for its publication in Soft Matter (DOI: 10.1039/c7sm01747b).

4.1. Introduction

Waterborne-polymer-inorganic hybrid dispersions have attracted plenty of attention because in addition to the improvement of the performance in stablished applications, they allow targeting new applications that are out of reach of the conventional waterborne polymer latexes[1]. Thus, the inorganic materials offer the possibility to new functionalities. Although, commonly the incorporation of a single type of inorganic material is challenging, the incorporation of multiple inorganic nanoparticles with complementary functionalities is pursued in recent research works. The production of hybrid polymer/inorganic materials with multiple functionalities including quantum dots have already been studied; particularly for the fields of photovoltaics and biological applications[2–15].

Many examples of preparation of bifunctional polymeric fluorescent-magnetic particles bringing together different types of quantum dots and magnetic nanoparticles using diverse techniques can be found in literature[2–8,13–15]. Gaponik et al.[3] encapsulated together water-soluble CdTe quantum dots and magnetic nanoparticles in poly(styrene-sulfonate)-poly(allylamine hydrochloride) microcapsules (5.6 μm diameter) obtaining fluorescence stability in physiological buffer solutions during two weeks. In order to avoid the reabsorption of emitted light they used a concentration of magnetic nanoparticles more than an order of magnitude lower than for QDs. They obtained fluorescent capsules that can be externally externally controllable by a magnetic field. Mandal et al.[5] produced oil droplets containing core/shell CdSe/ZnS QDs and a ferrofluid composed of Fe_2O_3 nanoparticles. They studied the optical properties of the droplets by varying the concentration of QDs and Fe_2O_3 nanoparticles, observing that when increasing the concentration of ferrofluid in the droplets, fluorescence intensity decreased due to both static and dynamic fluorescence quenching. More recently,

Fischer et al.[15] synthesized magneto and light-responsive polymer particles. Magnetite was incorporated into polystyrene particles functionalized with phosphonate groups. This magnetic particles were further functionalize by crystalline CdS nanoparticles on their surface, obtaining raspberry like hybrid polymer particles.

Other important combinations have been made in the area of photovoltaics, in which the rise of solar cells market has motivated the improvement of their efficiency. For this, dye-sensitized solar cells have been developed, and as exposed in Chapter 1, taking advantage of the growth of quantum dots technology three different systems can be differentiated[10,12]. Semiconductor sensitized or p-n junction system is a clear example of combination of QDs with other semiconductors. This system takes advantage of the wide absorbance wavelength range of quantum dots, using them as light harvesters, for transferring the electrons to the TiO_2 nanoparticles contained in the electrode[10–12]. Kamat[12] studied deeply the QDs/TiO_2 system describing how fluorescence bleaching appears and depends on the QDs particle size when combining these two nanoparticles. This observation confirms the electron transfer from quantum dots to titanium oxide.

In this Chapter, the synthesis of multiparticle hybrid latexes and films by co-encapsulation of octadecylamine coated CdSe/ZnS quantum dots and cerium oxide nanoparticles is presented. The aim was to explore the potential synergies of the combination of both nanoparticles in a waterborne polymer dispersion and film. CeO_2 is known by good UV-Vis absorbance properties[16], and quantum dots present, as shown in previous chapters, exceptional fluorescence emission properties.

For this, and profiting from the good dispersability of both nanoparticles in styrene, their encapsulation into cross-linked core/shell PS/PMMA polymer particles was carried out by seeded semi-batch emulsion polymerization[17]. Furthermore, film-forming latexes were synthesized by the production of an additional MMA/BA/AA shell to the cross-linked core/shell particles, ending up with core/shell/shell hybrid polymer particles containing both QDs and CeO_2 nanoparticles.

The effect of cerium oxide nanoparticles on the optical properties of quantum dots was studied by measuring fluorescence emission intensity during storage at sunlight of toluene dispersions, latexes and films in which both nanoparticles were present.

4.2. Toluene dispersions of quantum dots and cerium oxide nanoparticles

As already discussed in previous Chapters octadecylamine coated CdSe/ZnS quantum dots were purchased in powder state, and hence it could be directly dispersed in the solvent or monomer. However, cerium oxide provided by Altana (BYK3812) was received in mineral spirits. Thus, they were first dried at 60ºC for two days in an oven and then the solid was powdered prior to use.

The study of the combination of quantum dots and cerium oxide was started in the simplest system, i.e. dispersions of both nanoparticles in different proportions exposed to daylight. Both quantum dots and cerium oxide nanoparticles were easily dispersed in toluene, obtaining transparent and stable dispersions independently of their concentration. Taking

advantage of this, toluene was the chosen as solvent to study the influence of cerium oxide on the emission fluorescence of quantum dots during storage. Mixtures of both types of nanoparticles at different ratios were prepared (Table 4.1) and left at daylight and ambient temperature in order to study how the increase in the concentration of CeO_2 nanoparticles affected the fluorescence emission intensity and the UV absorbance of the quantum dots during time. The concentration of QDs was maintained for all the samples.

Table 4.1 Mixture of quantum dots and cerium oxide dispersed in toluene in different weight ratios.

Sample	QDs/CeO_2 ratio
1	1:0
2	2:1
3	1:1
4	1:2
5	1:3
6	1:4
7	1:5

Fluorescence emission intensity of the different toluene dispersions were measured right after their preparation (Figure 4.1). It was observed that the emission intensity of dispersion with the lowest amount of CeO_2 (2:1 ratio) did not vary substantially compared to the QDs dispersion. However, when increasing the concentration of CeO_2 in the system, fluorescence intensity decreased proportionally.

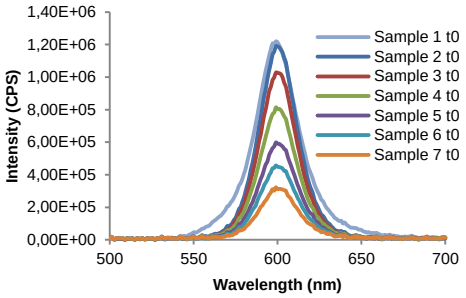

Figure 4.1 Fluorescence emission intensity of toluene dispersions containing different QDs:CeO_2 ratio.

Scattering measurements for samples 1 to 6 were carried out using a Zetasizer Nano Series (Malvern Instruments). The counts per second were analyzed observing an increase while increasing the concentration of CeO_2 in the dispersion. As it can be seen in Figure 4.2, adding CeO_2 to the system, fluorescence emission intensity decreases to more than a half the value obtained for a pure QDs dispersion, while scattering increases nearly to double its value. Therefore, the light scattering of the CeO_2 nanoparticles probably cause the decrease of the fluorescence emission intensity

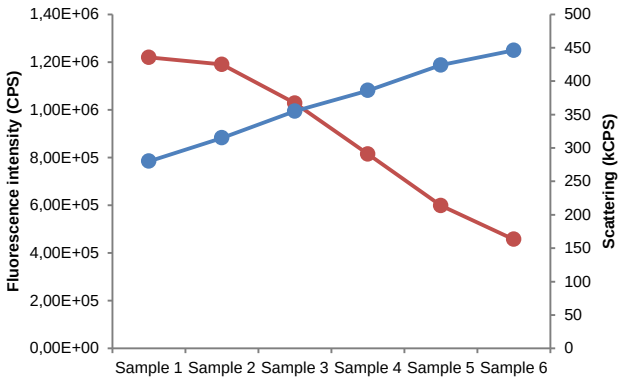

Figure 4.2 Comparison between the decrease of the fluorescence emission intensity and the increase of the scattering of samples 1 to 6.

The seven toluene dispersions were stored at daylight measuring their fluorescence emission intensity during time (Figure 4.3). In the case of the QDs dispersion, no changes in the emission intensity were observed over time under sunlight exposure. Regarding the dispersions containing both QDs and CeO_2, the same variations during time were observed in all the cases. Emission intensity slightly decreased during time when exposing the samples to sunlight in similar proportions independently of the ratio between the nanoparticles.

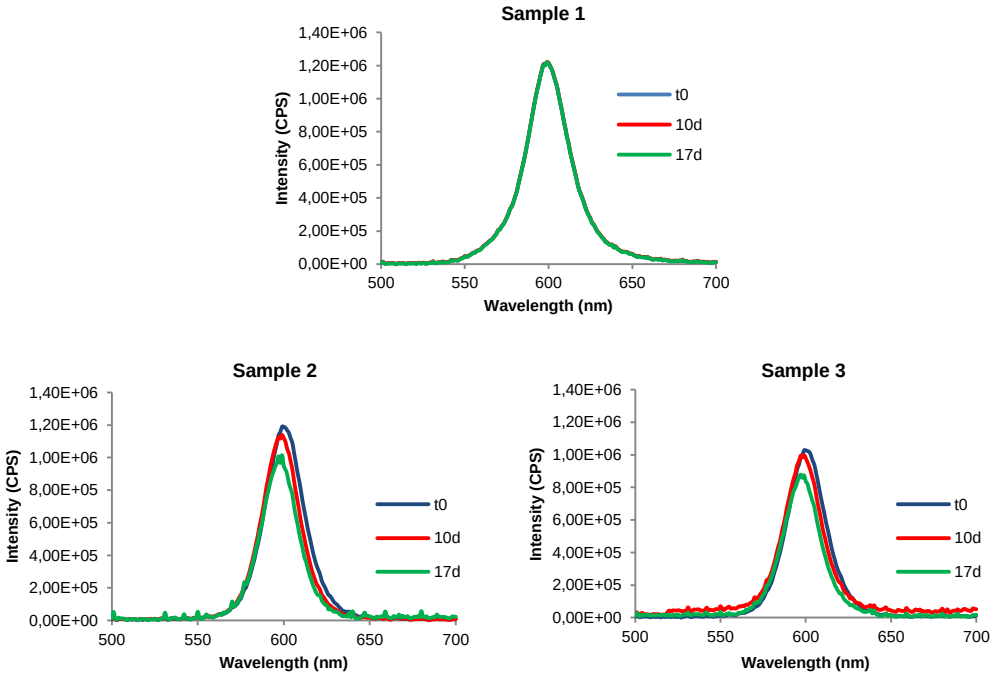

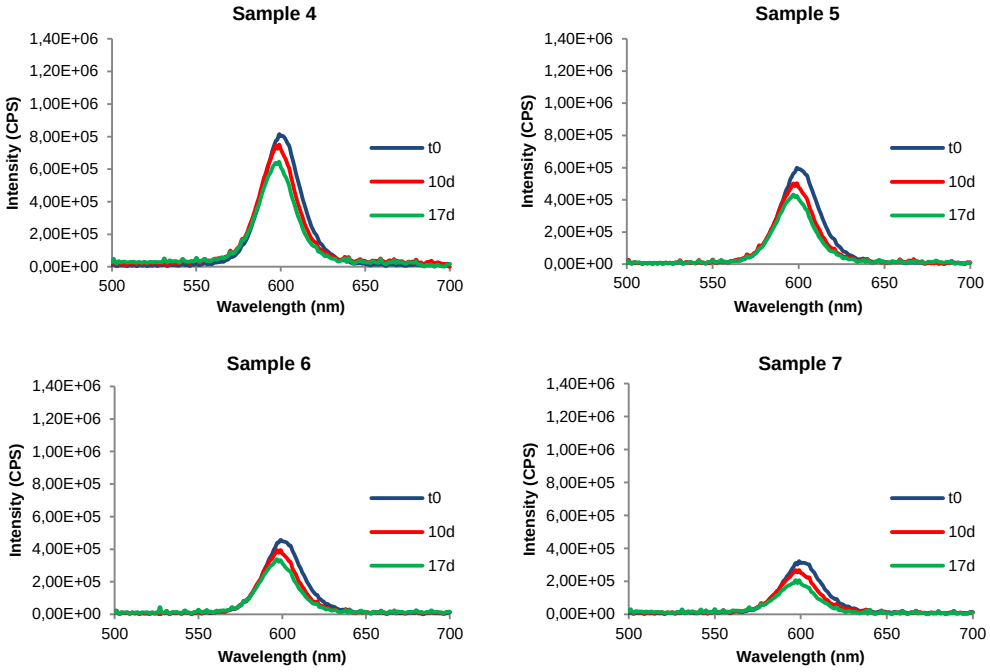

Figure 4.3 Fluorescence emission intensity evolution during exposure to daylight of the different toluene dispersions.

4.3. Multiparticle latexes

Hybrid cross-linked core/shell polymer particles were synthesized by seeded semi-batch emulsion polymerization following the same procedure described in Chapter 2 for the encapsulation of quantum dots. First, the seed latex was produced by miniemulsion polymerization of styrene and divinyl benzene in presence of the nanoparticles (QDs + CeO_2). Then a cross-linked polymethyl methacrylate shell was synthesized by feeding to the reactor a mixture of methyl methacrylate and divinyl benzene in starved conditions.

4.3.1. Morphology of hybrid cross-linked core/shell polymer/QDs-CeO_2 particles.

Morphology of the multifunctional cross-linked core/shell PS/QDs-CeO_2/PMMA polymer particles was studied by TEM. Figure 4.4 presents a TEM micrograph of a cross-linked core/shell latex with co-encapsulated QDs:CeO_2 in a weight ratio 1:1. It is remarkable that most of the polymer particles contained nanoparticles. Additionally, all the nanoparticles observed were placed in the polymer particles, not observing any in the aqueous phase, confirming a good encapsulation efficiency of both quantum dots and CeO_2 nanoparticles.

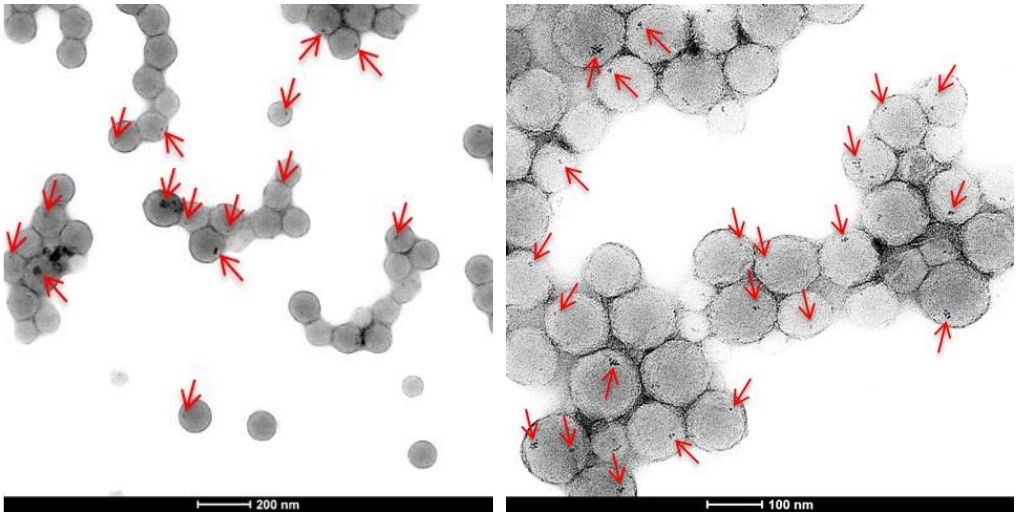

Figure 4.4 TEM micrograph of PS-DVB/QDs-CeO_2/PMMA-DVB polymer particles

In order to shed light on the identification of both types of nanoparticles, EDX analysis was carried out on this sample. For this, a High Resolution Transmission Electron Microscope (HRTEM-TITAN) was used in STEM mode. It is important to highlight that in this mode the

contrast is inverted with respect to normal TEM mode, that is, the more dense areas are seen in white and the less electron dense parts are seen darker. This can be observed in Figure 4.5a, in which the background is completely dark, observing the cross-linked core-shell PS/PMMA polymer particles in a light grey and white spots inside them that correspond to the inorganic nanoparticles. In the selected area, three out of four polymer particles contain inorganic nanoparticles. Moreover, the top polymer particle contains two inorganic nanoparticles. An EDX map of this area was done, highlighting the main elements that form the quantum dots and the cerium oxide (Cd, Se, Zn, S and Ce) (Figure 4.5b). Unfortunately, only the signals from the cadmium and the cerium elements (red and orange pixel images), were relevant; for the other elements only noise was measured (not presented). Based on these two elements (Cd and Ce) it is noticed that the bottom left polymer particle contains a quantum dot and the center polymer particle contains a CeO_2 aggregate. Regarding the top polymer particle, both Cd and Ce signals are observed next to each other, concluding that one QD nanocrystal and one CeO_2 nanoparticle are present. These results confirm the encapsulation of QDs and CeO_2 nanoparticles into the cross-linked core-shell PS/PMMA polymer particles, either into different or the same particle.

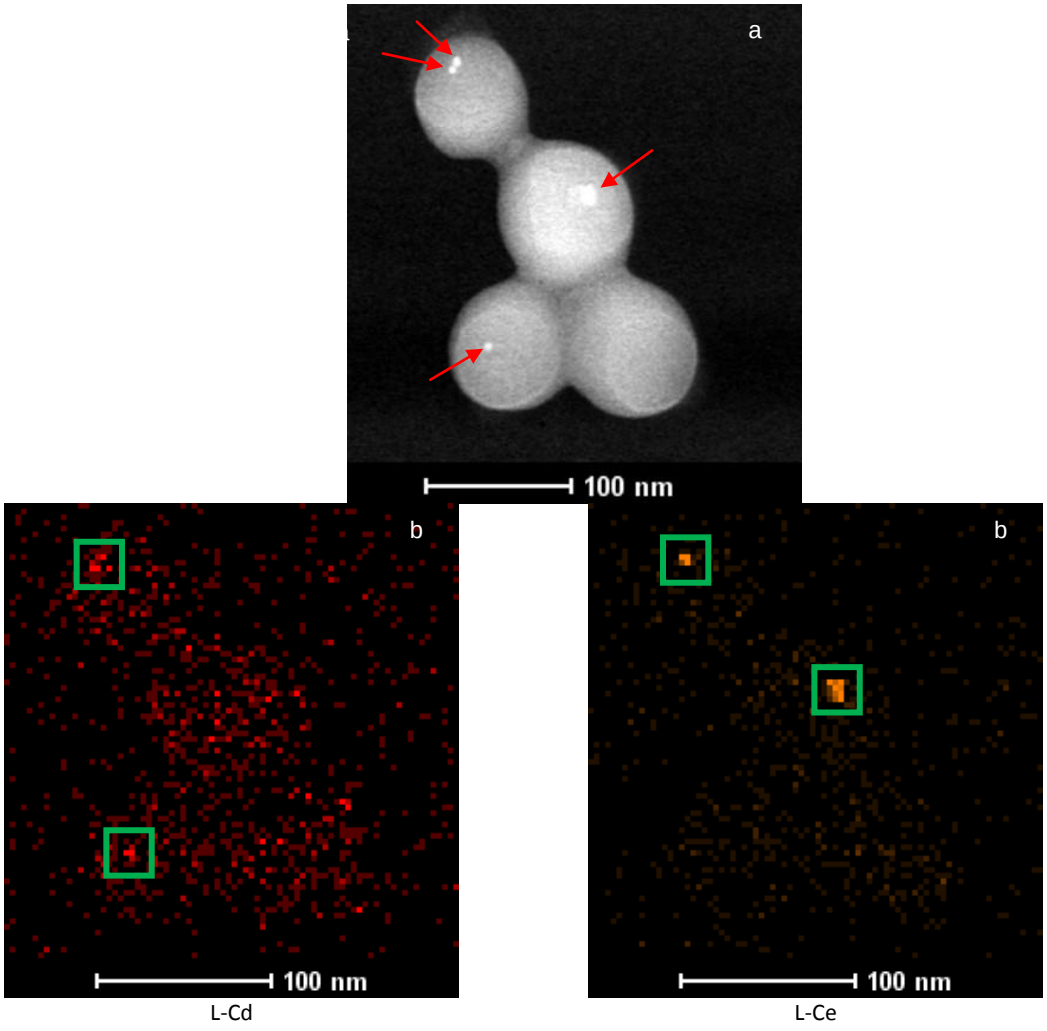

Figure 4.5 EDX analysis of a sample containing QDs and CeO_2 co-encapsulated into cross-linked PS/PMMA polymer particles (ratio 1:1). a) STEM image of the selected area. b) EDX mapping of the elements of interest (Cd, Ce).

4.3.2. Optical properties of QDs-CeO_2 multiparticle latexes

The effect of the addition of CeO_2 nanoparticles in the system in terms of optical properties was studied by comparing latexes containing QDs and CeO_2, in a ratio 2:1, and latexes containing only QDs. The latexes were diluted at the same QDs concentration and measured under the same conditions of excitation wavelength and slit opening. Figure 4.6 shows a comparison of their fluorescence emission spectra observing that both latexes presented the same emission intensity right after their synthesis. Hence, the coencapsulation of CeO_2 nanoparticles and CdSe/ZnS QDs did not change the fluorescence properties of the later.

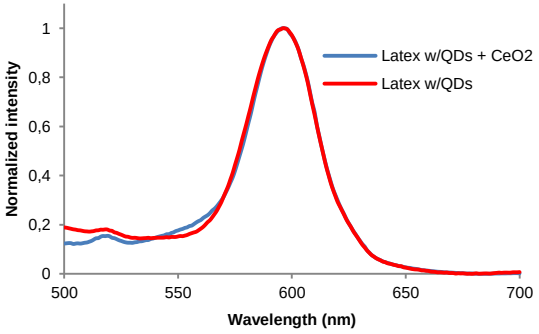

Figure 4.6 Comparison of fluorescence emission for latexes with the same concentration of quantum dots, with and without nanoceria.

Latexes containing QDs and CeO_2 and latexes only containing QDs were exposed to sunlight and stored in the dark monitoring their fluorescence emission intensity during storage time. Figure 4.7a presents the time evolution of the fluorescence spectrum of a latex containing QDs and CeO_2 in a ratio 2:1 in weight of nanoparticles, and Figure 4.7b presents the spectrum for a latex only containing QDs, being both exposed to daylight during the same time. A clear

increase in the fluorescence was observed for the one containing nanoceria and QDs, whereas for the hybrid QDs-polymer latex the variation in fluorescence intensity was negligible. Fluorescence emission intensity in the case of latexes containing QDs and CeO_2 increased 31% during the 18 days of exposure, while for the latex without nanoceria the variation observed was 0.8%.

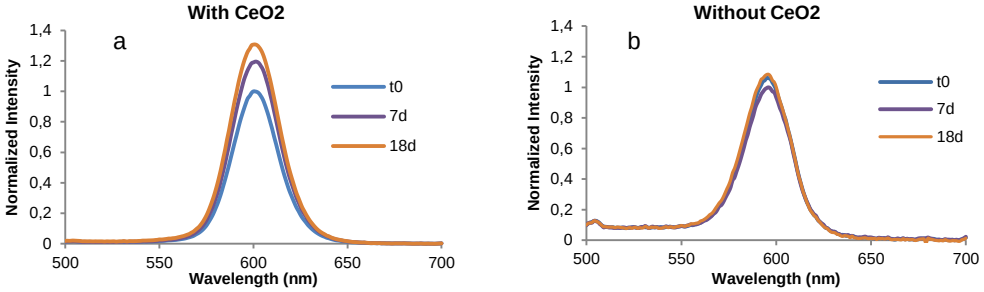

Figure 4.7 a) Fluorescence emission spectrum of latex containing both QDs and CeO_2 nanoparticles exposed to daylight during 18 days. b) Fluorescence emission spectrum of latex containing QDs exposed to daylight during 18 days.

In contrast, when the latexes where kept in the dark, the same behavior was found regardless of the presence or not of nanoceria in the polymer particles (Figure 4.8). A small decrease in fluorescence emission intensity was observed during the first three weeks but no further changes were measured afterwards. This is in agreement with the results presented in Chapter 2 in which emission intensity of the latexes containing QDs remained stable after a small decrease during 3 weeks of storage.

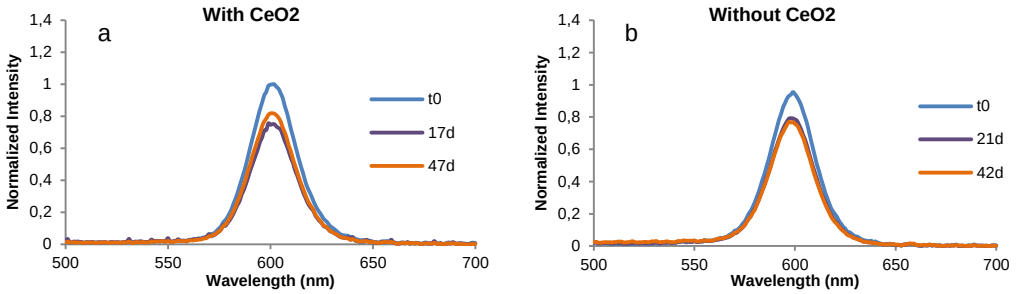

Figure 4.8 a) Fluorescence emission spectrum of latex containing QDs and CeO_2 nanoparticles stored in the dark during 47 days. b) Fluorescence emission spectrum of latex containing QDs stored in the dark during 42 days.

These results clearly indicate that CeO_2 nanoparticles are influencing the optical properties of the QDs when exposed to daylight. This behavior can be related to the antenna effect that CeO_2 nanoparticles can have on receiving incident optical radiation and transferring it to QDs enhancing their fluorescence[18,19]. This plasmonic effect could not explain the time dependence of the fluorescence increase by itself, but a change in the dielectric constant of the surrounding medium when exposed to light could account for the enhancement of the antenna phenomenon[20]. It must be said that the photoactivation of CdSe/ZnS observed in this work in the presence of CeO_2, cannot be directly related to the activation observed by other authors due to photocorrosion of freshly prepared QDs[21]. In these cases, the photoactivation is due to the oxidation of the surface defects in the presence of O_2 and light excitation, and it is accompanied by a blue shift due to a decrease in QD nanoparticle size. In our case, the fluorescence of bare QDs was completely stable under O_2 and light both in toluene and encapsulated in polymer particles, and it is the presence of CeO_2 which produces the photoactivation.

In an attempt to understand the effect of the CeO_2 nanoparticles on the fluorescence emission of QDs when both are co-encapsulated into polymer nanoparticles, latexes containing different weight ratios of QDs:CeO_2 nanoparticles were synthesized by means of the method

described above, and their fluorescence emission intensity during storage at daylight was monitored over time. Figure 4.9 shows how fluorescence emission intensity varied when latexes were exposed to daylight during 17 days and Table 4.2 summarizes the increase of fluorescence emission intensity for each case taking the value at t_0 as reference. It can be seen that, contrary to what happened for the toluene dispersions, when increasing the concentration of nanoceria up to five times the concentration of QDs, fluorescence emission intensity increased during storage at daylight. It was observed that, the nanoparticle ratio strongly influenced the increase in fluorescence emission. Interestingly, the highest increase in fluorescence emission intensity was obtained for a QDs:CeO_2 ratio of 1:2. For this ratio the intensity increased by 225% after 10 days, and it even kept increasing after those days of exposure, while for 1:1 and 1:5 ratios the increment was of 80% and 125% respectively after 10 days, but then the emission intensity was maintained almost constant. In the case of ratio 1:2 the increase of fluorescence emission intensity did not stop after 17 days but after around 40 days. However, this increase was very low compared to the one observed during the period showed.

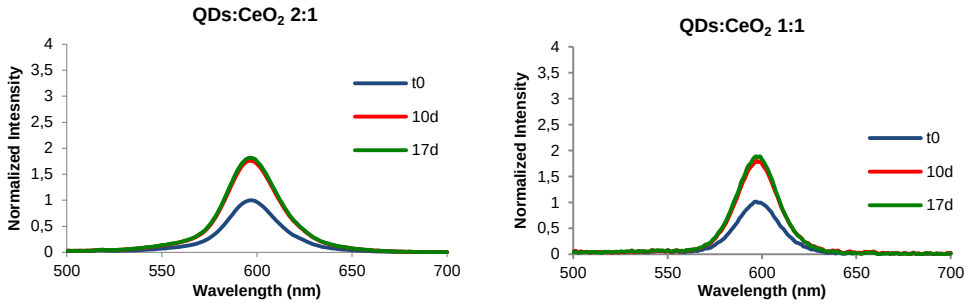

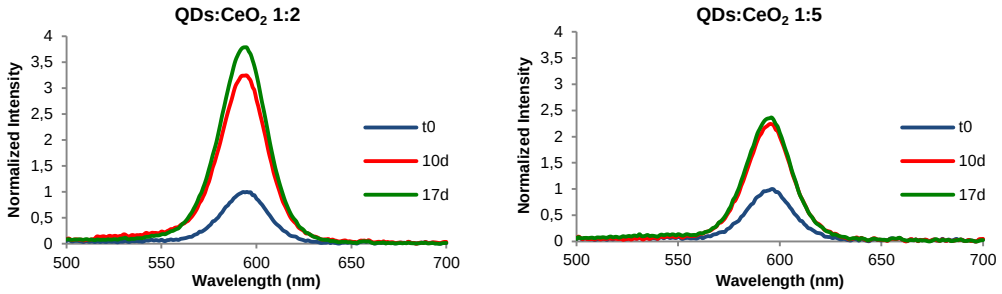

Figure 4.9 Fluorescence emission spectra of latexes containing different QDs:CeO_2 ratios when exposed to daylight.

Table 4.2 Fluorescence emission intensity increase during storage at daylight of latexes with different QDs:CeO_2 ratios.

Sample	t_0 - day 10	Day 10 - day 17	Total increase
1:0.5	76%	6%	82%
1:1	80%	9%	89%
1:2	225%	54%	279%
1:5	124%	12%	136%

For the sake of understanding the reasons of the interaction of the CeO_2 nanoparticles on the fluorescence emission of QDs, the nanoparticles were encapsulated individually in polymer particles and then blended. The fluorescence emission of the blend was monitored during time. Blends were prepared by mixing the latexes for obtaining weight ratios 1:1 and 1:2 of QD:CeO_2 nanoparticles.

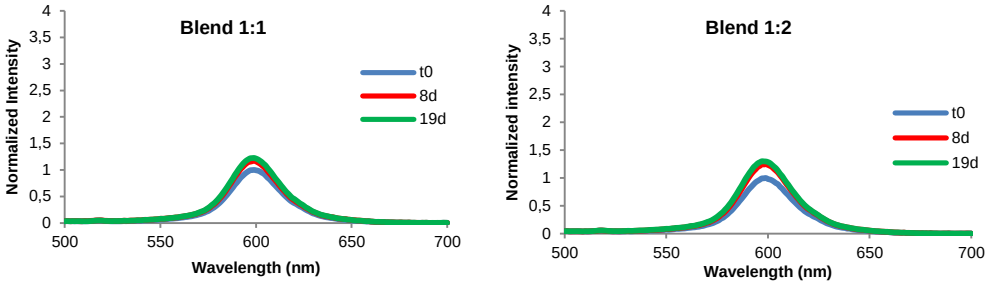

Figure 4.10 Fluorescence emission intensity evolution during exposure to sunlight of the blend latexes in a ratio of nanoparticles QDs:CeO_2 1:1 and 1:2 in weight.

Both were stored at daylight as done for the co-encapsulated hybrid latexes, and fluorescence was measured over time. The same behavior was observed in both cases; a small increase of the fluorescence emission intensity during the first 8 days of exposure, and then stable emission during time (Figure 4.10). The increment was slightly higher in the case of the 1:2 blend, which was in agreement with the behavior found for the hybrid latexes with co-encapsulated QDs and CeO_2 nanoparticles. However, the magnitude of increase for each ratio is substantially smaller, 23% for the blend 1:1 and 30% for the blend 1:2 in 19 days, whereas for the co-encapsulated latexes this increase was of 89% and 279%, respectively.

This result indicated that the presence of the CeO_2 nanoparticles in separate polymer particles and hence at longer distances, does not affect the environment of the QDs and their fluorescence emission intensity in the same manner. The shorter the distance between the nanoparticles, the higher the influence on the optical properties of the environment of the QDs, and hence stronger the effect on the fluorescence emission.

Based on these results for cross-linked core/shell hybrid latexes with co-encapsulated quantum dots and cerium oxide nanoparticles, it is clear that cerium oxide has a strong impact on the optical properties of the quantum dots leading to an enhancement of their fluorescence emission when exposing the latex to daylight. This influence was found to be stronger when the ratio QDs/CeO_2 was 1:2. On the other hand, it is worth to point out that CeO_2 nanoparticles did not affect the fluorescence stability during storage when the samples were not exposed to light.

4.4. Synthesis of hybrid films containing QDs and CeO_2

The hybrid cross-linked core/shell PS/QDs-CeO_2/PMMA latexes did not produce continuous films at room temperature because of the high Tg and the cross-linking of the polymer that do not favor the deformation of the particles in order to produce continuous films at room temperature. Therefore, in order to obtain good quality continuous and transparent hybrid films, the hybrid core/shell latex was used as seed in semi-batch emulsion polymerization aiming the production of a film forming shell by copolymerizing MMA/BA/AA under starved feed conditions. The seeded semi-batch emulsion copolymerization was carried out in a 50 ml round bottom flask adding the seed, the initiator solution (KPS 0.5 wbm%) in a shot and feeding the monomer mixture MMA/BA/AA in a ratio 39.5%/59.5%/1% employing a syringe pump at a feeding rate of 0.12 g/min. The polymerization was carried out at 75ºC for 3 hours obtaining latexes with 20% S.C.

Regarding the thickness of this second shell, it was proved that it has to be at least as thick as the cross-linked polymethyl methacrylate shell to obtain continuous and transparent

films; namely the MMA/BA/AA monomer mixture should be at least 60% of the total polymer in weight.

Minimum film formation temperature of the films was determined using a minimum film forming temperature bar obtaining a result of 15ºC. Taking this into account, films were casted into silicon molds and dried at 23±2ºC and 55±5% humidity obtaining continuous, transparent and flexible material.

4.4.1. Morphological analysis of film forming latexes and films

The analysis of the morphology of the hybrid core-shell-shell latex was done by TEM. According to some reports, the addition of hydroxyethyl cellulose (HEC) to low Tg latexes keeps the spherical shape of the polymer particles preventing from deformation during the sample preparation[22]. Figure 4.11 presents the TEM images of the film forming latex particles prepared by this method. Figure 4.11a shows a low magnification image which one can clearly distinguish the hard core (dark) and the soft film forming shell (grey) but not the inorganic nanoparticles. Some of the inorganic nanoparticles can be better distinguished in the high magnification images (Figure 4.11b and c), and they are at the edge or at the interface between the hard and soft phases.

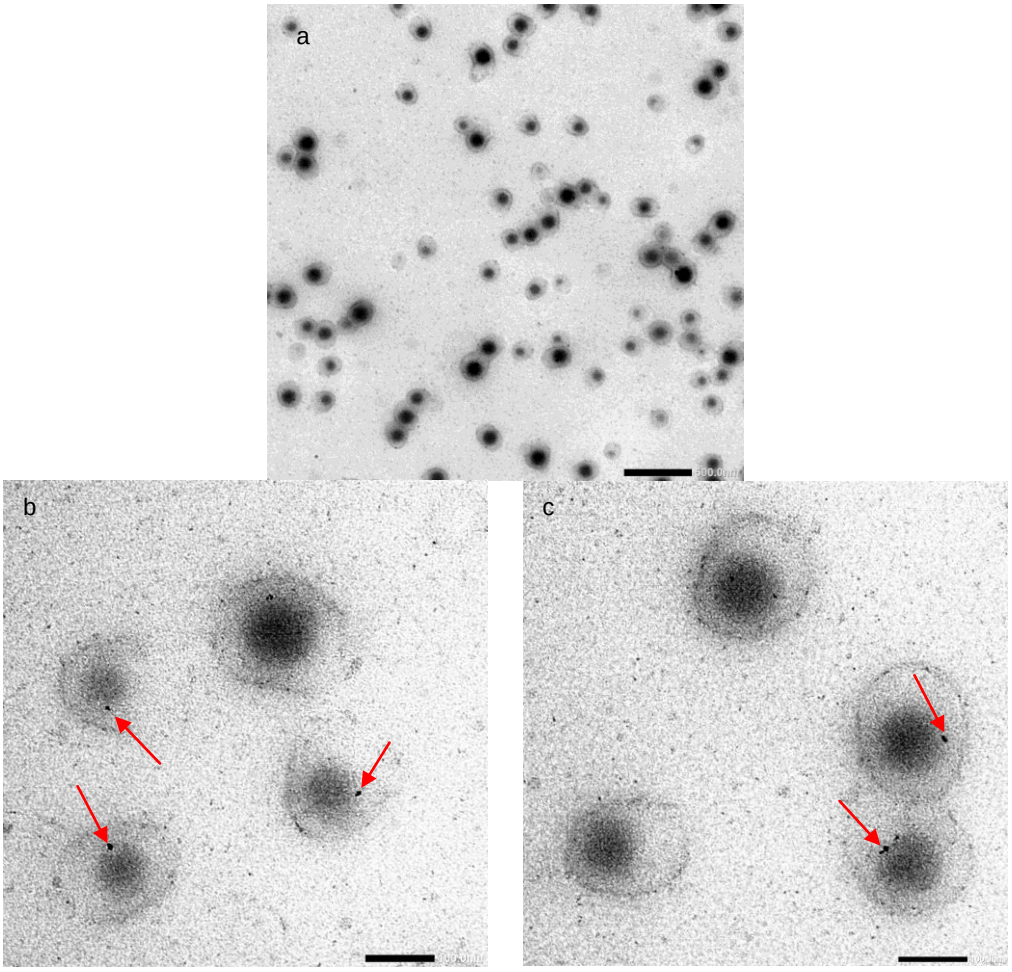

Figure 4.11 TEM micrographs of core/shell/shell hybrid polymer particles containing QDs and CeO_2 nanoparticles after the addition of a 0.06% wt HEC, a) at low magnification (scale bar 500 nm), b) c) at higher magnification distinguishing the inorganic nanoparticles into the hard part of the polymer particles (scale bar 100 nm).

Regarding the morphology of the films, those were cast in silicon molds as described above, at 23ºC and 55% humidity and trimmed with an ultra microtome device (Leica EMFC6) equipped with a diamond knife. The sections of 100 nm thickness obtained were placed on 300 mesh copper grids and observed by TEM without further treatment (Figure 4.12).

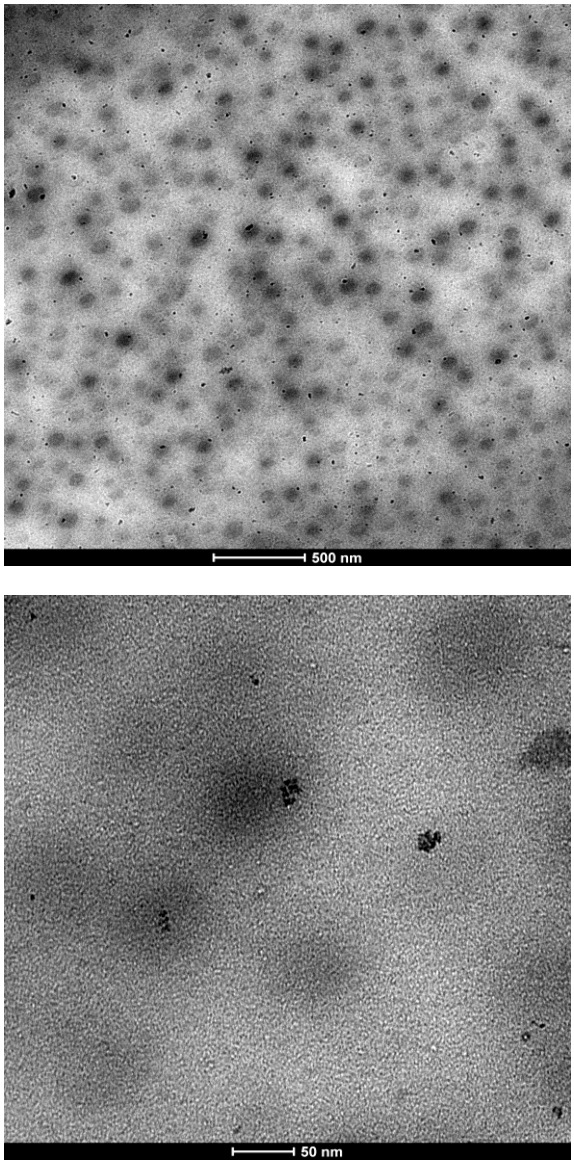

Figure 4.12 TEM micrographs of hybrid films containing QDs and CeO_2 nanoparticles.

As it can be observed in the above micrographs, the hardest part of the film forming particles (PS/PMMA) stands out as dark grey particles from the poly(MMA-co-BA-co-AA) background that forms the film. The inorganic nanoparticles are distinguished as black spots at the edge of the hard particles, showing that the formation of the film does not affect the position of the nanoparticles in the polymer particles.

4.4.2. Optical properties of the films

Films were cast from latexes containing both QDs and CeO_2 and only QDs. During the drying time, no differences in color between a film containing both quantum dots and cerium oxide and a film only containing quantum dots were observed. However, when the films containing both nanoparticles was removed from the mold and exposed to daylight it became reddish as seen in Figure 4.13a. Clearly the film was emitting light under the influence of normal daylight. In contrast, a film cast from a latex containing only quantum dots (Figure 4.13b) did not show such a reddish color and was transparent.

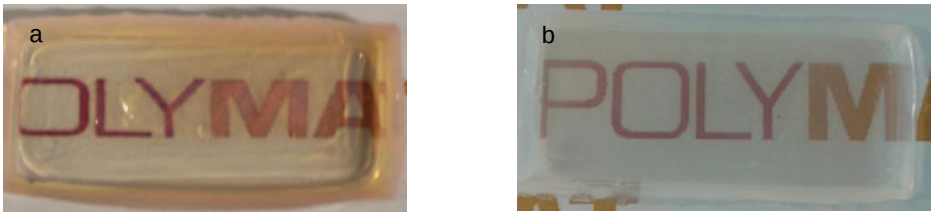

Figure 4.13 a) Hybrid QDs/CeO_2 film exposed to daylight. b) Hybrid QDs film exposed to daylight.

The homogeneity of the fluorescence in the hybrid film was studied by fluorescence microscopy. Figure 4.14 shows homogeneous fluorescence along the film, concluding that the QDs did not aggregate during the film formation.

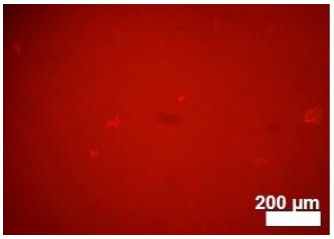

Figure 4.14 Fluorescence image of a film with a homogeneous fluorescence distribution.

Moreover, as done for the toluene dispersions and the latexes where QDs and CeO_2 were mixed and co-encapsulated respectively, fluorescence of the films was measured during storage at daylight.

Figure 4.15 shows a comparison between the fluorescence emission intensity of a film containing only QDs and a film in which both QDs and CeO_2 nanoparticles were present. Both films were stored at daylight during 20 days measuring their fluorescence emission intensity along time. Measurements were done to thin films cast in a quartz support, and carried out directly in the spectrofluorometer taking advantage of the homogeneous distribution of the fluorescence showed above.

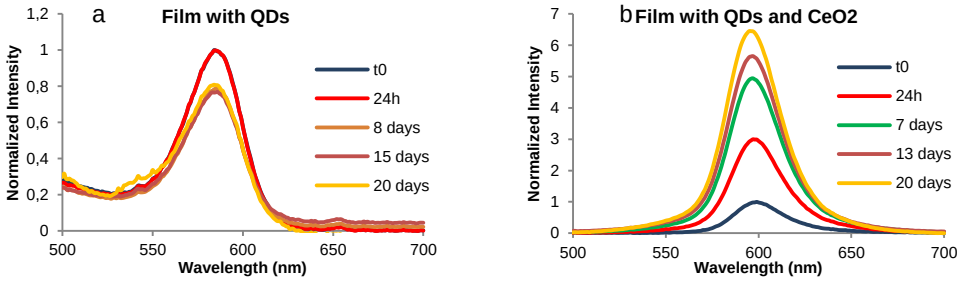

Figure 4.15 Fluorescence emission intensity evolution of a) hybrid polymer/QDs film and b) hybrid polymer/QDs/CeO_2 film during storage at sunlight.

As it can be observed in Figure 4.15a, the film containing only quantum dots did not present any variation on the fluorescence emission intensity during storage at daylight.

In the case of the hybrid QDs/CeO_2 films enormous variations in fluorescence emission intensity were measured (Figure 4.15b). Note that the nanoparticles´ ratio in the film forming latex was QDs/CeO_2 1:2, for which in the core/shell latex a much smaller increase in the emission intensity was noticed (see Figure 4.9 and Table 4.2). Nevertheless, in the film the intensity increase was large during the first 24 hours and kept growing during the 20 days of measurement. The total increase was calculated to be of 545%, much higher than the 82% calculated for the corresponding hybrid core/shell latex.

The higher increase of fluorescence emission intensity observed for the hybrid films with respect to hybrid latex when exposed to sunlight, can be explained considering the different environments surrounding the QD nanoparticles when they are dispersed in polymer particles or when they are fixed upon film formation. Neighboring particles that might also contain CeO_2 nanoparticles are substantially closer and hence affecting their optical properties. This is illustrated with a cartoon in Figure 4.16. As it can be seen in the dispersed system (hybrid latex) the environment of the QDs is only affected by the CeO_2 in polymer particles that contain both inorganic nanoparticles (note that the inorganic nanoparticles are statistically distributed in the polymer particles based on their abundance during the miniemulsification step, as already seen in Chapter 2 for hybrid particles containing QDs). However, in the hybrid films the environment of the QDs, in absence of the surrounding water, might also be affected by neighboring polymer particles that contain CeO_2 (or both nanoparticles). As indicated by the green circles the number of particles affecting the environment of QDs in substantially enhanced and this is likely the reason for the increase in the fluorescence emission of the films.

In fact, if the average interparticles space (IPS) is calculated for inorganic nanoparticles in the latex (QD/CeO_2 1:2 latex), assuming a random and homogenous distribution, it would be 106 nm, while the IPS of the inorganic nanoparticles in the polymeric dry film would be 58 nm. This explanation is also valid for the differences found in the fluorescence emission intensity between toluene dispersions of both nanoparticles, latex particles containing both nanoparticles and blends of latexes containing QDs on one side and CeO_2 nanoparticles on the other.

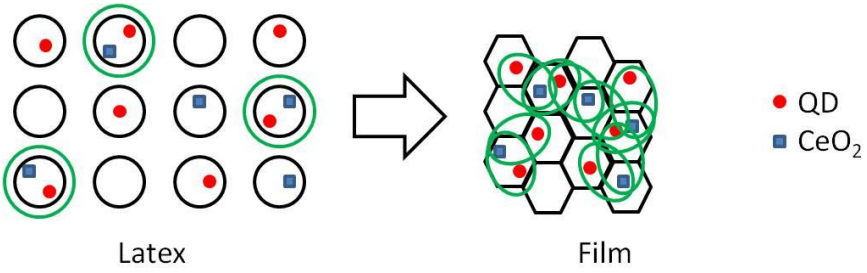

Figure 4.16 Cartoon of the environments seen by QD nanoparticles in a polymer latex and film made out of the same latex.

Further proof of the hypothesis presented above was obtained by preparing two latexes: one containing only CeO_2 nanoparticles (synthesized following the procedure described in Aguirre et al[23]) and the other containing only QDs synthesized the seeded semi-batch emulsion polymerization procedure described along this thesis. A film was made out of this mixture with a QD/CeO_2 ratio 1:2, and its fluorescence was monitored over time when stored in daylight. The evolution of the fluorescence is presented in Figure 4.17. Clearly, the fluorescence intensity increases substantially (more than 300% in 12 days), which again indicated that the environment of the QD nanoparticles is affected by CeO_2 nanoparticles located at short

distances in the film, in agreement with the cartoon in Figure 4.16. However, in this case the distances are not as short as when both nanoparticles were co-encapsulated and hence this is reflected in a lower increase of the fluorescence.

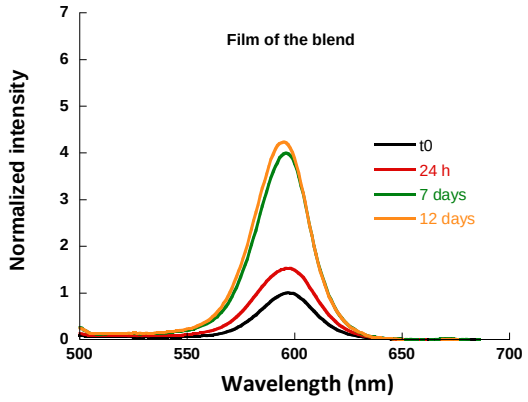

Figure 4.17. Fluorescence emission intensity over time in daylight of a film obtained from the mixture of two latexes: one containing only encapsulated CeO_2 and other containing only encapsulated QDs.

4.5. Conclusions

A deep study of the effect of CeO_2 on QDs optical properties has been done. Starting from the simplest system, toluene dispersions of mixtures of both nanoparticles in different ratios in which no relevant variations in fluorescence emission were observed. Then, latexes with four different QDs:CeO_2 ratios were synthesized and fluorescence emission intensity was measured over storage at daylight observing in all the cases an increase of the emission intensity during time. A dependence between the variation of the emission and the ratio of the weight of the nanoparticles was observed, obtaining a greater increase for the case of the ratio QDs:CeO_2 1:2.

Blends between one latex with encapsulated quantum dots and another one with encapsulated CeO_2 were done in two different ratios observing the same behavior in both cases. In those cases, there were only slight variations in the fluorescence emission intensity, determining that, as the distance between both nanoparticles was higher, the effect of CeO_2 was attenuated.

In the last part, core/shell/shell film forming latexes with QDs and QDs and CeO_2 co-encapsulated in the core were synthesized. From these latexes good quality homogeneous and transparent films were obtained at ambient temperature. Fluorescence of the films was studied by fluorescence microscopy observing that it was homogeneous along them, not observing aggregates of the nanoparticles. A long-term study of the evolution of fluorescence in films containing only QDs or QDs and CeO_2 was carried out by exposing them to daylight during 20 days. It was observed that, in the case of a film containing both nanoparticles fluorescence emission intensity increased 545% in 20 days, whereas for the film only containing QDs, fluorescence was stable during time.

Fluorescence enhanced latexes and films were obtained by the successful co-encapsulation of octadecylamine coated CdSe/ZnS quantum dots and cerium oxide nanoparticles into colloidal polymer particles.

4.6. References

(1) Paulis, M.; Asua, J. M. Knowledge-Based Production of Waterborne Hybrid Polymer Materials. *Macromol. React. Eng.* **2016**, *10* (1), 8–21.

(2) Caruge, J. M.; Halpert, J. E.; Wood, V.; Bulović, V.; Bawendi, M. G.; Caruge, J. M.; Halpert, J. E.; Wood, V.; Bulovic, V. Colloidal Quantum-Dot Light-Emitting Diodes with Metal-Oxide Charge Transport Layers. *Nat. Photonics* **2008**, *2* (4), 247–250.

(3) Gaponik, N.; Radtchenko, I. L.; Sukhorukov, G. B.; Rogach, A. L. Luminescent Polymer Microcapsules Addressable by a Magnetic Field. *Langmuir* **2004**, *20* (4), 1449–1452.

(4) Wang, D.; He, J.; Rosenzweig, N.; Rosenzweig, Z. Superparamagnetic Fe 2 O 3 Beads − CdSe / ZnS Quantum Dots Core − Shell Nanocomposite Particles for Cell. *Nano Lett.* **2004**, *4* (3), 3–7.

(5) Mandal, S. K.; Lequeux, N.; Rotenberg, B.; Tramier, M.; Fattaccioli, J.; Bibette, J.; Dubertret, B. Encapsulation of Magnetic and Fluorescent Nanoparticles in Emulsion Droplets. *Langmuir* **2005**, *21* (9), 4175–4179.

(6) Selvan, S. T.; Patra, P. K.; Ang, C. Y.; Ying, J. Y. Synthesis of Silica-Coated Semiconductor and Magnetic Quantum Dots and Their Use in the Imaging of Live Cells. *Angew. Chemie - Int. Ed.* **2007**, *46* (14), 2448–2452.

(7) Tu, C.; Yang, Y.; Gao, M. Preparations of Bifunctional Polymeric Beads Simultaneously Incorporated with Fluorescent Quantum Dots and Magnetic Nanocrystals. *Nanotechnology* **2008**, *19* (10), 105601.

(8) Zeng, H.; Sun, S. Syntheses, Properties, and Potential Applications of Multicomponent Magnetic Nanoparticles. *Adv. Funct. Mater.* **2008**, *18* (3), 391–400.

(9) Shockley, W.; Queisser, H. J. Detailed Balance Limit of Efficiency of P-N Junction Solar Cells. *J. Appl. Phys* **1961**, *32* (3), 510–519.

(10) Nozik, A. . Quantum Dot Solar Cells. *Phys. E Low-dimensional Syst. Nanostructures* **2002**, *14* (1–2), 115–120.

(11) Robel, I.; Kuno, M.; Kamat, P. V. Size-Dependent Electron Injection from Excited CdSe Quantum Dots into TiO 2 Nanoparticles. *J. Am. Chem. Soc.* **2007**, *129* (14), 4136–4137.

(12) Kamat, P. V. Quantum Dot Solar Cells. Semiconductor Nanocrystals as Light

Harvesters. *J. Phys. Chem. C* **2008**, *112* (48), 18737–18753.

(13) Erogbogbo, F.; Yong, K.-T.; Hu, R.; Law, W.-C.; Ding, H.; Chang, C.-W.; Prasad, P. N.; Swihart, M. T. Biocompatible Magnetofluorescent Probes: Luminescent Silicon Quantum Dots Coupled with Superparamagnetic Iron(III) Oxide. *ACS Nano* **2010**, *4* (9), 5131–5138.

(14) Ning, Y.; Wang, C.; Ngai, T.; Yang, Y.; Tong, Z. Hollow Magnetic Janus Microspheres Templated from Double Pickering Emulsions. *RSC Adv.* **2012**, *2* (13), 5510.

(15) Fischer, V.; Bannwarth, M. B.; Jakob, G.; Landfester, K.; Muñoz-Espí, R. Luminescent and Magnetoresponsive Multifunctional Chalcogenide/polymer Hybrid Nanoparticles. *J. Phys. Chem. C* **2013**, *117* (11), 5999–6005.

(16) Aguirre, M.; Paulis, M.; Leiza, J. R. UV Screening Clear Coats Based on Encapsulated CeO2 Hybrid Latexes. *J. Mater. Chem. A* **2013**, *1* (9), 3155.

(17) De San Luis, A.; Bonnefond, A.; Barrado, M.; Guraya, T.; Iturrondobeitia, M.; Okariz, A.; Paulis, M.; Leiza, J. R. Toward the Minimization of Fluorescence Loss in Hybrid Cross-Linked Core-Shell PS/QD/PMMA Nanoparticles: Effect of the Shell Thickness. *Chem. Eng. J.* **2017**, *313*, 261–269.

(18) Pelton, M.; Aizpurua, J.; Bryant, G. Metal-Nanoparticle Plasmonics. *Laser Photonics Rev.* **2008**, *2* (3), 136–159.

(19) Novotny, L. From near-Field Optics to Optical Antennas. *Phys. Today* **2011**, *64* (7), 47–52.

(20) Motl, N. E.; Smith, A. F.; DeSantis, C. J.; Skrabalak, S. E. Engineering Plasmonic Metal Colloids through Composition and Structural Design. *Chem. Soc. Rev.* **2014**, *43* (11), 3823–3834.

(21) Wang, Y.; Tang, Z.; Correa-Duarte, M. A.; Pastoriza-Santos, I.; Giersig, M.; Kotov, N. A.; Liz-Marzán, L. M. Mechanism of Strong Luminescence Photoactivation of Citrate-Stabilized Water-Soluble Nanoparticles with CdSe Cores. *J. Phys. Chem. B* **2004**, *108* (40), 15461–15469.

(22) Geng, X.; Zhai, M. X.; Sun, T.; Meyers, G. Microscopy Microanalysis Morphology Observation of Latex Particles with Scanning Transmission Electron Microscopy by a Hydroxyethyl Cellulose Embedding Combined with RuO 4 Staining Method. *Microsc. Microanal.* **2013**, *19*, 319–326.

(23) Aguirre, M.; Paulis, M.; Leiza, J. R. UV Screening Clear Coats Based on Encapsulated CeO2 Hybrid Latexes. *J. Mater. Chem. A* **2013**, *1* (9), 3155.

Chapter 5. Potential applications of the synthesized hybrid polymer/quantum dots latexes

*This work has been carried out in collaboration with Tecnalia.

5.1. Introduction

As presented in Chapter 1, quantum dots can be used for several applications such as biological labeling, multiplexing assays, solar cells and LEDs in combination with polymers, in photocatalysis and as volatile organic compounds (VOCs) sensors. This is possible thanks to their exceptional optical and electronic properties, that lead to an improvement of either the optical stability or the electron transport in the device. In this project, an efficient encapsulation of CdSe/ZnS quantum dots into cross-linked core-shell PS/PMMA polymer particles with a good optical stability was achieved opening the door to some applications. Moreover, in Chapter 3 a great control of the fluorescence of the hybrid latexes containing different QDs sizes was demonstrated, introducing the possibility of using the produced blends for biological labeling and multiplexing assays.

Gas and/or VOC sensing is a recent area of interest for quantum dots[1–6]. Gas sensing for semiconductor gas sensors is based on interactions on the surface of the sensor such as adsorption-desorption (reduction-oxidation) that generates an electrical signal upon contacting with a gas or vapor (Figure 5.1). The adsorption process of oxygen takes place in absence of the gas of interest. The atmospheric oxygen adsorbs on the sensor´s surface taking an electron from the semiconductor material and forming species as O^-, O^{2-} or O_2^-. This leads to a reduction in the number of charges on the surface of the sensor, so to an increase of the resistance, which is the parameter usually used for the characterization of a sensor against a gas or vapor. Adsorption is both temperature and composition dependent, so studies carried out with different QD types and at different temperatures can be found in literature[7]. When exposing the sensor to the gas or vapor of interest, this reacts with the previously adsorbed

oxygen on the surface of the sensor, injecting electrons to the surface and resulting in a decrease of the resistance of the sensor. Thanks to this increase and decrease of the resistance the sensitivity and selectivity of the sensor can be characterized[8,9].

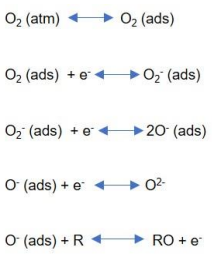

Figure 5.1 Adsorption-desorption process taking place in the sensor surface before and when exposed to a gas or vapor[7].

The resistance of semiconductor metal oxides such as ZnO and SnO_2 is very sensitive to these processes, so they have been extensively used as gas sensors[10]. However, this process can be improved by using quantum dots. Their large surface to volume area enhances the selectivity and sensitivity of the gas sensor[11,12]. Some recent articles show this improvement using metal oxide QDs synthesized using different techniques and validated against different gases. For example, Forleo et al[1] synthesized ZnO QDs by a wet chemical procedure[13] obtaining nanoparticles ranging in size from 2.5 nm to 4.5 nm in diameter. The sensor device was prepared by drop-casting deposition of the nanocrystals onto an alumina substrate. Their response was studied by applying a voltage of 4 V between the electrodes and measuring the circulating current when exposing the sensor to a gas or vapor. The response of the sensor was assessed when exposed to NO_2, acetone and methanol at different temperatures. They achieved a good and selective response to NO_2 at low concentration and temperature, but poor responses to methanol and acetone. On the other hand, Nath et al[2]

synthesized ZnO quantum dots embedded in a polyvinylpyrrolidone (PVP) matrix by quenching method, to measure the response to acetone vapor. The authors of this publication carried out the sensing test to acetone into a silica tube introduced into a tubular furnace, controlling both the temperature (200-360ºC) and the acetone concentration (100-500 ppm). They observed response of the ZnO sensor at low concentrations of acetone vapor (100 ppm), being maximum at 300ºC. Other metal oxides, such as SnO_2, have been used as gas sensors[3]. In this work, the authors synthesized SnO_2 QDs by sonochemical method, and showed the selectivity of the sensor to carbon monoxide over methane in a mixture of both gases below 375ºC. However, not only metal oxides are suitable as gas sensors, colloidal PbS has also been studied to detect gases as NO_2[4] and H_2S[5]. In the first case, a flexible device constructed on a paper substrate with fast response and high selectivity to NO_2 at room temperature was designed. Based on this, the same authors demonstrated the high sensitivity and selectivity of PbS QDs as sensors for H_2S. In this case they used an aluminum substrate onto which the PbS QDs were spin-coated by a layer-by-layer process. As in the previous examples, the resistance of the device was measured in a range of temperatures and at different gas or vapor concentrations. In this case, a highly sensitive, selective and recoverable device for the detection of H_2S over SO_2, NO_2 or NH_3, at 135ºC was obtained. Recently, an optical gas sensor for CO_2 diluted in water using graphene quantum dots has been reported[6]. In this case, instead of electrical changes, authors observed a variation of the photoluminescence spectrum of the QDs when putting them in contact with a solution of CO_2 in water.

In the examples exposed above quantum dots were used in a bare form, they were put directly in contact with the vapor or gas of interest. However, this does not avoid the problems

of toxicity and manipulation. A reported alternative is the incorporation of QDs into polystyrene-polystyrene-co-maleic anhydride and the synthesis of nanofibers by electrospinning out of those hybrid latexes[14]. Homogeneous fluorescent and conductive nanofibers. The variation of the conductivity was studied when exposed to chloroform, DMF and THF thanks to the presence of QDs. However, the variation of the fluorescence was not studied when exposing the nanofibers to the different vapors.

In the reports presented here, quantum dots have been used taking advantage either of their semiconductor nature, their large surface area or of their fluorescence properties, obtaining sensitive and selective sensors, most of them at high temperatures. However, to the best of our knowledge, the combination of fluorescence and conductivity in the same gas sensor has not been reported. In this Chapter, the synthesis of hybrid nanofibers containing CdSe/ZnS QDs by electrospinning and their optical and resistance response to volatile organic compounds (VOCs) at room temperature is described. Latexes containing cross-linked core-shell PS/QDs/PMMA particles synthesized as described in Chapter 2 were used. However, as the viscosity of those latexes is very low for the electrospinning process, a polymeric thickener was employed to achieve the appropriate viscosity of the dispersion. Two different polymers were used, polyvinyl alcohol (PVA) and polyethylene oxide (PEO) for this goal. The differences in terms of synthesis, morphology and response to VOCs depending on the polymer used are shown in this Chapter.

5.2. Synthesis of fluorescent nanofibers by electrospinning

The nanofibres containing commercial octadecylamine coated CdSe/ZnS quantum dots were produced by electrospinning. The working conditions in terms of viscosity of the latex and of the set-up as well as the characterization of the obtained hybrid nanofibers are described in the next sections.

5.2.1. Synthesis of the latexes and optimization of the viscosity of the electrospun dispersions

Cross-linked PS/QD/PMMA core-shell hybrid latexes were synthesized following the same protocol described in Chapter 2. However, these latexes have a low solids content, 12%. Therefore, viscosity is low and not suitable for the production of nanofibers by electrospinning. In order to obtain good quality and continuous nanofibers, viscosity had to be increased to be in the range of 100-500 cP. Water soluble polyvinyl alcohol (PVA) and polyethylene oxide (PEO) have been used as thickeners for this purpose. Two samples with latexes containing different types and concentration of QDs were prepared, NF1 and NF2. To prepare NF1, 10 g of latex were taken and 1.5 g of PVA were added. To dissolve the PVA the mixture was heated at 70ºC during 24 hours under magnetic agitation. On the other hand, NF2 was prepared by dissolving 0.5 g of PEO in 10 g of latex at room temperature. Homogeneous and stable dispersions were obtained. Table 5.1 summarizes the most relevant data of the obtained dispersions including a Blank prepared with PVA as thickener.

Table 5.1 Characteristics of the nanofibers samples synthesized in terms of type and concentration of QDs, final particle size, and thickening type and concentration.

Sample	QDs type	%QDs (%wbm)[#]	Dp	Thickening type	Thickening concentration (%wt)
Blank	-	-	180	PVA	15%
NF1	QD560	0.05	135	PVA	15%
Blank 2	-	-	132	PEO	5%
NF2	QD600	1.03	154	PEO	5%

[#]Weight based on total monomer (S+MMA+DVB).

To get these thickener concentrations different samples were prepared using blank core-shell latex and adding different concentrations of the thickeners. The apparent viscosity of the dispersions was measured using a rheometer (TA Instruments-AR1500ex). Flow procedures using a 60 mm diameter steel plate as geometry were carried out at 25ºC in all the measurements. Three different steps were set. A conditioning step in which the working temperature is set, a first continuous ramp from 0.1 to 1000 s^{-1} and a second continuous ramp from 1000 to 0.1 s^{-1}. Figure 5.2a and b presents the viscosity as a function of the thickeners concentration for a shear rate of 200 s^{-1} for the studied thickeners. Suitable viscosities for the production of nanofibers were obtained for a concentration of PVA of 15% in weight, 0.25 Pa.s (Figure 5.2a) and for a concentration of 5% in weight of PEO, 0.52 Pa.s (Figure 5.2b). Additionally, Figure 5.2c and d shows the non-newtonian behavior of the dispersions containing QDs (NF 1 and NF 2) plotting the viscosity as a function of the shear rate.

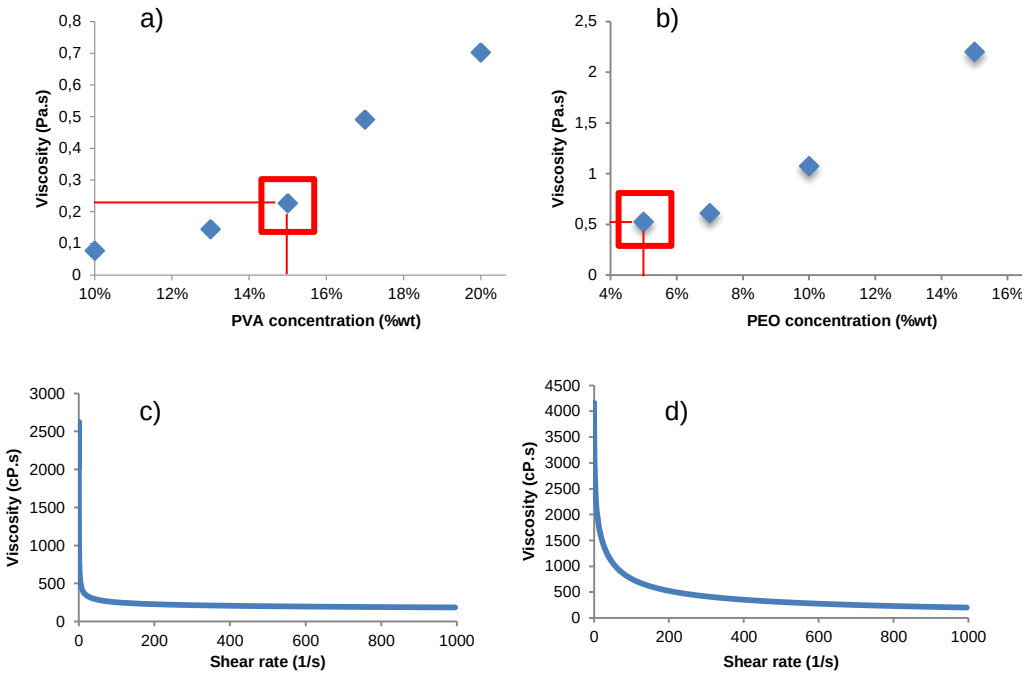

Figure 5.2 a) Viscosity vs PVA concentration at a shear rate of 200s^{-1}; b) Viscosity vs PEO concentration at a shear rate of 200s^{-1}; c) and d) Apparent viscosity of samples a) NF1 and b) NF2.

5.2.2. Electrospinning set-up and synthesis of the nanofibers

The experimental set-up used is a home-made equipment available in Tecnalia research center (Donostia-San Sebastián). The equipment is composed by a syringe pump, a polyamide tube that connects the syringe with a needle of 0.6 mm internal diameter, an aluminum foil collector connected to earth and a voltage generator. The voltage, the feeding rate and the needle to collector distance are controlled by a computer. As it can be seen in Figure 5.3, the set-up is placed onto a chamber were the temperature and the humidity are controlled to be 20ºC and 45-50%, respectively.

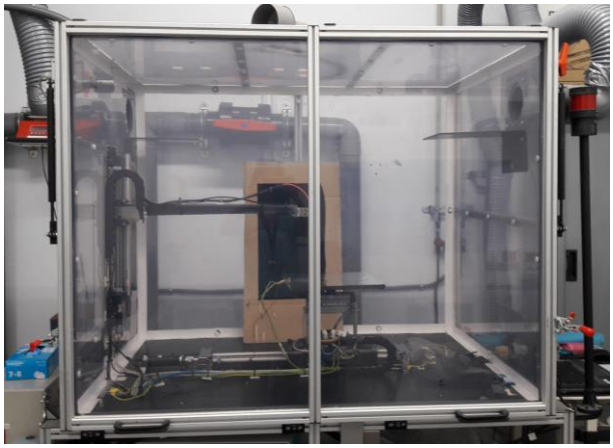

Figure 5.3 Experimental electrospinning set-up from Tecnalia research center (Donostia-San Sebastián).

The following procedure was used to produce the nanofibers. The polymeric dispersion was placed into a 3 ml plastic syringe, taking care of removing the air bubbles. The dispersion is brought up to the outlet of the syringe at high feeding rate but once this point the optimum feeding rate is implemented. Optimum conditions in terms of applied voltage, needle-collector distance and feeding rate for each sample are listed in Table 5.2. Those optimum conditions depend, among others, on the viscosity of the sample, the vapor pressure of the solvent (in this case water), and the desired morphology of the nanofibers.

Table 5.2 Optimum electrospinning conditions for each sample.

Sample	Voltage (kV)	Needle-collector distance (mm)	Feeding rate (ml/h)
Blank	15	200	0.08-0,1
NF1	15	200	0.08-0.1
NF2	15	200	0.2-0.3

Once the voltage is applied, the latex comes out of the needle, and due to the high electrostatic forces produced the nanofibers are produced and deposited on the collector (Figure 5.4).

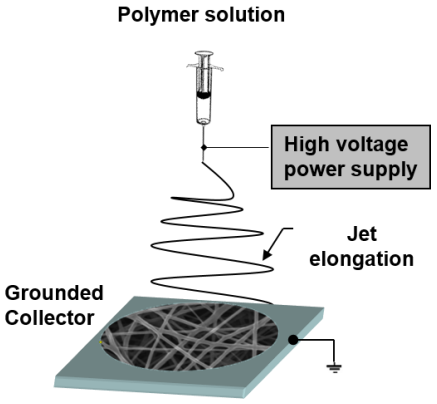

Figure 5.4 Scheme of the electrospinning process.

Due to the difference in viscosity, the area covered by the nanofibers on the aluminum foil was different, 20 cm in diameter for sample NF1 and 10 cm for sample NF2. A glass slide or transmission electron microscopy grid was placed on the middle of this area collecting there the nanofibers for their later characterization by scanning electron microscopy, transmission electron microscopy and fluorescence microscopy (Figure 5.5a and b). Furthermore, deposition was also done on an interdigitated electrode of 22.8 x 7.6 mm size with platinum electrodes fabricated onto a glass substrate with a trail distance of 5 μm for the electrical measurements. The electrospinning conditions were maintained as in the case of the deposition onto glass slides, however, in this case it is of special importance to connect the electrode to earth due to the high tension generated between the needle and the collector for the production of

nanofibers. The electrodes were connected to earth using two alligator clips on the pads as it can be observed in Figure 5.5c. This way the amount of nanofibers deposited on the electrode trails is maximized.

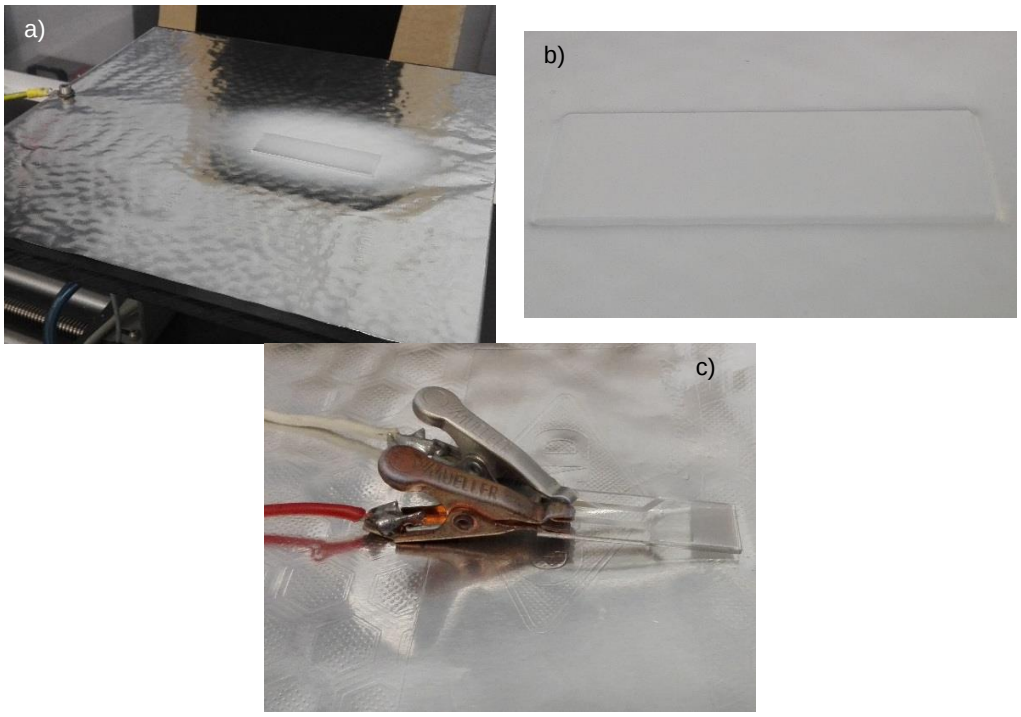

Figure 5.5 a) General image of the deposition area of NF2 sample on the aluminum foil collector during 5 min; b) Detail of NF1 sample deposited onto a glass slide for 30 min; c) NF2 nanofibers deposited onto an interdigitated electrode for 1.5 min. (Property of Tecnalia. All the rights reserved)

5.3. Morphological characterization of the nanofibers

The morphology of hybrid nanofibers was analyzed by SEM and TEM. On one hand, SEM was used for the characterization of the fibers themselves such as their thickness, their homogeneity and the possible defects. On the other hand, by TEM the interior of the nanofibers was investigated; the shape of the cross-linked core-shell PS/PMMA polymer particles, their distribution into the PVA or PEO matrix and the final distribution of the QDs.

5.3.1. Scanning electron microscopy

A Scanning Electron Microscope (SEM) QUANTA 250 from FEI at high voltage (10 kV) using a standard detector was used for the analysis of the shape and homogeneity of the nanofibers of the Blank, samples NF1 and NF2. Nanofibers were electrospunned on a microscope glass slide for five minutes for their characterization. Figure 5.6 shows SEM images for samples NF1 and Figure 5.7 for NF2. In both cases, good quality nanofibers with a continuous phase of PVA (NF1) or PEO (NF2) and no defects were observed.

Figure 5.6 displays the morphology of the nanofibers at different magnification. The diameter of the fibers is between 200-250 nm and the surface of the fibers is not flat but “sinusoidal”. The size of the fibers indicates that a single polymer particle (average diameter of 135 nm) fits. QDs cannot be distinguished in these images.

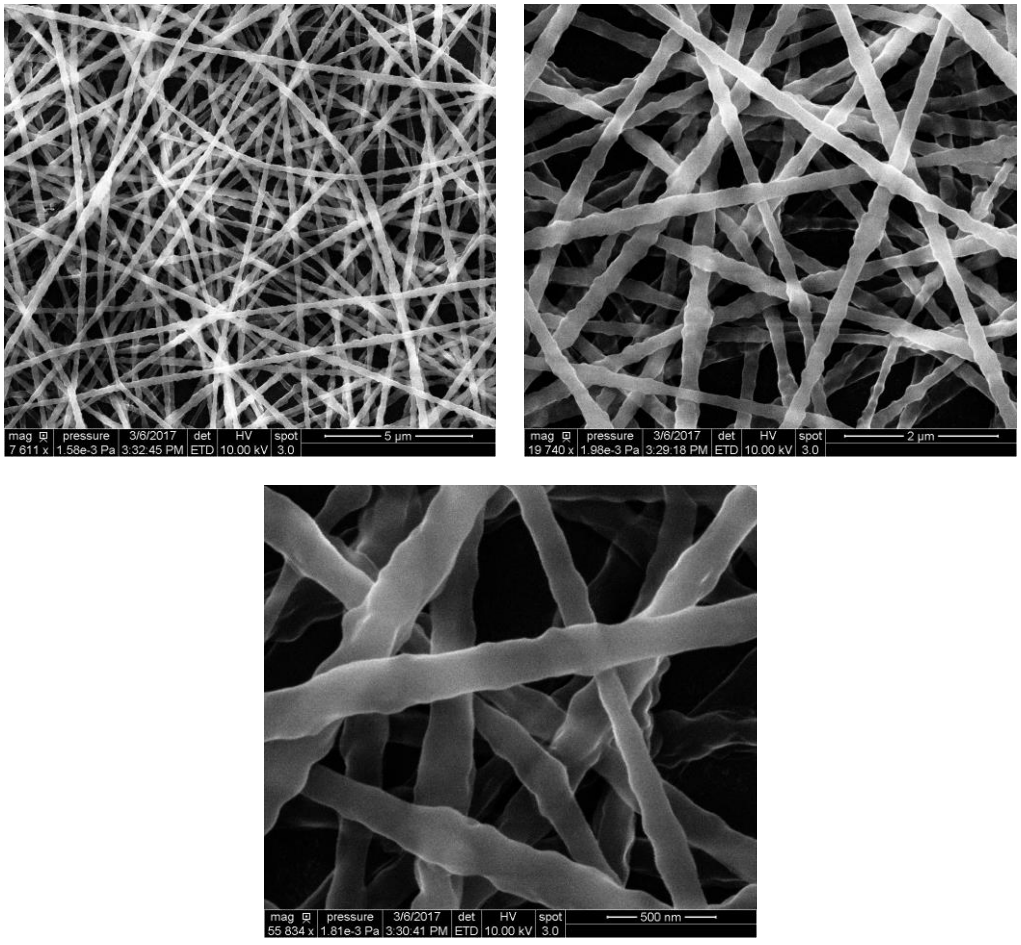

Figure 5.6 SEM micrographs of sample NF1.

Figure 5.7 shows the SEM micrographs of the nanofibers corresponding to sample NF2 at different magnifications. Continuous fibers of diameters ranging in size between 200 nm at 3.5 µm were obtained, indicating the possibility of having multiple polymer particles (average diameter of 154 nm) next to each other in the wider parts of the nanofibers. Regarding the

surface of the nanofibers, it is not completely smooth but bumpy. Due to the low magnification of the micrographs, QDs cannot be identified.

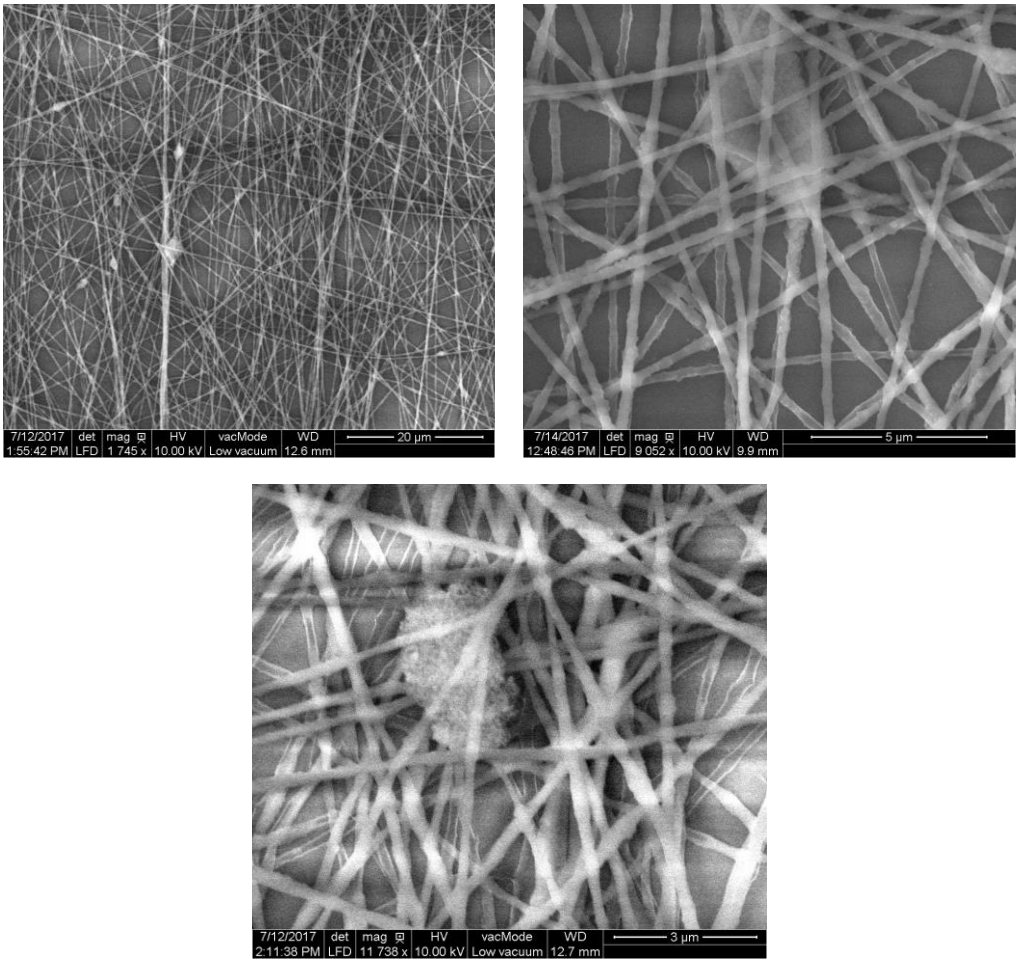

Figure 5.7 SEM micrographs of sample NF2.

5.3.2.Transmission electron microscopy

In order to characterize in further detail the nanofibers and the localization of the quantum dots, transmission electron microscopy was used. For this, nanofibers were directly deposited by electrospinning on the copper grids for a very short time to avoid large thickness that might prevent an appropriate TEM analysis. Figure 5.8 confirms that the nanofibers´ surface is not smooth. Indeed, it is bumpy and TEM clearly shows that there is a single polymer particle along the thickness of the fiber, which is seen darker in the micrographs. Surprisingly, the cross-linked particles appeared in some cases elongated or partially deformed in the direction of fiber formation. As the concentration of QDs was low in dispersion NF1 (0.5 QD/particle; namely not all the particles have a QD), visualizing the QDs was not easy. Figure 5.8c presents a fiber section composed by 3 polymer particles one of them clearly presenting a QD.

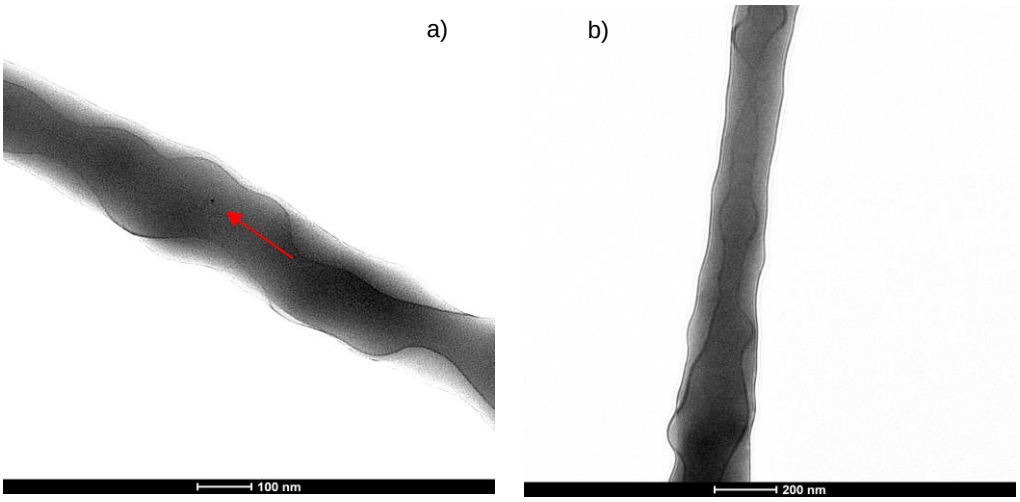

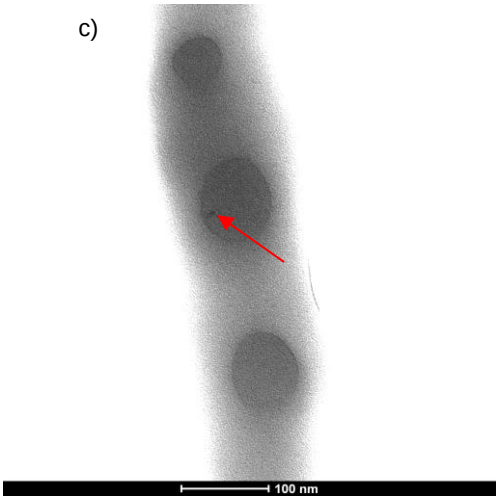

Figure 5.8 TEM micrographs of sample NF1.

The elongation of the polymer particles in emulsion electrospinning has been reported in literature, and is due to the huge electrostatic forces generated during the electrospinning process (Figure 5.9). On the other hand, the deformation of the core-shell polymer particles is a consequence of electrostatic interactions and physical confinement of the PVA layer. This difference in the internal morphology of the nanofibers might be due to inhomogeneity of the sample combined with an excess of PVA.

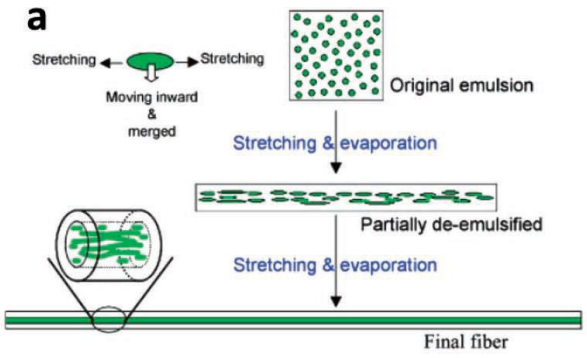

Figure 5.9 Elongation of the polymer particles when producing nanofibers by electrospinning of a polymer emulsion[15].

Concerning sample NF2, the morphology was completely different. In this case, and as it can be seen in Figure 5.10a, a discontinuous distribution of the polymer particles in the nanofibers occurred. Dark areas corresponding to the polymer particles were mixed with lighter areas corresponding to the PEO nanofiber. Moreover, focusing on these dark areas aggregation of the polymer particles was observed (Figure 5.10b). Contrary to the deformation of the polymer particles observed for sample NF1, in this case most of them maintained their spherical morphology during the electrospinning process.

As explained above, the final morphology of the nanofibers in electrospinning depends on many factors. In this case, the thickener polymer was changed (PEO instead of PVA) driving to a change in the viscosity, the surface tension…, what clearly affected the final morphology and the distribution of the polymer particles into the nanofibers.

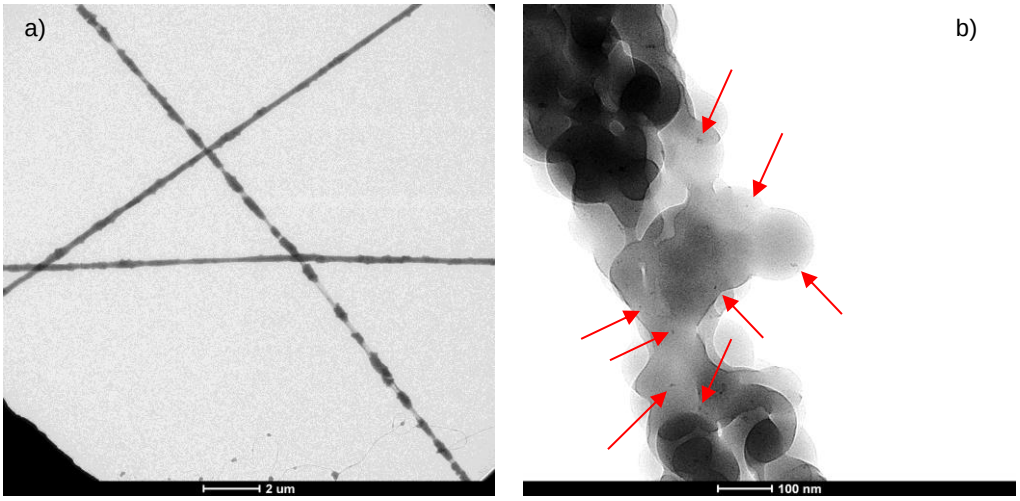

Figure 5.10 TEM micrographs of sample NF2.

This change in the thickener was done after observing, in the spectrofluorometer, that PVA emitted fluorescence at the same wavelength as the QD560 quantum dots present in sample NF1. Figure 5.11 shows this circumstance, the Blank PVA and the NF1 samples show an emission peak of different intensity but at the same wavelength. This causes an interference that does not allow reliable fluorescence measurement.

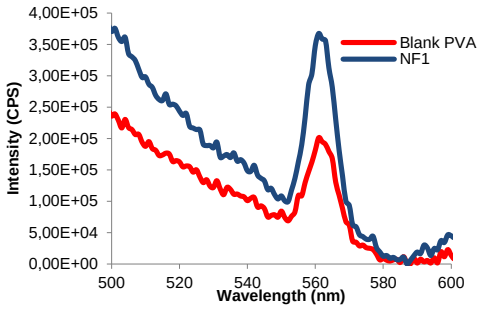

Figure 5.11 Fluorescence emission spectrum of the PVA blank compared to NF1 sample.

Quantum dots can be distinguished in Figure 5.10b. As it can be seen a higher amount was present in the polymer particles in contrast to sample NF1, as their concentration is higher (4 QDs/particle).

5.4. Fluorescence characterization of the nanofibers

Fluorescence emission intensity of the samples deposited on microscope glass slides was measured using a fluorescence microscope Olympus BX-51 coupled to a Horiba spectrofluorometer. For all the cases, the samples were covered in order to avoid the influence and detection of the external light during the measurements. This way the QDs present in the nanofibers could be focused obtaining higher emission intensity rather than measuring directly through the spectrofluorometer. This technique was especially useful in the case of sample NF1, in which, as it was explained above PVA emitted fluorescence at the same wavelength as the QD560 quantum dots when measuring the Blank PVA and the NF1 sample in the spectrofluorometer.

Figure 5.12a shows a fluorescence microscopy image of sample NF1. It was observed that the fluorescence distribution was neither high nor homogenous along the sample due to the low concentration of quantum dots in the sample. However, some fluorescent aggregates were perceived showing the presence of quantum dots. Taking advantage of this, the interference of the PVA could be avoided by focusing on the QDs aggregates and measuring there the fluorescence emission. In contrast to the measurement in the spectrofluorometer, the Blank PVA emission was not observed due to the filter used, specific for QDs detection (U-

MNU2), and therefore the fluorescence emission intensity of sample NF1 could be quantified (Figure 5.12b).

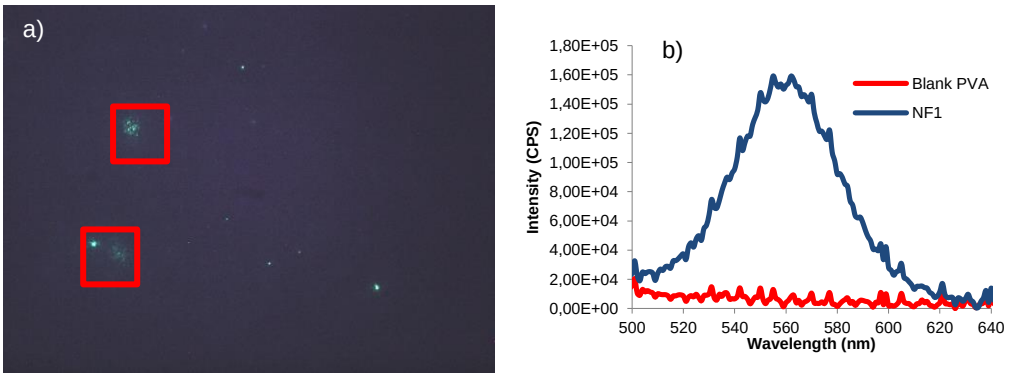

Figure 5.12 a) Fluorescence emission spectrum from the blank PVA measured in the spectrofluorometer; b) Fluorescence microscopy image of an area of NF1 sample; c) Fluorescence emission spectrum of sample NF1 measured through the fluorescence microscope focusing on an aggregate.

As observed in Figure 5.13a, fluorescence for sample NF2 was more homogeneous along the sample than for NF1, but still some fluorescent aggregates were observed, which is in good agreement with the morphology observed by SEM and TEM. PEO did not present fluorescence, so the interference between the polymer and the QDs was avoided, but still fluorescence emission was measured through the fluorescence microscope. This way, and as the fluorescence in the sample is not completely homogeneous, always the same fluorescent point could be focused making the measurements reproducible on time. Figure 5.13b shows the fluorescence emission spectrum of the point highlighted as a green square on the microscope image. A greater intense and smother peak than for sample NF1 was obtained due to the much higher concentration of QDs in this sample.

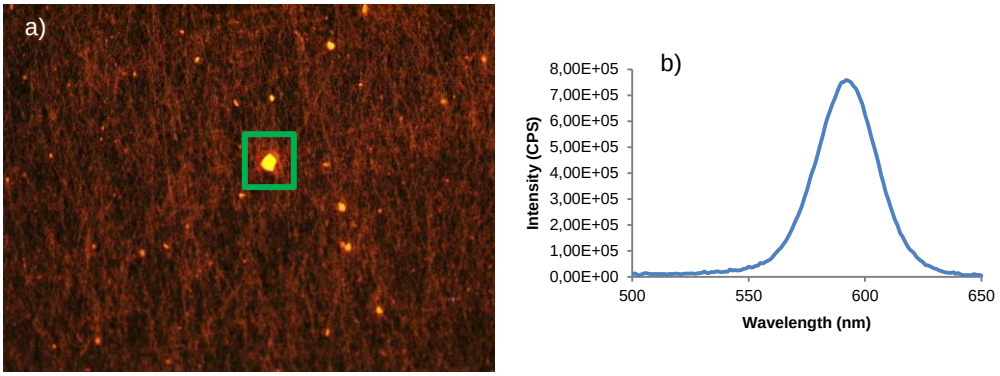

Figure 5.13 a) Fluorescence microscopy image of sample NF2; b) Fluorescence emission spectrum obtained using the fluorescence microscope focusing on one aggregate (highlighted in green).

5.5. Hybrid nanofibers as VOCs sensors

5.5.1. Optical VOCs sensors

The sensitivity of the synthesized nanofibers (samples NF1 and NF2) to VOCs was studied by monitoring the fluorescence emission intensity of the sample during time upon contact of the nanofiber with volatile organic compounds (VOCs) vapor. The sample was first covered to avoid the influence of the light on the sample and on the detector. Then, fluorescence was measured at time cero and afterwards a beaker containing the VOC was placed next to the sample. In order to generate a steam-rich atmosphere, both the sample and the beaker were covered during the whole experiment. The influence of three different solvents was studied, acetone, toluene and methanol. In the case of sample NF1 only acetone was used because of the complexity of finding areas with a measurable fluorescence emission intensity due to the low concentration of QDs.

Sample NF1 was exposed to acetone, and the fluorescence emission intensity of fluorescence of a chosen area was measured at different times, so while increasing the concentration of acetone vapor in the system (Figure 5.14a). A fast decrease of the fluorescence emission intensity was observed, 3 times in 20 minutes. Moreover, the emission peak suffered a blue shift showing a degradation of the QDs when being exposed to acetone vapor, probably due to the degradation of the QDs during their exposition to acetone.

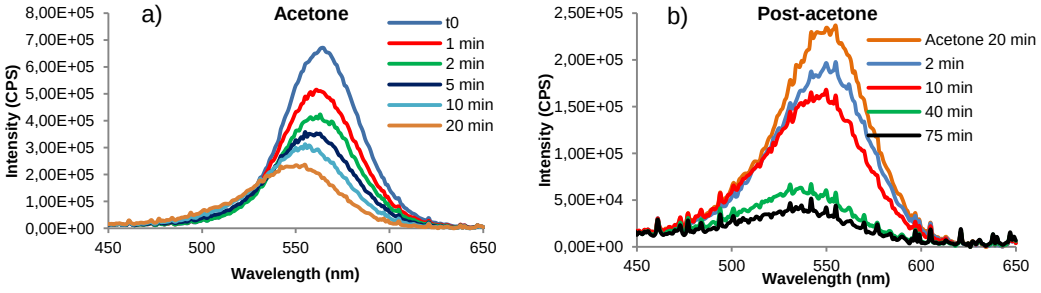

Figure 5.14 Fluorescence emission spectrum of a fluorescent aggregate in sample NF1 a) during exposure to acetone; b) after exposure to acetone.

The recovery of the fluorescence for this sample was also studied. This was done by first taking out the beaker with acetone and ventilating the area for a few minutes. Then, fluorescence emission intensity was measured during time observing a continuation of the decrease of the emission intensity and the blue shift of the peak even after more than one hour (Figure 5.14b). This fact is likely due to the degradation of the QDs during the exposition to acetone that makes them loosing fluorescence even after removing the solvent, making these hybrid PVA nanofibers non-recoverable.

Sample NF2 was exposed to three different compounds, acetone, toluene and methanol. In the case of exposition to methanol (Figure 5.15a) the response was fast,

comparable to the one observed for sample NF1 when exposed to acetone, but then it increased again until stability. In the case of toluene (Figure 5.15b) some fluctuations occurred during 2 hours, but it was not until exposing the sample overnight when a high decrease of the emission intensity occurred. A much more progressive decrease was observed for the exposition to acetone. In this case the fluorescence emission intensity decreased around 1.2 times in 3 hours, much less than for NF1 sample (Figure 5.15c).

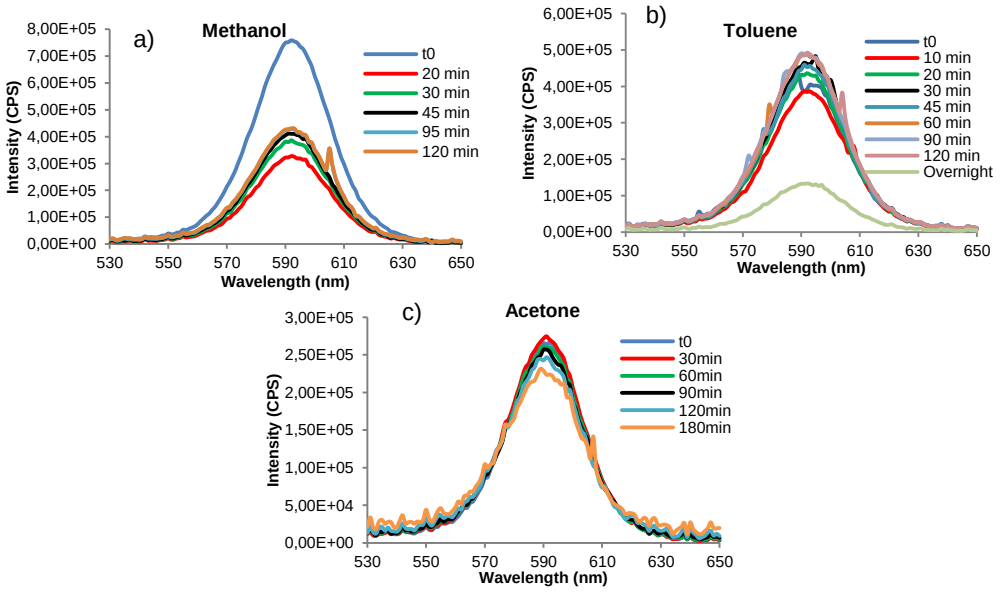

Figure 5.15 Fluorescence emission spectrum of an aggregate of sample NF2 when exposed to a) methanol; b) toluene; c) acetone.

An essay to check the recovery of the initial fluorescence emission intensity was carried out for the case of the sample exposed to acetone. As it can be seen in Figure 5.16 fluorescence emission intensity decreased after 60 min of non-exposition of the sample to acetone, being almost stable after 120 min of post-acetone exposition. After 5 days the

fluorescence emission intensity was recovered. According to these results, the nanofibers could be reused in an additional acetone exposition cycle.

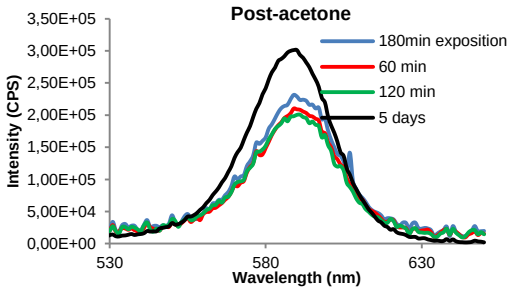

Figure 5.16 Fluorescence emission spectra during 5 days of sample NF2 after exposition to acetone.

In the second cycle of acetone detection by fluorescence emission intensity measurements (Figure 5.17a), the intensity decreased fast during the first hour and then it decreased progressively as in the case of the first acetone cycle. The recovery of the initial optical properties was also studied in this case, by taking out the acetone beaker and measuring the fluorescence emission intensity for two days (Figure 5.17b). In this second cycle, recovery of the initial emission intensity was not obtained, but it increased back to the values measured after 60 minutes of exposition to acetone. This uncomplete recovery of the fluorescence emission intensity shows that at every cycle some fluorescence is lost.

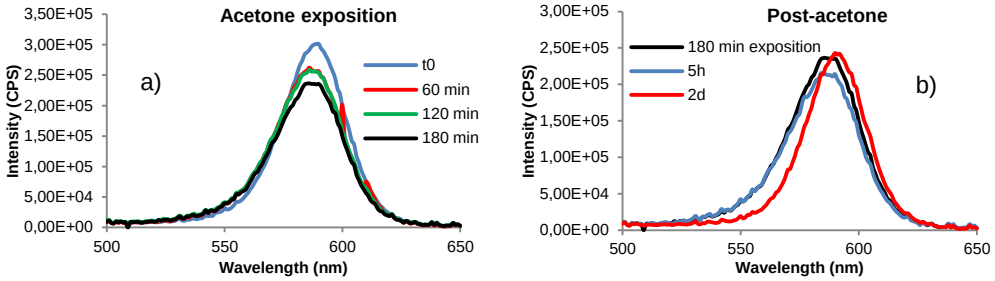

Figure 5.17 a) Fluorescence emission intensity evolution of cycle 2 of sample NF2 exposed to acetone; b) Fluorescence emission intensity evolution after the exposition of sample NF2 to a second cycle of acetone.

According to these results it can be concluded that the synthesized nanofibers are optically responding to VOCs. Furthermore, the increase in the concentration of quantum dots in the nanofiber is not accelerating the process, the main differences are due to the variation of the polymer (PVA or PEO). Moreover, in the case of nanofibers composed by PEO, a second detection cycle of acetone was possible. The possible use of these nanofibers in further cycles has to be further investigated, as well as the use of different thickeners and their impact on the detection of different VOCs.

5.5.2. Resistance of the VOCs sensors

Additionally to the optical response of the nanofibers to different VOCs, sample NF2 was also electrically characterized in Tecnalia research center (Donostia-San Sebastián). For this, as mentioned above, the nanofibers were deposited onto an interdigitated electrode (22.8x7.6 mm) with platinum electrodes fabricated onto a glass substrate with a trail distance of 5 µm (Figure 5.18).

Figure 5.18 Interdigitated electrode. (Property of Tecnalia. All the rights reserved)

Resistance was measured with a multimeter. Two electrospinning tests were carried out, with deposition times of 1.5 min (D06E23) and 4 min (D03E24) in order to study the influence of the deposition time on the resistance measurements. For sample D06E23 a value of 110-120 MΩ was obtained, while for sample D03E24 the resistance value was of 5-6 MΩ. This showed that the deposition time had a great influence on the resistance of the electrode, being much higher when less nanofibers were deposited on the electrode, so less quantum dots were present in the sample.

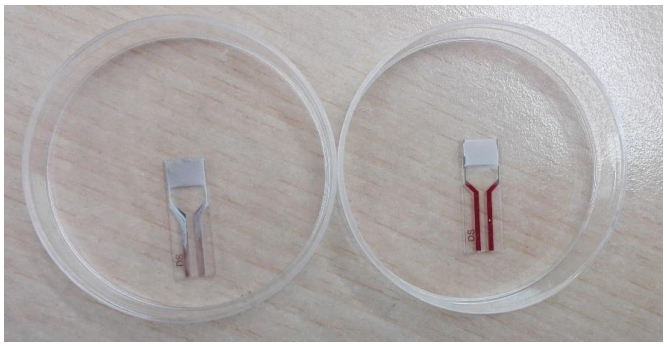

Figure 5.19 Electrodes deposited with NF2 nanofibers, sample D03E23 on the right and sample D03E24 on the left. (Property of Tecnalia. All the rights reserved)

In order to get reasonable resistance values, sample D06E24 was the chosen one for studying the resistance evolution when exposed to acetone vapor. This study was done by placing the chosen electrode connected to the multimeter together with a petri dish containing acetone under a beaker (Figure 5.20). This way, as done for the optical measurements, an acetone vapor-rich atmosphere was generated.

Figure 5.20 D03E24 electrode into an acetone steam-rich atmosphere prepared for the resistance measurements.

Measurements were carried out at 24.7ºC and 56% humidity for 50 minutes. As it can be observed in Figure 5.21, the resistance increased from 6 to 13 MΩ almost immediately when introducing the electrode into the acetone vapor atmosphere. Small fluctuations of the signal were observed during time, probably because of changes in the humidity as it was checked that this had a great influence on the resistance. When taking the electrode out to the air, the original resistance value was recovered almost at the same moment, meaning that the electrode could be reused for at least another cycle.

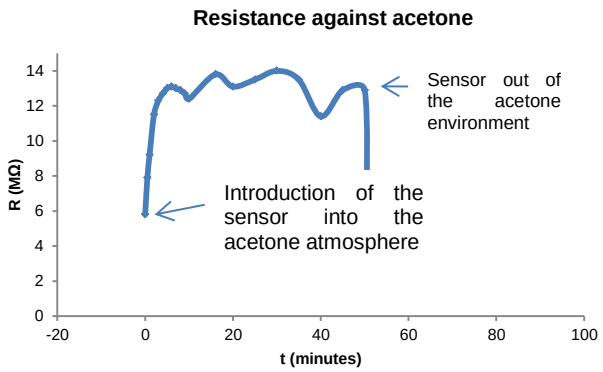

Figure 5.21 Resistance evolution of electrode D03E24 against acetone.

The electrode was left in the air overnight measuring the resistance again and obtaining a value of 3.5 MΩ, much lower than the one measured initially in the air and after the test with acetone. This can be explained by the increase of humidity, from 56% to 70%, which demonstrates the great influence that this parameter has on the resistance measurements, meaning that the sensor is also sensitive to water vapor.

5.6. Conclusions

The potential application of the hybrid PS/QD/PMMA dispersions as volatile organic compounds sensor was studied in this Chapter. Hybrid nanofibers with different types and concentration of QDs were produced by electrospinning. For this, first the viscosity of the PS/QD/PMMA dispersions had to be increased to appropriate values for the electrospinning process. Two different thickeners, polyvinyl alcohol (PVA) and polyethylene oxide (PEO), were used for this goal. The morphology of the resulting nanofibers was studied by SEM and TEM

obtaining a different effect on the polymer particles depending on the thickener used. Nanofibers produced with PVA resulted in a deformation of the polymer particles during the electrospinning process, while in the nanofibers produced with PEO aggregation of the polymer particles was observed. Regarding the QDs, they were present in both cases, showing that they were not lost during the production of the nanofibers.

Fluorescence measurements were done by fluorescence microscopy exposing the nanofibers to different VOCs (acetone, toluene and methanol). Nanofibers produced with PVA were exposed to acetone and showed a progressive decrease of the fluorescence emission intensity as well as a blue shift of the peak. The nanofibers produced with PEO responded to the three compounds showing a decrease of the fluorescence emission intensity. Additionally, conductivity measurements were carried out to the PEO sample in an acetone atmosphere. Conductivity increased during the exposition to the vapor recovering its original resistance value when taking it out the acetone environment.

In conclusion, the hybrid PEO synthesized nanofibers can be used both as optical and electrical VOCs sensors. On the other hand, PVA hybrid nanofibers can be applied at least as optical sensors. These are preliminary results to prove that the hybrid PS/QD/PMMA dispersions are good candidates to be used as optical and electrical sensors for VOC detection. Further work is needed to optimize the composition and morphology of the fibers, but this is out of the scope of this PhD thesis.

5.7. References

(1) Forleo, A.; Francioso, L.; Capone, S.; Siciliano, P.; Lommens, P.; Hens, Z. Synthesis and Gas Sensing Properties of ZnO Quantum Dots. *Sensors Actuators, B Chem.* **2010**, *146* (1), 111–115.

(2) Nath, S. S.; Choudhury, M.; Chakdar, D.; Gope, G.; Nath, R. K. Acetone Sensing Property of ZnO Quantum Dots Embedded on PVP. *Sensors Actuators, B Chem.* **2010**, *148* (2), 353–357.

(3) Mosadegh Sedghi, S.; Mortazavi, Y.; Khodadadi, A. Low Temperature CO and CH4 Dual Selective Gas Sensor Using SnO2 Quantum Dots Prepared by Sonochemical Method. *Sensors Actuators, B Chem.* **2010**, *145* (1), 7–12.

(4) Liu, H.; Li, M.; Voznyy, O.; Hu, L.; Fu, Q.; Zhou, D.; Xia, Z.; Sargent, E. H.; Tang, J. Physically Flexible, Rapid-Response Gas Sensor Based on Colloidal Quantum Dot Solids. *Adv. Mater.* **2014**, *26* (17), 2718–2724.

(5) Li, M.; Zhou, D.; Zhao, J.; Zheng, Z.; He, J.; Hu, L.; Xia, Z.; Tang, J.; Liu, H. Resistive Gas Sensors Based on Colloidal Quantum Dot (CQD) Solids for Hydrogen Sulfide Detection. *Sensors Actuators, B Chem.* **2015**, *217*, 198–201.

(6) Raeyani, D.; Shojaei, S.; Kandjani, S. A.; Wlodarski, W. Synthesizing Graphene Quantum Dots for Gas Sensing Applications. *Procedia Eng.* **2016**, *168*, 4–7.

(7) MADHUCHHANDA CHAKRABORTY. Preprartion of Metal Oxide Semiconductor Quantum Dots and Their Applications as Nano Gas Sensor (Chapter 5), Assam University, 2015.

(8) Hellegouarc'h, F.; Arefi-Khonsari, F.; Planade, R.; Amouroux, J. PECVD Prepared SnO2 Thin Films for Ethanol Sensors. *Sensors Actuators B Chem.* **2001**, *73* (1), 27–34.

(9) Sahay, P. P. Zinc Oxide Thin Film Gas Sensor for Detection of Acetone. *J. Mater. Sci.* **2005**, *40* (16), 4383–4385.

(10) Comini, E. Metal Oxide Nano-Crystals for Gas Sensing. *Anal. Chim. Acta* **2006**, *568* (1–2), 28–40.

(11) Yamazoe, N. New Approaches for Improving Semiconductor Gas Sensors. *J. Sensors Actuators B. Chem.* **1991**, *5* (1–4), 7–19.

(12) Xu, C.; Tamaki, J.; Miura, N.; Yamazoe, N. Grain Size Effects on Gas Sensitivity of Porous SnO2-Based Elements. *Sensors Actuators B. Chem.* **1991**, *3* (2), 147–155.

(13) Schwartz, D. a; Norberg, N. S.; Nguyen, Q. P.; Parker, J. M.; Gamelin, D. R. Magnetic Quantum Dots: Synthesis, Spectroscopy, and Magnetism of Co2+ - and Ni2+-Doped ZnO Nanocrystals. *J. Am. Chem. Soc.* **2003**, *125* (43), 13205–13218.

(14) Tatavarty, R.; Hwang, E. T.; Park, J. W.; Kwak, J. H.; Lee, J. O.; Gu, M. B. Conductive

Quantum Dot-Encapsulated Electrospun Nanofibers from Polystyrene and Polystyrene-Co-Maleic Anhydride Copolymer Blend as Gas Sensors. *React. Funct. Polym.* **2011**, *71* (2), 104–108.

(15) Xu, X.; Zhuang, X.; Chen, X.; Wang, X.; Yang, L.; Jing, X. Preparation of Core-Sheath Composite Nanofibers by Emulsion Electrospinning. *Macromol. Rapid Commun.* **2006**, *27* (19), 1637–1642.

Chapter 6. Conclusions

Quantum dots are inorganic nanoparticles that have demonstrated exceptional optical and electronic properties with a myriad of potential applications. However, the implementation of new technologies based on QDs requires solving some important drawbacks (toxicity, small size and hence difficult manipulation, degradability…). This has been investigated in this thesis. The first and main goal of this work was the encapsulation of the quantum dots into colloidal polymer particles, in order to preserve their properties, but also to protect the environment from their toxicity.

To accomplish this objective, octadecylamine coated CdSe/ZnS quantum dots purchased to OceanNanotech were used, and a two-step encapsulation method was developed to ensure an efficient encapsulation and stability of the nanocrystals: seeded semi-batch emulsion polymerization. In a first step, cross-linked polystyrene-QDs particles were synthesized by miniemulsion polymerization. The resulting latex was not optically stable, as the QDs diffused out the polymer particles being degraded by the action of the water and the remaining radicals, and therefore losing their fluorescence during storage. Efficient encapsulation was ensured in the second step of the process. The core cross-linked hybrid PS/QDs particles were used as a seed, and a mixture of methyl methacrylate and divinyl benzene was fed into the reactor. As a result, cross-linked core-shell

polystyrene/QDs/polymethyl methacrylate hybrid polymer particles with high fluorescence stability (up to 9 months) were obtained (Figure 6.1). The influence of the shell thickness was also investigated, concluding that a minimum shell thickness of 12 nm was necessary in order to achieve this fluorescence stability.

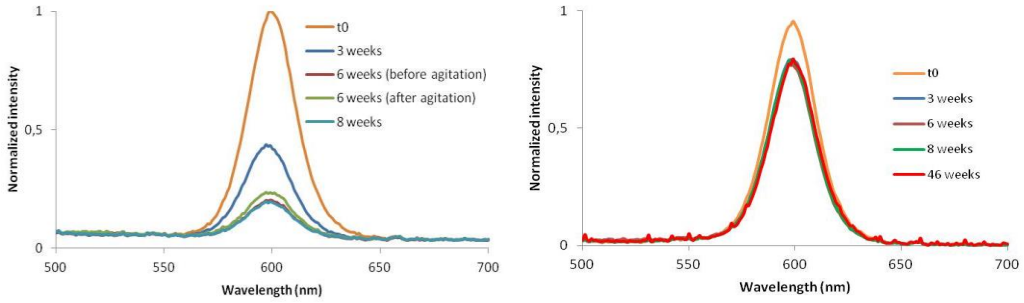

Figure 6.1 Comparison of fluorescence emission spectrum of the PS-DVB/QDs core vs the PS-DVB/QD/PMMA-DVB core-shell latexes.

Once this key objective was fulfilled, the encapsulation of quantum dots of different sizes was investigated to open the door to multiplexing applications. During the internship, done at ICMCB (Bordeaux-France), oleylamine coated CdSe core and hexadecylamine-TOPO coated CdSe/CdS core-shell quantum dots were synthesized in supercritical hexane. Those nanocrystals showed good optical properties when dispersed in organic solvents such as hexane, chloroform or toluene. However, when carrying out the miniemulsion for their encapsulation into cross-linked core-shell PS/PMMA polymer particles, fluorescence was lost. Therefore, commercial octadecylamine coated CdSe/ZnS quantum dots of four different sizes were used (that is four different emission wavelengths). One latex per QD type was prepared by seeded semi-batch emulsion polymerization. Then, blends of the different latexes were

prepared considering the emission wavelengths of the QDs. It has been shown that the number concentration of QD nanocrystals determines their fluorescence emission intensity. Taking this into account, mixtures of two or three latexes could be prepared with characteristic fluorescence spectra corresponding to each type of QDs. This strategy, that led to a great control and stability of the fluorescence emission intensity, is the first step in the potential use of these latexes and blends as biological markers and in multiplexing assays. For this, the polymer particles have to be modified in their surface with, for example, an amino acid as lysine that is recognised by a specific protein. The modification of the surface of the particles with different modifiers would allow specific recognition of different proteins (Figure 6.2).

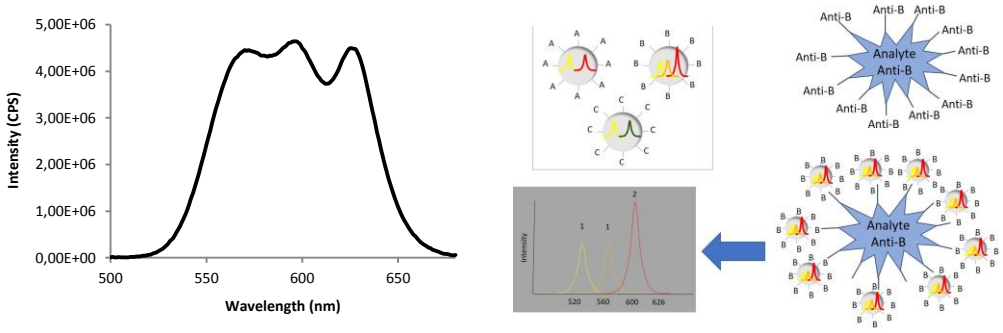

Figure 6.2 Left: Fluorescence emission spectrum of a blend of three different latexes; Right: Multiplexing scheme.

The combination of the commercial CdSe/ZnS quantum dots with CeO_2 nanoparticles was also studied in this thesis. Taking advantage of the excellent emission properties of QDs and of the excellent UV-absorption properties of CeO_2 nanoparticles, those two types of nanoparticles were co-encapsulated into the same polymer particle. The seeded semi-batch emulsion polymerization strategy used for the encapsulation of QDs was also used in this case. Additionally, a film forming formulation was developed. By producing a second shell of

MMA/BA/AA good quality and transparent films cast at room temperature were obtained. Latexes and films containing both QDs and CeO_2 nanoparticles in different ratios (in weight) were exposed to sunlight, studying their fluorescence emission intensity evolution during exposition. An enhancement of the fluorescence emission intensity was observed in both cases: 280% in the latex with a ratio 1:2 QDs:CeO_2 and 545% for a film with a ratio 1:2 QDs:CeO_2. This increase in the emission intensity is likely due to the effect of CeO_2 nanoparticles on the QDs. Moreover, the increase proportion depends on the different environments surrounding the QD nanoparticles when they are dispersed in polymer particles or when they are fixed upon film formation. Neighboring particles that might also contain CeO_2 nanoparticles are substantially closer in the case of the film and hence affecting much more the optical properties of the QDs (Figure 6.3).

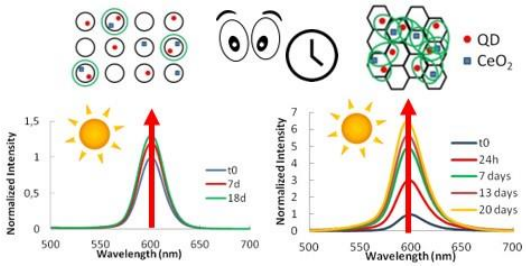

Figure 6.3 Enhancement of the fluorescence emission intensity in a latex and in a film containing QDs and CeO_2.

The potential application of the stable hybrid polymer/QDs latexes as gas sensors was studied in the last part of this work. Two hybrid latexes containing different QD sizes at different concentrations and mixed with different thickeners (PVA and PEO) were chosen for this goal. Nanofibers were produced by electrospinning, obtaining very different morphologies for each case, concluding that this was intimately related with the thickener used (Figure 6.4). Taking

advantage of the fluorescence of the nanofibers, their use as optical gas sensors for acetone, methanol and toluene was investigated, concluding that both PVA and PEO nanofibers optically responded to VOCs. However, it was observed that this response depended on the thickener used and on the vapor to which the nanofibers were exposed to. PEO nanofibers deposited on an electrode were responsive to acetone showing an increase in the resistance. Moreover, the starting resistance value was recovered instantaneously after finishing the exposition to acetone. Therefore, the synthesized nanofibers containing QDs and PEO as thickener were recoverable for additional detection cycles.

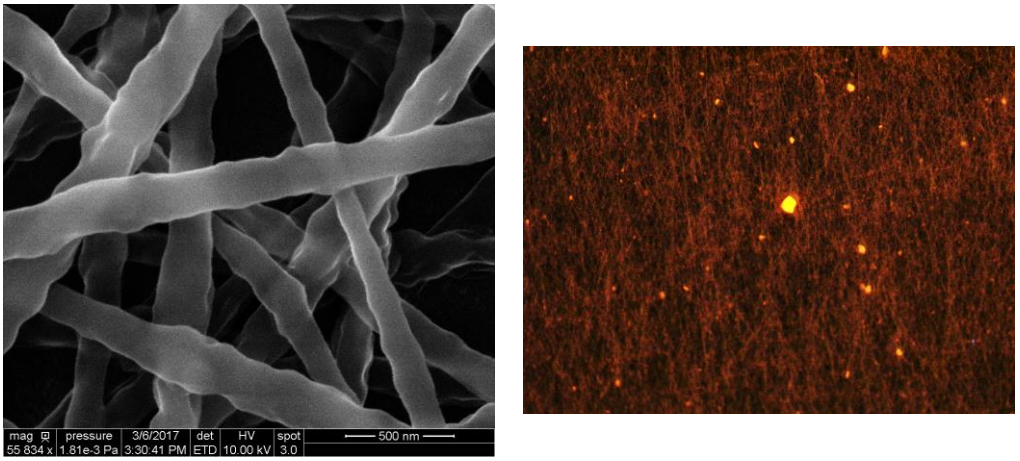

Figure 6.4 Right: SEM image of the hybrid polymer/QD latex with PVA nanofibers. Left: Fluorescence microscopy image of the hybrid polymer/QD latex with PEO nanofibers.

As a general conclusion, CdSe/ZnS quantum dots were successfully encapsulated into cross-linked core-shell PS/PMMA polymer particles, obtaining stable latexes during long periods of time. Additionally, a great control of the fluorescence when mixing latexes containing different types of quantum dots was achieved, allowing for labelling and multiplexing assays. A

big enhancement of the fluorescence was accomplished when co-encapsulating the quantum dots and nanoceria nanoparticles and exposing the latexes and the films to sunlight. Finally, the preliminary work of the potential use of those hybrid latexes as VOCs sensors was shown.

Appendix I. Materials and characterization methods

I.1. Materials

Commercial octadecylamine coated CdSe/ZnS quantum dots (QDs) of four different sizes were purchased to Ocean NanoTech in solid form. The needed amount of nanocrystals for each case was directly dispersed in the solvent or in the monomer without further treatment.

The following reagents were used for the synthesis of TOPO/hexadecylamine coated CdSe/CdS quantum dots in supercritical fluids. Cadmium deoxycholate [$(Cd(DCh)_2$], previously synthesized in the lab, elemental selenium (Se, Sigma Aldrich), elemental sulfur (S, Sigma Aldrich) and trioctyl phosphine (TOP, Sigma Aldrich, technical grade 90%) were used for the synthesis of the cadmium, selenium and sulfur precursors. Oleylamine (OA, Sigma Aldrich, technical grade 70%) was used as surface modifier for CdSe quantum dots. Trioctyl phosphine oxide (TOPO, Stem Chemicals, 90%) and hexadecylamine (HDA, Sigma Aldrich) were used as surface modifiers in the synthesis of CdSe/CdS QDs. Hexane (Sigma Aldrich, anhydrous 95%) was used as solvent in the preparation of the precursors and as supercritical fluid during the synthesis. All the mentioned reagents were used without further treatment.

Hydrophobic CeO_2 nanoparticles dispersion in mineral spirit with 49 wt% was kindly supplied by Altana. The dispersion was first dried for 48 hours at 60ºC and then grinded before use.

Toluene (Acros, 99.5%) was used as solvent for the dispersion of QDs and CeO_2 for fluorescence measurements. Styrene (S, Quimidroga), methyl methacrylate (MMA, Quimidroga), butyl acrylate (BA, Quimidroga), acrylic acid (AA, Sigma Aldrich) and methacrylic acid (MAA, Sigma Aldrich) monomers were used as received. Divinyl benzene (DVB, Fluka) as cross-linked, sodium dodecyl sulfate (SDS, Sigma Aldrich) as anionic emulsifier and hexadecane as co-stabilizer (HD, Sigma Aldrich) were used as received. Potassium persulfate (KPS, Sigma Aldrich) was used as initiator without further treatment. Deionized water was used for the preparation of the aqueous phase of the miniemulsions and hydroquinone (HQ, Sigma Aldrich) for stopping the reaction when withdrawing a sample from the round bottom flask. Polyvinyl alcohol (PVA, Sigma Aldrich) and polyethylene oxide (PEO, Sigma Aldrich) were used as thickeners for increasing the viscosity of the hybrid core-shell latex for the synthesis of the nanofibers by electrospinning.

I.2. Miniemulsion stability measurement

As introduced in Chapter 2, the miniemulsion stability was followed by studying the evolution of the backscattered light using the Turbiscan LAb^{expert} equipment. The reading head of this device consists of a pulsed near infrared light source (λ = 880 nm) and two synchronous detectors. The transmission detector receives the light flux transmitted through the sample while the backscattering detector measures the backscattered light. The detection head scans

the entire length of the sample (55 mm) acquiring transmission and backscattering data every 40 µm. A representation of the equipment is presented in Figure I.1. The curves that are obtained provide the transmitted and backscattered light flux in percentage relative to standards (suspension of monodisperse spheres and silicon oil) as a function of sample height (in mm).

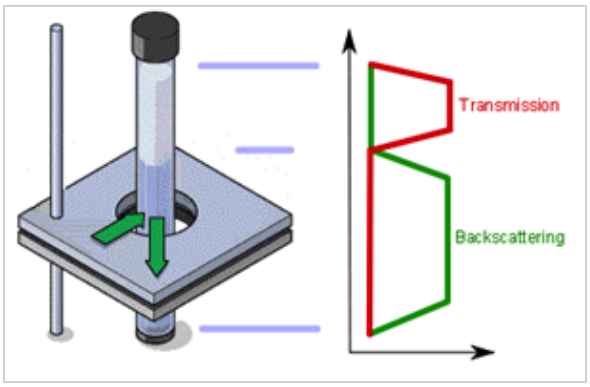

Figure I.1 Representation of the Turbiscan LAbexpert detection principle.

This technique allows very early visualization of creaming, sedimentation and coalescence/flocculation. Creaming takes place when the dispersed phase has a lower density than the continuous phase. It can be easily detected because the backscattering flux decreases at the bottom of the sample and increases at the top due to the increase in the dispersed phase concentration. Sedimentation takes place when the density of the dispersed phase is greater than the continuous one. In this case, the backscattering increases at the bottom of the sample due to an increase in the sample concentration. Coalescence/flocculation

leads to the fusion of interfaces increasing the droplet size. The particle size leads to a variation (usually a decrease) of the backscattering over the whole height of the sample.

I.3. Solids content and monomer conversion

Approximately 1mL of the latex was withdrawn from the reactor during the polymerization process, placed in a pre-weighed aluminum pan and immediately thereafter a drop of a 1 wt% hydroquinone solution was added to stop the reaction. The pan was dried until constant weight was achieved. The solids content (SC) was obtained gravimetrically and is given by:

$$SC = \frac{weight\ of\ the\ solid\ dried\ material}{weight\ of\ the\ latex} \qquad (I.1)$$

The instantaneous conversion (*X*) was determined by the following equation,

$$X(t) = \frac{Polymerized\ Monomer}{Total\ Monomer} = \frac{(SC \cdot Latex) - NPS}{MW} \qquad (I.2)$$

Where, NPS is the non-polymerizable materials (QDs, CeO_2, surfactant, costabilizer and initiator) and MW is the amount of monomer plus polymer at each time.

I.4. Nd and Np calculations

Miniemulsion droplets and polymer particle sizes were measured by dynamic light scattering (DLS) using a Malvern Zetasizer Nano ZS (laser: 4mw, He-Ne, λ=633 nm, angle

173º). The equipment determines the particle size by measuring the rate of fluctuations in light intensity scattered by particles as they diffuse through a fluid.

Samples were prepared by diluting a fraction of the latex or miniemulsion with deionized water. To measure the size of miniemulsion droplets, H_2O saturated with monomer is normally used to avoid droplet destabilization by thermodynamic reasons. However, similar results were found when saturated H_2O and no-saturated H_2O was used. The analyses were carried out at 20°C and each run consisted in two size measurements per sample, from which the final size was obtained as the average of both measurements.

Results obtained from DLS were used to determine the number of droplets (N_d) and number of particles (N_p).

$$N_d = \frac{V_d}{V_t} = \frac{6 \cdot (W_{mon}/\rho_{mon})}{\pi \cdot {d_d}^3} \quad (I.3)$$

$$N_p = \frac{V_p}{V_t} = \frac{6 \cdot (W_{pol}/\rho_{pol}) \cdot X}{\pi \cdot {d_p}^3} \quad (I.4)$$

N_d was calculated using Equation I.3, where W_{mon} was the amount of monomer (g), ρ_{mon} the monomer density (0.909 g/cm^3), and d_d the average droplet size (nm) calculated by DLS. N_p was determined following Equation I.4. In this case, W_{pol} corresponds to the amount of polymer (g) at each time, and it was calculated from the monomer conversion (*X*). ρ_{polym} refers to the polymer density (1.04 g/cm^3) and d_p to the average particle size. N_d and N_p involved some uncertainty because the third power of d_d and d_p was used in their calculation.

Equation I.4 was also used to calculate the Np of the nanoparticles QDs and CeO_2 being their density 5.82 g/cm^3 and 7.2 g/cm^3 respectively.

I.5. Fluorescence measurements

Fluorescence emission intensity of quantum dots dispersions, hybrid latexes and hybrid films was measured using a Fluoromax-4 spectrofluorometer (Horiba Jobin Yvon) equipped with a Xe arc-lamp as excitation source, detecting the signal at 90º with a photon counting detector. Quartz cuvettes of 10 mm path length clear on all four sided were used for the measurement of dilutions and latexes, whereas square quartz supports 1.5 cm side were used for the analysis of the films that were casted on them.

Coupled to the spectrofluorometer, a fluorescence microscope Olympus BX51 furnished with a Hg lamp excitation source and a specific filter cube (U-MNU2), was used for measuring the fluorescence in a specific area of the film and to take pictures of the distribution of the QDs along a film.

I.6. UV-Vis measurements

The UV-Vis absorption measurements were carried out using a Shimadzu spectrophotometer (model UV-2550 230V). The measurements were done in the 200-800 nm range at room temperature using a quartz cuvette 10 mm path length and quartz supports where the films were cast.

I.7. Viscosity measurements

Apparent viscosity of the PVA and PEO dispersions was measured using a TA Instruments-AR1500ex rheometer. Flow procedures using a 60 mm diameter steel plate as geometry were carried out at 25ºC in all the measurements. Three different steps were set. A conditioning step in which the working temperature is set, a first continuous ramp from 0.1 to 1000 s^{-1} and a second continuous ramp from 1000 to 0.1 s^{-1}.

I.8. Conventional 2D TEM

The morphology of the latex particles as well as the films cast from the latexes, and the quantum dot sizes were characterized by Transmission Electron Microscopy (TEM), TECNAI G2 20 TWIN (FEI, Eindhoven, The Netherlands), operating at an accelerating voltage of 200 KeV in a bright-field image mode.

Preparation of the samples was done as follows. For the analysis of the core and core-shell particles, the latex was diluted and directly deposited on a copper grid. For the analysis of the soft core-shell-shell particles, hydroxyethyl cellulose (HEC) was added to the latex (0.06% wt) prio to the deposition of the sample on the copper grid. This prevents the deformation of the low Tg polymer particles during sample preparation by forming a thin film around the particles and keeping their spherical morphology[1]. On the other hand, in the case of the films, those were cast at room temperature and trimmed at -40ºC using an ultramicrotome device (Leica

EMFC6) equipped with a diamond knife. The ultrathin sections (100 nm) were placed on a 300 mesh copper grid. In all cases no further preparation or staining was necessary. Finally, for the characterization of the QDs´ sizes, toluene dispersions were deposited on the copper grids and analyzed without further preparation.

I.9. Cryo-TEM

Cryo-TEM was used to analyze the position of the QDs into the monomer droplets in the miniemulsion. Briefly, one drop of the diluted hybrid miniemulsion (~3 μL) was vitrified by fast freezing in liquid ethane using a Vitrobot Mark IV (FEI, Eindhoven, The Netherlands). This vitrified sample grid was then transferred through a 655 Turbo Pumping Station (Gatan, France) to a 626 DH Single Tilt Liquid Nitrogen Cryo-holder (Gatan, France), where it was maintained bellow -170ºC. A copper grid (300 mesh Quantifoils) was hydrophilized by glow-discharge treatment. The sample was then examined in the Transmission Electron Microscope TECNAI G2 20 TWIN (FEI, Eindhoven, The Netherlands) mentioned above, operating at an accelerating voltage of 200 keV in a bright-field and low-dose image mode.

I.10. Electron tomography (3D-TEM)

The use of 2D-TEM to determine the location of the nanoparticles into the polymer particles conventional 2D-TEM can be ambiguous due to a wrong interpretation of the images because of the artefacts intrinsic to the technique[2]. To accurately determine the location of, in this case, the quantum dots into the polymer particles, a 3D reconstruction is needed in order

to get a general view of the whole hybrid particle. For this Electron Tomography or 3D-TEM was carried out to the hybrid core and core-shell particles.

To reconstruct a 3D object by electron tomography a tilt series (projections) of micrographs are taken at angular increments. This is done by tilting the sample around the eucentric axis of the holder rod, usually from -60º to +60º (see Figure I.2a). Each projection in real space is equivalent to a central slice in Fourier space and thus, by recording images at successive tilt angles, the 3D Fourier space is built slice by slice[3]. The images collected by tilting the sample are back-projected along their original tilt directions into a three-dimensional object space as shown in Figure I.2b. The overlap of the back-projections defines the reconstructed object.

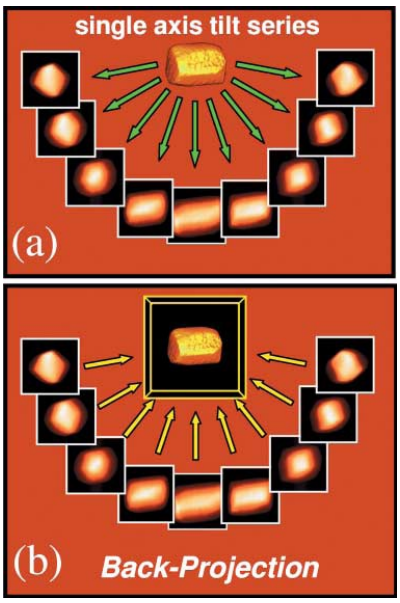

Figure I.2. A schematic diagram of the tomographic reconstruction using the back-projection method. a) images at tilted angles and b) the images projected into a three dimensional object[3].

In order to assess the degree of encapsulation of the nanoparticles, a 3D tomographic reconstruction of core and core-shell samples was carried out. On one hand, the polystyre/QDs sample was characterized using tilt series of micrographs and their subsequent 3D reconstruction acquired in the same TEM microscope as for the 2D analysis exposed above, TECNAI G2 20 TWIN (FEI, Eindhoven, The Netherlands) in bright field and low dose conditions. The tilt series was obtained tilting the sample from +60º to -60º every 2º with a pixel size of 0.22 nm/pixel. The images were aligned using a homemade plugging for Digital Micorgraph (http://www.christophtkoch.com/FRWR/index_tools.html) and Inspect 3D software (http://www.fei.com). The reconstruction was carried out using Simultaneous Iterative Reconstruction Technique (SIRT) (10 iteration) employing the Inspect 3D software. On the

other hand, the core-shell polystyrene/QDs/polymethyl methacrylate sample was tilted from -55º to +70º every 2º. The images were acquired at 100kV in a JEOL JEM-1230 thermionic emission TEM (JEOL, Japan) in bright field and low dose image mode with a pixel size of 0.34 nm/pixel. The images were aligned using the Midas utility of the IMOD 4.3.3 package[4] and reconstructed with weighted back projection (WBP) algorithm in IMOD 4.3.4 package.

Some differences between the XY and YZ planes were present due to the elongation of the objects inherent to the TEM tomography technique. This is due to the missing wedge, some information is missing at certaing angles, in these cases the images missing to cover 360º. To correct this distortion the resulting 3D reconstruction was rescaled in the electron beam direction.

The 3D-TEM analyses were carried out in eMERG and Department of Mining and Metallurgical Engineering and Materials Science University of the Basque Country UPV/EHU, Pº Rafael Moreno Pitxitxi, 3, 48013, Bilbao, Spain.

I.11. Image processing

Statistics of the distribution of the nanoparticles into the polymer particles as well as of the size of the polymer particles and the quantum dots used during this work, around 500 polymer particles and nanoparticles were counted and measured using the open access software Image Processing and Analysis in Java (Image J). Different average values were calculated, precisely, in number, in weight and in volume.

$$Dp_{Number} = \frac{\sum n_i \cdot dp}{\sum n_i} \qquad I.5$$

$$Dp_{Weight} = \frac{\sum n_i \cdot dp^4}{\sum n_i \cdot dp^3} \qquad I.6$$

$$Dp_{Volume} = \left(\frac{\sum n_i \cdot dp}{\sum n_i}\right)^{1/3} \qquad I.7$$

I.12. Energy-dispersive X-ray spectroscopy

Discern of quantum dots over nanoceria nanoparticles was not possible visually due to the similar size of the nanoparticles. Therefore, an Energy-dispersive X-ray (EDX) mapping of the samples was carried out. Samples containing core-shell hybrid polymer particles were diluted and directly deposited on copper grids. On the other hand, the samples containing soft core-shell-shell hybrid polymer particles were, as mentioned above, mixed with HEC (0.06% wt) prior to their deposition on the copper grid. A High-Resolution Transmission Electron Microscope (HRTEM) TITAN (FEI, Eindhoven, The Netherlands) operating in Scanning Transmission Electron Microscopy (STEM) mode was used, which makes observing the background of the sample in dark, the polymer particles in grey and the inorganic nanoparticles as white spots. An electron beam stimulated the emission of characteristic X-rays of the elements present in the area focused. This allows doing an EDX mapping of the area of interest and identify the nanoparticles present.

The EDX analysis were carried out using the HRTEM facilities of the Electron-Microscopy Laboratory in NanoGUNE, Avd. Tolosa 76, 20018, Donostia-San Sebastián, Spain.

I.13. References

(1) Geng, X.; Zhai, M. X.; Sun, T.; Meyers, G. Microscopy Microanalysis Morphology Observation of Latex Particles with Scanning Transmission Electron Microscopy by a Hydroxyethyl Cellulose Embedding Combined with RuO 4 Staining Method. *Microsc. Microanal.* **2013**, *19*, 319–326.

(2) Drummy, L. F.; Wang, Y. C.; Schoenmakers, R.; May, K.; Jackson, M.; Koerner, H.; Mauryama, B.; Vaia, R. A.; Farmer, B. L.; Mauryama, B.; et al. Morphology of Layered Silicate - (NanoClay-) Polymer Nanocomposites by Electron Tomography and Small-Angle X-Ray Scattering. *Macromolecules* **2008**, *41*, 2135–2143.

(3) Midgley, P. A.; Weyland, M.; Yates, T. J. V.; Arslan, I.; Dunin-Borkowski, R. E.; Thomas, J. M. Nanoscale Scanning Transmission Electron Tomography. *J. Microsc.* **2006**, *223* (3), 185–190.

(4) Kremer, J. R.; Mastronarde, D. N.; McIntosh, J. R. Computer Visualization of Three-Dimensional Image Data Using IMOD. *J. Struct. Biol.* **1996**, *116* (1), 71–76.

(5) Kremer, J. R.; Mastronarde, D. N.; McIntosh, J. R. Computer Visualization of Three-Dimensional Image Data Using IMOD. *J. Struct. Biol.* **1996**, *116* (1), 71–76.

(6) Agulleiro, J. I.; Fernandez, J. J. Fast Tomographic Reconstruction on Multicore Computers. *Bioinformatics* **2011**, *27* (4), 582–583.

(7) Schindelin, J.; Arganda-Carreras, I. Frise, E.; Kaynig, V.; Longair, M.; Pietzsch, T.; Preibisch, S.; Rueden, C.; Saalfeld, S.; Schmid, B.; Tinevez, J. Y.; et al. Fiji:an Open-Source Platform for Biological-Image Analysis. *Nat. Methods* **2012**, *9*, 676–682.

Appendix II. Additional experiments

II.1. Optical study of the combination of QDs with TiO_2 nanoparticles

In view of the effect of nanoceria nanoparticles on the optical properties of the quantum dots presented Chapter 4, other interesting semiconductor inorganic nanoparticles were analyzed. TiO_2 (Degussa-P25) was the chosen nanoparticle for this study, which was first explored in toluene dispersions. The election of this nanoparticle was made based on the good UV-Vis absorbance capacity of TiO_2, the similar band gap value to the one of CeO_2, and its use in solar cells.

A dispersion in toluene of quantum dots and titanium oxide in a ratio 1:1 in weight was prepared. As done with the QDs-CeO_2 dispersions, fluorescence was measured during storage at daylight. In this case a clear decrease in the emission intensity was observed, together with a blue shift in the maximum emission peak (Figure II.1a), which indicated a reduction of the size of the nanocrystals, so a degradation of their surface. Nevertheless, if the dispersion was purged with N_2 overnight, a decrease in the fluorescence emission intensity was also observed but not a shift on the emission wavelength (Figure II.1b). Moreover, differences in color from the non-purged to the purged dispersions were also observed (Figure II.1c-d).

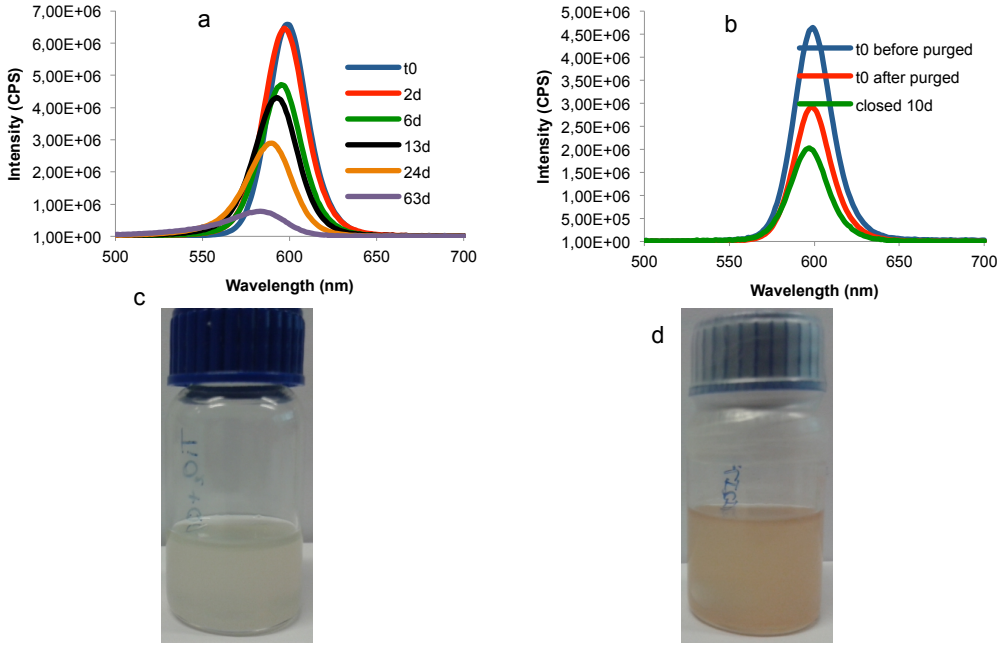

Figure II.1 a) Fluorescence emission intensity evolution of a toluene QDs-TiO_2 dispersion exposed to daylight. b) Fluorescence emission intensity evolution of a toluene QDs-TiO_2 dispersion purged with N_2 and exposed to daylight. c) QDs-TiO_2 toluene dispersion after exposure to daylight. d) N_2 purged QDs-TiO_2 toluene dispersion after exposure to daylight.

In the case of QDs-CeO_2 toluene dispersions, a slight decrease of the fluorescence emission intensity was observed over time. However, this decrease was much lower than for QDs and TiO_2, and the blue shift was not observed. At this point it is important to highlight the high photocatalytic activity that titanium oxide nanoparticles present. This means that, the electron-hole generated when an electron jumps from the valence band to the conduction band when the nanoparticle absorbs light reacts with oxygen, water or hydroxyl groups generating radicals. Taking this into account, together with the already discussed effect that radicals have in the surface of QDs (Section 2.4), it was concluded that, when a dispersion containing both

TiO_2 and QDs was in contact with oxygen, degradation of the QDs´ surface took place driving to a loss of fluorescence and a shift of the emission peak.

Those are preliminary results; more research can be done on the co-encapsulation of QDs and TiO_2 nanoparticles into polymer particles or on the encapsulation of QDs and use of the TiO2 nanoparticles as a stabilizer of the polymer particles, to study the effect on the optical properties of the QDs as done for the CeO_2 nanoparticles. However, this is out of the scope of this PhD thesis.

II.2. Modification of the hybrid core-shell polymer particles for their use in multiplexing assays

As shown in Chapter 3 fluorescence spectra can be modulated at will by blending latexes containing commercial CdSe/ZnS quantum dots of different sizes. This opens the door to the use of the synthesized hybrid latexes for multiplexing assays. However, for this the surface of the hybrid polymer particles has to be functionalized so it reacts with an analyte present in the sample of study.

This functionalization is being currently studied by a master student of the group (Ms. Idoia Guruceaga), using L-lysine, based on the method shown previously by Holzapfel et al[1].

First the surface of the polymer particles is functionalized with carboxylic acid groups, which are then activated for coupling the lysine. Functionalization of the surface of the polymer

particles with carboxylic acid group has been done by producing an additional MMA-MAA or AA shell on the top of the cross-linked core-shell polymer particles. This second shell has been synthesized by seeded semi-batch emulsion polymerization using the core-shell latex as a seed, adding a 2% wt of emulsifier (SDS), and feeding with a syringe pump a 1% wt of MAA or AA. The final shell thickness was about 30 nm. The resulting latex was centrifuged for one hour at 30.000 r.p.m in order to remove the carboxylic acid groups that were not attached to the surface. Then, activation of the carboxylic acid groups was done using a molar ratio 1:1 of carboxylic acid groups and activation reagents in order to get all the carboxylic acid groups functionalized with L-lysine. The activation of the carboxylic acid groups works as shown in Figure II.2. The 1-ethyl-3-(3-dimethylaminopropyl) carbodiimide hydrochloride (EDC) works as a carbodiimide cross-linker, which reacts with the carboxylic acid groups forming an unstable O-acylsourea ester intermediate. In order to improve the efficiency of the lysine coupling and to avoid the hydrolysis of the O-acylsourea intermediate, sulfo-N-hydroxysuccinimide (sulfo-NHS) is included in the method. The activation reaction is carried out in 4-morpholinoethanesulfonic acid (MES) buffer at pH 6.5 for 20 minutes at room temperature by dissolving the EDC with sulfo-NHS in the buffer. After the activation of the carboxylic acid groups L-lysine dihydrochloride is added. The coupling reaction is carried out under agitation for 3 hours at room temperature.

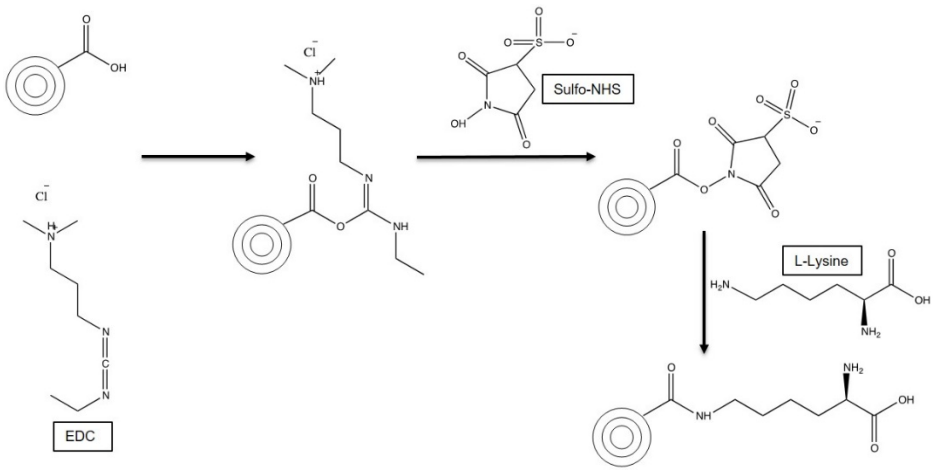

Figure II.2 Carboxylic acid group activation with 1-ethyl-3-(dimethylaminopropyl) carbodiimide hydrochloride (EDC) and sulfo-N-hydroxysuccinimide (sulfo-NHS).

II.3. References

(1) Holzapfel, V.; Lorenz, M.; Weiss, C. K.; Schrezenmeier, H.; Landfester, K.; Mailänder, V. Synthesis and Biomedical Applications of Functionalized Fluorescent and Magnetic Dual Reporter Nanoparticles as Obtained in the Miniemulsion Process. *J. Phys. Condens. Matter* **2006**, *18*, 2581–2594.

Resumen y conclusiones

Los puntos cuánticos (PCs) o quantum dots (QDs) son nanocristales semiconductores con un tamaño que oscila entre los 2 nm y los 10 nm. Fueron descubiertos en 1981 por Alexey Ekimov y estudiados durante los años 80 por L. E. Brus y sus colaboradores. De especial interés fue el estudio de la influencia de su tamaño en sus propiedades. Su reducido tamaño, menor al radio de Bohr, les confiere unas propiedades ópticas y electrónicas especiales. Entre ellas destaca su capacidad de variar la longitud de onda de emisión, únicamente variando el tamaño del nanocristal sin modificar su composición (Figura 1). También cabe destacar su emisión a una longitud de onda muy determinada y su capacidad de absorción de luz en un amplio rango de longitudes de onda.

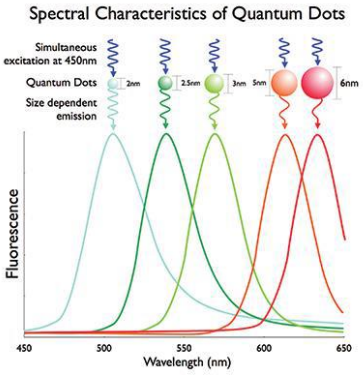

Figura 1. Variación de la longitud de onda de emisión en función del tamaño de los puntos cuánticos CdSe/ZnS. (Imagen tomada de la referencia Chen, J.; Imam, P. Causes of Asset Shortages in Emerging Markets. *Rev. Dev. Financ.* **2013**, *3* (1), 22–40).

Estas propiedades los hacen ser útiles para diversas aplicaciones. Por ejemplo, en biomedicina se pueden utilizar uno o varios tipos de puntos cuánticos simultáneamente, formando una especie de código de barras que permita la detección de analitos de interés. Esto es posible gracias a su estrecho pico de emisión, que permite diferenciar varios tipos de puntos cuánticos a la vez, excitando la muestra a una única longitud de onda. Los puntos cuánticos también se utilizan para la producción de placas solares y LEDs. En combinación con polímeros conductores hacen el transporte de electrones hacia los electrodos más eficiente. Otras aplicaciones menos conocidas pero de gran importancia son su uso como sensores de compuestos orgánicos volátiles (COVs) y como foto-sensibilizadores en procesos de fotocatálisis para el tratamiento de agua.

Sin embargo, también hay que tener en cuenta sus inconvenientes; su difícil manipulación, debida a su pequeño tamaño y su toxicidad, dado que los PCs de mayor calidad están mayoritariamente compuestos por metales pesados.

Para sacar el mayor partido a las excelentes propiedades ópticas de estas nanopartículas, pero sin olvidar los problemas de toxicidad que presentan, en este trabajo se han encapsulado en partículas de polímero, utilizando puntos cuánticos comerciales (OceanNanotech) de morfología núcleo corteza, con un núcleo de CdSe y una corteza de ZnS, modificados en su superficie con octadecilamina. La presencia de una corteza minimiza la pérdida de electrones debida a defectos en la superficie del núcleo. Por otra parte, el recubrimiento con octadecilamina permite la dispersión de los PCs en disolventes orgánicos como tolueno o cloroformo, así como en diferentes monómeros como el estireno.

El primer objetivo de esta tesis fue el de la encapsulación de estos PCs en partículas de polímero dispersas en agua para mantener su fluorescencia durante largos periodos de tiempo y conseguir una mayor protección frente a su potencial toxicidad. Una vez conseguido esto, el siguiente paso fue la combinación de PCs de diferentes tamaños para la creación de un código de barras con el fin de utilizarlo para detección múltiple en sistemas biológicos. Por otra parte, también se investigó la combinación de los puntos cuánticos con otras nanopartículas inorgánicas, más concretamente con óxido de cerio. Por último, se abordó la posible aplicabilidad de las dispersiones híbridas sintetizadas como sensores ópticos y eléctricos de compuestos orgánicos volátiles.

La encapsulación de los puntos cuánticos en partículas de polímero se realizó en dos etapas. La primera fue la formación de un núcleo de poliestireno reticulado mediante polimerización en miniemulsión, y la segunda la formación de una corteza de polimetilmetacrilato reticulado sobre el núcleo mediante la polimerización en emulsión en semicontinuo. En la primera etapa, los PCs se dispersaron en el monómero (estireno, S) junto con el reticulante (divinil benceno, DVB) y un co-estabilizador (hexadecano, HD) obteniendo la fase orgánica. Por otra parte, se preparó la fase acuosa en la que se disolvieron parte del emulsificante (SDS) y el tampón ($NaHCO_3$) en agua. Ambas fases se mezclaron y se sonificaron creando la miniemulsión. En este punto se obtuvieron gotas de monómero conteniendo los PCs estabilizadas en medio acuoso. Estas gotas se polimerizaron durante 6 horas a 75ºC utilizando para ello un iniciador térmico (KPS), obteniendo un látex híbrido con 5% en contenido en sólidos. El látex resultante no era ópticamente estable, observando una pérdida de fluorescencia durante el tiempo por la difusión de los PCs hacia la interfase

partícula polimérica-agua (Figura 2a). Por ello, y para asegurar la encapsulación de las nanopartículas en las partículas de polímero se realizó una segunda etapa sintetizando una corteza alrededor del núcleo. En ella se utilizó el látex de partículas reticuladas de poliestireno como siembra, KPS como iniciador y una mezcla de metil metacrilato y divinil benceno como monómeros a alimentar, llevando a cabo la reacción a 75°C durante 3 horas. La inyección de la mezcla de monómeros en el reactor se hizo utilizando una bomba jeringa . El contenido en sólidos final fue del 12%. Al finalizar este proceso se logró una efectiva encapsulación de PCs CdSe/ZnS modificados con octadecilamina en su superficie en partículas reticuladas núcleo-corteza PS/PMMA. La morfología de dichas partículas híbridas se estudió mediante microscopía de transmisión electrónica en tres dimensiones, observando que los PCs se encontraban rodeados por polímero en todas las direcciones. También se hizo un estudio de la fluorescencia de los látex durante el tiempo, observando estabilidad de la intensidad de emisión durante al menos 9 meses (Figura 2b).

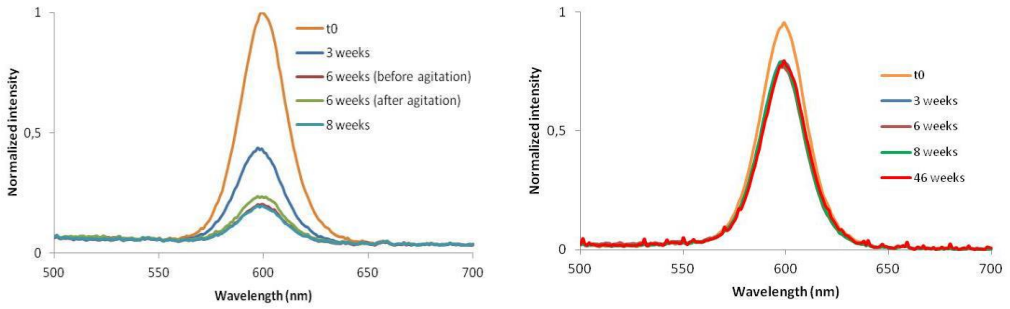

Figura 2. a) Espectro de fluorescencia para un látex PS-DVB/PCs. b) Espectro de fluorescencia para un látex PS-DVB/PCs/PMMA-DVB durante nueve meses.

Una vez desarrollado el método de encapsulación se investigó la encapsulación de múltiples puntos cuánticos de cara a su aplicación como marcadores. Durante el segundo año de tesis se realizó una estancia corta en el Institut de Chimie de la Matière Condensée de Bordeaux (ICMCB) bajo la supervisión del profesor Cyril Aymonier, con el objetivo de sintetizar puntos cuánticos de diferentes tamaños y posteriormente encapsularlos siguiendo el método anterior. Se sintetizaron PCs núcleo-corteza CdSe/CdS de diferentes tamaños recubiertos con trioctil fosfina y hexadecilamina en hexano supercrítico. Los puntos cuánticos sintetizados presentaban buenas propiedades ópticas en dispersión en hexano o cloroformo. Sin embargo, se observó una degradación de dichos nanocristales en el proceso de encapsulación, perdiendo sus propiedades ópticas. Por ello se utilizaron PCs CdSe/ZnS comerciales de cuatro tamaños diferentes, es decir, de cuatro longitudes de onda de emisión diferentes. Se prepararon látex con cada uno de los diferentes tipos de PCs, y se realizaron mezclas de dos o tres látex controlando el número de nanocristales de cada tipo en cada mezcla. Con ello se lograron controlar las intensidades y las relaciones de emisión, creando un amplio número de combinaciones posibles.

Durante este trabajo también se han estudiado los efectos de la combinación de los puntos cuánticos con nanopartículas de óxido de cerio, teniendo en cuenta la excelente emisión de los PCs y las buenas propiedades de absorción UV de las partículas de CeO_2. Ambos tipos de nanopartículas se co-encapsularon en las mismas partículas de polímero utilizando el método de encapsulación expuesto anteriormente. Así mismo se desarrolló una formulación que era capaz de formar films a temperatura ambiente. Para ello, se sintetizó una segunda corteza utilizando el látex híbrido de partículas reticuladas de poliestireno recubiertas

por una corteza de polimetil metacrilato reticulado como siembra. Esta segunda corteza está compuesta por metil metacrilato-butil acrilato y acido acrílico en una proporción 39.5/59.5/1% con el objetivo de reducir la Tg del polímero. Se obtuvieron films transparentes y de buena calidad a temperatura ambiente. Mediante fluorescencia se estudió el efecto que tienen las nanopartículas de CeO_2 sobre las propiedades ópticas de los puntos cuánticos. Tanto los látex como los films conteniendo diferentes proporciones de PCs:CeO_2 se expusieron a la luz solar midiendo la fluorescencia a lo largo del tiempo. Se observó un incremento de la emisión de fluorescencia durante el tiempo de exposición a la luz solar tanto para los látex como para los film (ej. 280% de incremento para un látex con una proporción PCs:CeO_2 1:2, y 545% para un film con una proporción PCs:CeO_2 1:2). Las diferencias en el incremento de la emisión se deben a la diferencia en las distancias entre las nanopartículas. En el látex esta distancia es mayor al estar las partículas de polímero en dispersión. Sin embargo, cuando se forma el film estas distancias se acortan y por lo tanto el efecto del óxido de cerio sobre los puntos cuánticos se acrecienta (Figura 3).

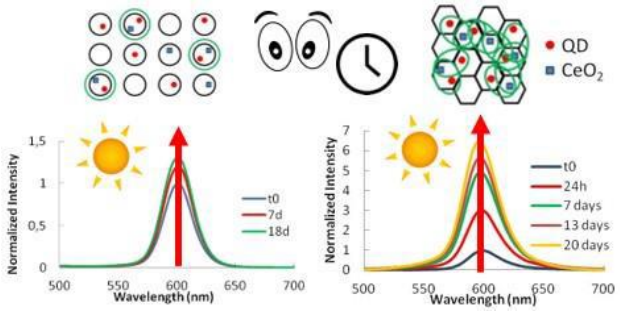

Figura 3. Incremento de la fluorescencia de un látex (izquierda) y de un film (derecha) expuestos a la luz solar.

Por último, la aplicabilidad de los látex híbridos núcleo-corteza se ha estudiado mediante la producción de nanofibras por electrohilado y su posterior contacto con

compuestos orgánicos volátiles (COVs). Dado que los látex sintetizados tienen una viscosidad demasiado baja para producir las nanofibras, ésta se aumentó mediante la adición de polivinil alcohol (15% wt) u óxido de polietileno (5% wt). La dispersión resultante se inyectó a través de una bomba jeringa, creando una diferencia de potencial entre la aguja y el colector para producir las nanofibras. Las condiciones óptimas utilizadas han sido: voltaje 15 kV, distancia aguja-colector 200 mm y un flujo de alimentación 0.08-0.1 mL/h para las dispersiones de PVA y 0.2-0.3 mL/h para las dispersiones de PEO. Las nanofibras sintetizadas se pusieron en contacto con vapores de diferentes disolventes (acetona, tolueno y metanol) y se midió la evolución de su fluorescencia durante el tiempo. Se observó que con el paso del tiempo, al aumentar la concentración de vapor, la intensidad de emisión de fluorescencia desciende. También se ha estudiado la respuesta eléctrica de las nanofibras producidas con PEO ante vapor de acetona. Para ello se midió la conductividad de las nanofibras depositadas en un electrodo interdigitado observando un aumento de la resistencia a lo largo del tiempo de exposición al vapor de acetona, recuperando su valor inicial al dejar de exponer el electrodo a la acetona.

Con el trabajo desarrollado para esta tesis doctoral se ha logrado una eficiente encapsulación de PCs de diversos tamaños en partículas poliméricas dispersas en agua, consiguiendo gran estabilidad de sus propiedades ópticas, así como un buen control de la fluorescencia al combinar diferentes PCs. Así mismo, se co-encapsularon los PCs con CeO_2 consiguiendo mejorar las propiedades ópticas tanto de los látex como de los films. Por último, se ha investigado la posible aplicabilidad de los látex híbridos sintetizados como sensores de COVs.